Tuning the interaction Potential in complex Plasmas

Lisa Wörner

München 2012

Tuning the interaction Potential in complex Plasmas

Dissertation

conducted in the framework
of a joint supervision (co-tutelle)

at the Fakultät für Physik
der Ludwig–Maximilians–Universität München

and the
Université d'Orléans

handed in by
Lisa Wörner
born in Darmstadt.

Munich, the 26. October 2012

First Referee: Prof. Dr. G. E. Morfill
Second Referee: Prof. Dr. L. Boufendi
Date of the oral Exam: 7. 12. 2012

Contents

Abstract

Plasmas are next to the solid, liquid and gaseous phase the fourth state of matter. It is established by ionizing a gas. About 99% of the visible matter in the universe is in the state of plasma. The industrial, medical and scientific benefits of plasmas led to a variety of artificially produced plasmas. In plasmas dust particles can grow. Especially in industrial plasmas particle formation in the plasma gas phase is very common. The fundamental understanding of the growth is of vital importance in order to suppress undesired particle formation or to deposit particles and films in a certain region.

In terms of this thesis the particle growth in a direct current (DC) discharge by using acetylene will be discussed. It has been observed that the particle growth depends on the neutral gas flow fed into the plasma chamber. Depending on the applied flow different growth frequencies and transport phenomena are shown. The observations recorded by a spectrometer will then be complimented by pictures from the particles taken by a scanning electron microscope.

Introducing artificial particles into a plasma rather than growing them there yields several advantages. The particle sizes can be controlled, including the possibility of particle mixtures. Furthermore, particles with bigger diameter can be introduced than what can be grown on reasonable time scales in a plasma.

Several possible experiments with injected particles underline the interdisciplinary character of the plasma environment. To understand the inter particle interactions the particle charge is a crucial parameter.

In this thesis several experiments determining the particle charge will be discussed. In this frame the experiments on board of the International Space Station have been performed to measure the residual charge in the particle afterglow.

In the last section experiments on particle cluster rotation as observed in an additional confinement will be discussed. It will be shown that the particles tend to form vertical strings due to the wake field that forms downstream of each particle. Finally the insight gained on the possibilities of tuning of the interaction potential by electric fields will be discussed. The results are then compared to the predictions of earlier simulations.

Résumé

A coté des solides, des liquides et des gaz, le plasma est le quatrième état de la matière. Il est généré en ionisant un gaz. Dans l'univers, 99% de la matière est l'état de plasma. L'émergence de plusieurs types de plasmas artificiels est due aux multiples et différentes applications, très intéressantes les unes que les autres, des plasmas dans des secteurs aussi variés que l'industrie, l'énergie, le biomédical et la science. Très souvent, des particules solides peuvent se former dans les plasmas. Ceci a tout particulièrement été observé dans ceux utilisés dans l'industrie. La compréhension des mécanismes de leur nucléation et croissance est d'une importance capitale en vue de trouver des solutions pour inhiber leur formation ou d'éviter qu'elles ne se déposent sur les surfaces en cours de traitement.

L'objectif du travail de recherche entrant dans le cadre de cette thèse est l'étude de la formation de particules dans un plasma généré par décharge électrique continue. Il a été observé que ce phénomène dépend du flux de gaz neutre injecté dans l'enceinte du réacteur. J'ai mis en évidence que la fréquence de formation est liée à ce paramètre. Les observations enregistrées à l'aide d'un spectroscope sont complétées et corrélées aux photographies obtenues par microscopie électronique à balayage.

L'injection de particules dans le plasma plutôt que de procéder à les faire croitre présente certains avantages. On peut contrôler leur taille y compris de la cas de mélanges de particules. On tout particulièrement injecter des particules ayant des tailles beaucoup plus importantes que celles que l'on forme sur des gammes de durées raisonnables des plasmas utilisés.

Plusieurs expériences réalisées avec des particules injectées ont mis en exergue le caractère pluridisciplinaire du milieu plasma. Afin de comprendre les interactions mutuelles entre particules il est crucial de déterminer la charge portée par les particules.

Plusieurs expériences réalisées au cours de cette thèse et présentées ici ont porté sur la détermination de ce paramètre fondamental. Dans ce cadre une série d'expérience a été réalisée à bore de la Station Spatiale Internationale (ISS) dans le but de déterminer la charge résiduelle des particules dans la phase de post-décharge.

Dans la dernière partie, seront présentées et discutées des expériences portant sur l'observation de la rotation de clusters de particules soumis à un confinement supplémentaire. On montre que les particules tendent à former des alignements verticaux dus au faible champ qui se forme en aval de chaque particule. Enfin, les connaissances acquises sur les possibilités de moduler le potentiel d'interaction par l'intermédiaire d'un champ électrique seront discutées. Les résultats sont comparés aux prédictions des simulations.

Kurzbeschreibung

Neben fester, flüssiger und gasförmiger Phase sind Plasmen der vierte Aggregatzustand der Materie. Ionisierte Gase machen etwa 99% der sichtbaren Materie im Universum aus. Neben den natürlich vorkommenden Plasmen führte der industrielle, wissenschaftliche und medizinische Nutzen zu einer Vielzahl von künstlich erzeugten Plasmen. Teilchenwachstum ist ein häufiges Phänomän in Plasmen. Besonders in der Gasphase industrieller Plasmen ist es weit verbreitet. Das grundlegende Verständnis des Wachstums ist von unmittelbarer Bedeutung für die Vermeidung der Bildung unerwünschter Partikel sowie für die Deponierung von Teilchen und Filmen in erwünschten Bereichen.

Im Zuge dieser Arbeit wird das Wachstum von Partikeln in einer Gleichstrom (DC) Entladung unter Verwendung von Acetylen beschrieben. Die Abhängigkeit des Wachstums von dem Neutralgasfluß, die erreichten Teilchengrössen und die, aus dem repetetiven Charakter des Wachstumsprozesses resultierende, Wachstumsfrequenz werden gezeigt. Des Weiteren werden Veränderungen des Plasmas und der Teilchentransport entlang der Kammer beschrieben. Die von einem Spektrometer aufgenommenen Daten werden durch Rasterelektronenmikroskopbilder der Teilchen ergänzt.

Neben der Teilchenformation können Teilchen injiziert werden. So kann die Teilchengrösse von vorneherein festgelegt werden und auch Mischungen aus Teilchen verschiedener Grössen sind möglich. Zusätzlich können Experimente mit Teilchen grösseren Durchmessers durchgeführt werden.

Die zahlreichen möglichen Experimente mit injizierten Teilchen betonen den interdisziplinären Charakter komplexer Plasmen. Die Ladung der Teilchen dominiert ihre Wechselwirkung und ist daher ein entscheidender Faktor.

In dieser Arbeit werden verschiedene Experimente zur Bestimmung der Teilchenladung vorgestellt. In diesem Zusammenhang wurden Experimente an Bord der Internationalen Raumstation durchgeführt. Die Restladung der Teilchen nach Erlöschen des Plasmas wird bestimmt. Verschiedene Situation mit und ohne zusätzlichem elektrischen Feld wurden untersucht. Ohne zusätzliches Feld verteilen sich die Ladungen um null, mit Feld zeigt sich ein Trend zu positiver Teilchenladung.

Im letzten Abschnitt werden Experimente zur Clusterrotation besprochen. Auftretende vertikale Teilchenketten und Experimente mit einzelnen Teilchen vervollständigen das Bild. Anhand der gewonnenen Daten wird abschließend eine Aussage über die möglichen Veränderung des Teilchenwechselwirkungspotentials anhand eines Vergleichs mit früheren Simulationen gemacht.

Outline

The main objective of this thesis is the tuning of the particle interaction potential in complex / dusty plasmas.

To understand the particle behavior, first an introduction on the basic plasma principles, chapter 1, will be given. Afterwards the behavior of particles levitated in a plasma will be discussed, chapter 2. This includes charging and particle interactions.

This is followed by a description of particle formation in plasmas in general, chapter 3. The results of the experiments on particle formation in a DC discharge are then discussed in chapter 4.

Since the particle charge is one of the most fundamental parameters in complex/dusty plasmas a way to determine the charge in the plasma afterglow will be described in chapter 5.

In chapter 6 earlier experiments on the tuning of the interaction potential are discussed.

The final two chapters 7 and 8 are then dedicated to experiments on the interaction potential. Furthermore, interesting side effects will be discussed.

I have to refer to my own publications throughout the description of my experiments. My publications are designated different numbers to distinguish them easily from the rest of the references.

- [MY1]: Effect of Rotating Electric Field on 3D Complex (Dusty) Plasma
- [MY2]: The Formation and Transport Phenomena of nanometer-sized Particles in a DC Plasma
- [MY3]: String Formation in Response to Rotating Electric Fields

Chapter 1

Plasmas

1.1 States of Matter

Molecules and atoms tend to organize themselves according to their properties and the surrounding conditions, e.g. pressure, temperature, and volume. The three basic states in which matter occurs are solid, liquid and gas.

Phase transitions can be displayed using a phase diagram. Phase diagrams describe the state of a given material depending on two thermodynamical parameters, e.g. pressure and temperature [136]. Transitions from one to another state occur along certain lines in these diagrams. In case of a phase transition the temperature and the pressure will stay constant until the system has been changed completely. The only difference is the critical point beyond which the system passes into a supercritical fluid where gaseous and liquid phase are no longer distinguished. This has for instance been reported by C. Eckert *et al.*, [59].

Ionizing a gas leads to a fourth state: the plasma. Even in an only weakly ionized gas the charged species dominate the behavior of the system. In difference to the other three states the border between a system being a plasma or a gas is not sharp since the gas will undergo a slow transition while being (partly) ionized.

Plasmas differ from gases in some major respects. Since the gas molecules are ionized more than one active species occur in the plasma. Collisions and external forces lead to a non-Maxwellian ion and electron velocity distribution inside the plasma. Collective phenomena in response to electromagnetic fields are characteristic for plasmas.

Plasmas are a very common state of matter. Actually about 99% of the visible[1] matter in the universe is in the state of plasma. Plasmas occur in astrophysical environments as well as on earth. In addition artificial plasmas are employed for instance in industrial, medical, and scientific applications.

Typical astrophysical plasmas are stars [56, 172], comet tails, supernova explosions [14], planetary spokes [74, 157], and interstellar nebulae [81]. Dust has been found responsible

[1] In this thesis the visible range means any wavelength in the regime visible to the human eye, i.e. 450nm - 700nm)

for comet and planetesimal formation in nebulae [215]. The simulations by Supulver *et al.* [202] demonstrate the condensation of sub micrometer sized particles from present gas and their coagulation in nebulae, forming planetesimal. In their paper the necessity of charged species during this process is emphasized. In earths environment flames, polar auroras, and lightning [175] are naturally occurring plasmas. Artificially produced plasmas include fluorescent lights, industrial processing [19], spacecraft propulsion [126], plasma torches, particle sources [11] particle beam collisions [84], and acceleration [23]. In addition to the industrial and every day life applications, plasmas have shown to be useful in health care [193]. This includes sterilization, skin treatment, wound healing, cancer treatment and dental care.

1.2 Temperatures

In systems being in thermal equilibrium the temperature describes the particles kinetic energy. Even though many plasmas are not in thermal equilibrium, and therefore the velocity distributions are far from being Maxwellian, a temperature for electrons and ions can be approximated. Depending on the relation between the temperatures of the electrons, ions and the remaining neutral gas atoms[2] plasmas can be classified.

If electron and ion temperatures do not differ much the plasma is called thermal. The opposite situation is called a non-thermal plasma. There the ion temperature is almost at the level of the neutral temperature whereas the electron temperature is much higher. In most cases the ion temperature in non-thermal plasmas is therefore the same as the surrounding room temperature.

The degree of ionization is linked to the ion and electron temperature as well as to the electron density. If the electron kinetic energy is too low the ions and electrons recombine and the plasma turns into gas.

1.3 Low temperature Plasmas

1.3.1 General

It is possible to produce thermodynamically open low temperature plasmas. In this case the ions are almost in thermal equilibrium with the neutral gas atoms and thus leading to a situation in which the plasma is operated at room temperature. However, the electron kinetic energy is much higher than the ion kinetic energy.

Collisions of ions with neutrals are dominating the ion-ion and ion-electron collisions leading to a temperature of the plasma of the order of that of the neutral gas. To achieve an environment like this a gas at up to atmospheric pressures is exposed to electric powers

[2] As it has been previously stated plasmas are (partly) ionized gases and include still some neutral gas atoms. These may however be in an excited state. These neutrals are in thermal equilibrium and their temperature can be estimated assuming a Maxwellian velocity distribution.

of several Watts. The simplest way to ionize a gas is to apply a direct current. This type of discharge is hence also called DC discharge or DC plasma. If the applied voltage is alternated with a frequency in the order of several MHz it is called RF (radio frequency driven) plasma. Due to availability of industrial and therefore cheaper generators, RF plasmas are usually ignited at frequencies of 13.56 MHz and 81.6 MHz. There are different types of RF plasmas depending on the way of ionization. In capacitively coupled discharges the plasma is ignited in between two electrodes. If both electrodes are powered the discharge can be operated in push-push or push-pull mode depending on the phase shift of the applied voltages. Different from this works the inductively coupled discharge. This discharge is ignited using a coil and the induction of magnetic and electric fields.

In most of the laboratory environments plasmas are based on noble gases as Neon, Krypton, and Argon. In addition reactive gases, such as Acetylene or Methane can be injected into the plasma changing its properties. Some applications have shown that electronegative plasmas have advantages with respect to the ones based on noble gases. Especially for sputtering and etching plasmas based on Oxygen are of advantage [42].

1.3.2 Ionization

By delivering energy to a gas its molecules can be excited. The excitation of a given molecule is determined by the electron energy levels. The levels are defined by the inhabited orbitals. An orbital describes the probability of electron appearance in the vicinity of the atoms nuclei. They are characterized by quantum numbers corresponding to the electrons energy and angular momentum. According to the angular momentum the orbitals are named s, p, d, and f orbital. They differ in shape and population [179].

An excited atom will regain its ground state by releasing energy in form of photonic emission. Since the energy levels are discrete a certain atom or molecule will emit photons of discrete energy and thereby wavelength. This can be used to determine the compounds of a given material as well as for calibrating optical tools. In case of argon the most important transitions lead to emissions at 751 nm and 811 nm [152].

If the energy delivered to a molecule is high enough electrons can be removed completely. In addition positive ions and neutrals can pick up electrons. However, in most cases the volume recombination is negligible compared to the loss of charged species on the confining walls. Thus ionization and recombination are present at all times and the plasma is only sustained by constantly applying an electric field of sufficient intensity.

The degree of ionization α is described by the number density of neutral gas atoms (n_n) and ions (n_i). The formula is given as:

$$\alpha = \frac{n_i}{n_i + n_n} \tag{1.1}$$

If $\alpha \ll 1$ the plasma is considered to be weakly ionized [68, 190]. Throughout the experiments described in this thesis the ionization degree $\alpha \approx 10^{-5} - 10^{-7}$.

Since there are equal numbers of positive and negative charges in the plasma it is in a state of quasi-neutrality. This can be mathematically simplified by setting the number

density of free electrons n_e equal to the number density of ions times the average ionization.

Using the Boltzmann equation and the plasma potential the number densities can also be written as [68, 159]:

$$\begin{aligned} n_e &= n_{e0} \cdot exp(-\frac{e\Phi}{k_B T_e}) \\ n_i &= n_{i0} \cdot exp(-\frac{e\Phi}{k_B T_i}) \end{aligned} \tag{1.2}$$

In this equation $n_{e0,i0}$ are the initial electron and ion densities. Due to thermal losses these are reduced depending on the plasma potential, and the electron respectively ion temperatures $T_{e,i}$.

1.3.3 Potentials

Plasmas being determined by electro-magnetic fields are best described by the Maxwell equations [200].

$$\begin{aligned} \vec{\nabla} \cdot \vec{E} &= \frac{\rho}{\epsilon_0} \\ \vec{\nabla} \cdot \vec{B} &= 0 \\ \vec{\nabla} \times \vec{E} &= -\frac{\partial \vec{B}}{\partial t} \\ \vec{\nabla} \times \vec{E} &= \mu_0 \vec{j} + \mu_0 \epsilon_0 \frac{\partial \vec{E}}{\partial t} \end{aligned} \tag{1.3}$$

In these equations ρ and $\vec{j}$ are the charge and current densities.

In plasmas the time variation of the magnetic field can usually be neglected [66]. Hence the electric field can be derived from a scalar potential Φ

$$E = -\nabla\Phi \tag{1.4}$$

leading to the Poisson equation.

$$\Delta\Phi = \frac{\rho}{\epsilon_0} \tag{1.5}$$

The solution to this equation is in linear approximation the so-called Debye-Hückel (Yukawa) potential [159].

$$\Phi(r) = \frac{q}{4\pi\epsilon_0 r} exp(-\frac{r}{\lambda_D}) \tag{1.6}$$

With

$$\lambda_D = (\lambda_{De}^{-2} + \lambda_{Di}^{-2})^{-\frac{1}{2}} \tag{1.7}$$

being the total Debye length. The individual Debye lengths for ions and electrons respectively are given by

$$\lambda_{Di,e} = \sqrt{\frac{\epsilon_0 k_B T_{i,e}}{n_{i,e} e^2}} \tag{1.8}$$

The total Debye length describes the distance in which the measured charge of a particle is declined to $\frac{1}{e}$ of the original value [159]. Hence it is a measure of the screening of a particle. Therefore the Debye length is also called Debye screening length or screening length. The screening length is the typical length along which particles see the strong electric field of another particle. Since plasmas are quasi-neutral the individual particle charge is of high importance. The interaction is described by the plasma condition [68]

$$N_e = \frac{4\pi}{3}\lambda_D^3 n_e \gg 1, \tag{1.9}$$

giving the total number of electrons inside the Debye radius around a certain particle.

In addition collective phenomena can be observed. A typical phenomenon are charge density oscillations traveling at a characteristic frequency, the so-called plasma frequency

$$\omega_{p\ i,e} = \sqrt{\frac{e^2 n_{i,e}}{\epsilon_0 m_{i,e}}}. \tag{1.10}$$

If any field with a frequency above the ion (electron) plasma frequency is applied, the ions (electrons) can not follow the excitation any more. As the plasma frequency is proportional to the square root of the inverse particle mass, the ion plasma frequency is much lower than the electron plasma frequency. Since this thesis has been dedicated on the manipulation of the ions in the plasma the plasma frequency will be of high importance.

1.3.4 Regions

General

Containing equal numbers of positively and negatively charged particles parts of plasmas are quasi-neutral. The volume in which the quasi-neutrality is preserved is called bulk plasma [128]. The combination of quasi-neutrality and free charge carriers leads to a situation of almost infinite electric conductivity of the bulk plasma.

However, every laboratory plasma interacts with the surrounding confinement. Close to the walls a positive space charge builds up introducing a potential barrier confining the electrons inside the plasma. This results in strong electric fields. The volume in which these fields are present and the quasi-neutrality is violated is called sheath [128]. In the sheath basically no electrons are present. Thus electron impact ionization, dissociation, and excitation take place only in the bulk plasma. The bulk can thus be distinguished from the sheath due to the increased glow level.

The electrons are responsible for impact dissociation and ionization. These two processes lead to the increased plasma glow in the vicinity of higher electron density. Electrons are mainly present in the bulk, see e.g. figure 1.3. Thus, the sheath edge can be distinguished from the bulk plasma by the increased luminosity.

In order to fulfill energy conservation, ion continuity, and to preserve the quasi-neutrality in the bulk plasma D. Bohm [24] showed that ions have to enter the sheath with velocities

higher than the Bohm velocity

$$v \geq u_B = \sqrt{\frac{k_B T_e}{m_i}}. \tag{1.11}$$

To fulfill Bohms criteria the electric field of the sheath has to penetrate into the bulk plasma forming a pre-sheath.

Due to the electric field in the sheath the ion stream velocity is very high. Thus, their contribution to the absolute screening is reduced. The Debye length in the sheath is therefore dominated by the electron Debye length. In the bulk the opposite behavior appears. The electron temperature in the bulk is much higher than the one of the ions. Hence the electron contribution to the Debye length can be neglected and the screening is determined by ions [128, 174].

DC Discharges

In direct current (DC) plasmas the axial plasma is not uniform. If a DC plasma is produced inside a long cylinder eight regions occur along the tube: anode dark space, anode glow, positive column, Faraday dark space, negative glow, Crookes dark space, cathode glow, and Aston dark space. The regions are shown in a sketch in figure 1.1 as reproduced from [128].

The strongest voltage drop occurs along the *Crookes dark space*[3]. In this dark space even the high energetic electrons are repelled and can not reach the cathode. The discharge is maintained by the production of secondary electrons by ions emerging from the cathode. Due to the current induced by the ionization the electron density and flux grow along the dark space. This exponential growth leads to the initial breakdown starting the discharge. The occurring hysteresis shown in figure 1.2 are due to the initial breakdown conditions of the discharge.

The increasing density of fast electrons leads to a bright region close to the cathode, the *negative glow*. In this region ionization and excitation of the gas is enhanced. In order to fulfill the conditions as present in the following positive column the fast electrons have to be dissipated and the electric field has to drop. Thus the electrons first loose their energy due to collisions and are then re-accelerated in the weak field. The acceleration length is approximately their mean free path. The resulting dark region is called *Faraday dark space*.

The conditions in the *positive column* are quite similar to the conditions in the ones in the bulk plasma. The electric field balances the energy loss due to ionization and excitation. The axial uniform plasma is sustained by a weak electric field.

Since the electron drift velocity in the weak electric field of the positive column is smaller than the thermal electron velocity an electric field is needed to prevent the thermal electrons from hitting the anode. This region is called *anode fall*. It has a double layer structure since the anode has to be positive with respect to the positive column in order to sustain the current.

[3]The Crookes dark space is also called cathode fall or cathode sheath.

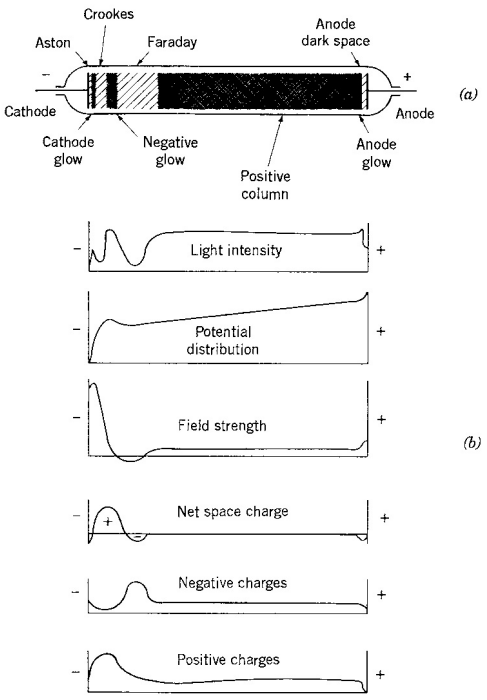

Figure 1.1: The different regions (a) in a DC glow discharge and the distribution of the fields and space charges(b), [128].

The remaining regions do not determine the behavior of the discharge and will not be discussed here. Any interested reader might read the according sections in Refs. [128, 174] from which also the information on the described regions has been taken.

In addition the characteristics of the discharge as a whole depend on the applied current. The established voltage depends on the pressure. A typical distribution for a pressure of 1 Torr ($\approx$ 133 Pa) is shown in figure 1.2. At low currents the glow discharge slowly builds up. Beneath I_A the discharge is called Townsend or dark discharge. At intermediate currents ($I_A < I < I_B$), where the slope of the distribution is negative, the normal glow establishes. This is the region in which most of the low temperature experiments are performed. It is followed by the abnormal glow ($I_B < I < I_C$) before the voltage drops suddenly and the plasma is called arc discharge.

DC discharges however are not always as uniform as discussed above. In the positive column regions of higher and lower emission intensity can occur. The brighter regions are called striations [100, 130, 216]. The striations form if electrons loose energy due to collisions with neutrals leading to regions of increased electron density. The increase in the electron intensity leads to higher electric fields and thereby a (re-)acceleration of electrons. The number and elongation of the striations depends on the applied current. The higher the current the more striations occur. The formation of striations is enhanced by lower energy loss in the collisions followed by an earlier establishing of the necessary excitation energy. Due to the distribution of the initial electron energy the dark and bright

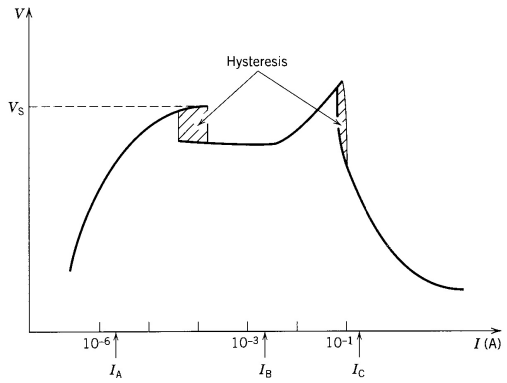

Figure 1.2: The graph demonstrates the U-I characteristics of a DC discharge, [128].

regions of the striations are sharply divided. The typical triangle or round shape of the striations is caused by a focusing effect. That the striations reach out to the walls is due to radial electron diffusion. The electrons far from the center experience weaker fields and need longer distances before having reached the energy necessary for excitation. Thus, the distances between the striations off-center are wider. Often moving or instable striations are observed, leading to a smearing of the glow.

RF Discharges

A plasma can also be induced by applying an alternating current to a gas-filled volume. The usual alternation frequencies are 13.56 and 81.6 MHz. Hence these plasmas are called radio frequency driven plasmas or RF plasmas. If the current is applied to one or two planar electrodes the discharge is called *capacitively coupled*. The choice of exact excitation frequencies is due to availability of industrial generators. In principle any RF current can be employed to induce a plasma with similar properties.

To excite and ionize gas atoms or molecules energy has to be delivered to them. In case of capacitively coupled RF discharges this is mainly due to two processes: *ohmic* and *stochastic heating* [128]. In a rather simple model in the bulk plasma the energy is transfered by electron-neutral collisions. This is called ohmic heating. In contrast to this the momentum transfer in the sheath is mainly due to the alternating high electric field. The process is therefore called stochastic heating [162].

Due to their higher mobility electrons react to the alternating electric field. In contrast to this ions can only react to time integrated potentials. Thus the electron density can be considered to be constant in the bulk plasma and zero in the sheath. This assumption is only true if the electron temperature is much lower than the potential across the sheath resulting in an electron Debye length much shorter than the time averaged sheath width. The ion density is almost constant over the whole volume. Furthermore the electric fields among the electrodes can be assumed constant neglecting phenomena such as the skin effect [128].

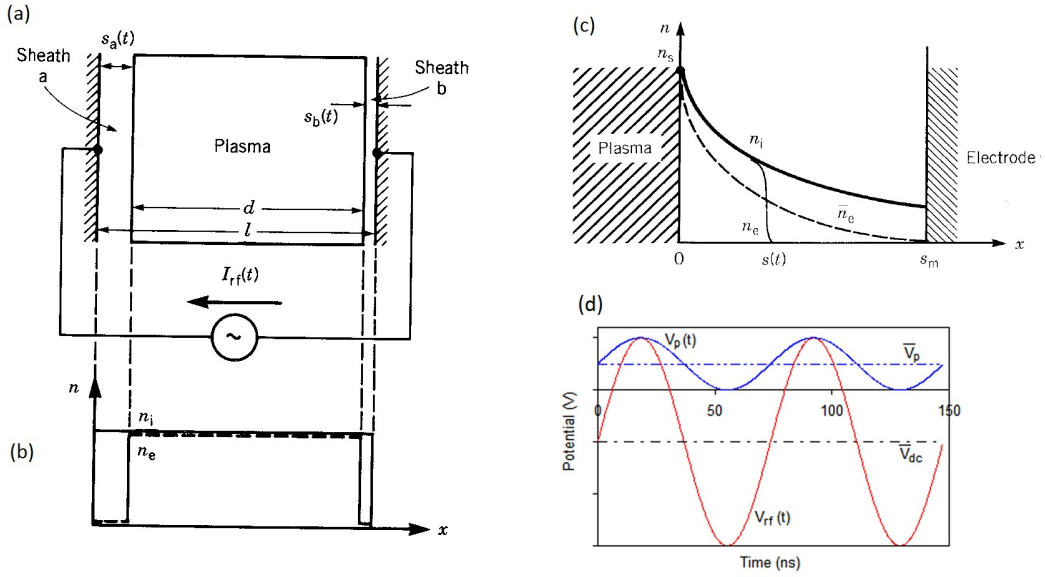

Figure 1.3: Sketch of a radio frequency driven plasma(a). Plot (b) displays the distribution of the electron and ion density along the plasma and the sheath, [128]. Next to it a more realistic distribution of the electron and ion densities in the sheath is given. This figure is reproduced from [127]. Furthermore, the development of the applied RF voltage V_p, the resulting plasma potential V_p, the corresponding time average $\overline{V_p}$, and the self bias $\overline{V_{dc}}$ is shown,[71].

A sketch of the situation in a RF discharge is shown in figure 1.3(a). The sheath that forms next to the powered electrode (left hand side) is usually bigger than the one that forms next to the grounded plate (right hand side). In between the two sheaths the quasi-neutral bulk plasma forms. Since the electron mobility is high enough to follow the electric fields the electrons will stay in the central region of the plasma whereas the slower ions penetrate into the sheath region. An ideal representation of this is shown in figure 1.3(b), [128]. A more realistic picture of the ion and electron density as well as the space averaged electron density in the sheath is shown in figure 1.3(c), [127]. Several simulations of the electrons passing through the volume between two electrodes including their density, temperature, and impact on the carrier gas have been conducted, [71, 212].

The strong potential difference between the electrode and the plasma results in a bias voltage which can be measured on the electrode. The bias voltage depends on the plasma parameters. Thus, further information on the plasma state and change can be gained by measuring it over time [125]. The development of the RF voltage V_{rf} and the plasma potential V_p are displayed in figure 1.3(d), [71]. Furthermore, it shows the time averaged plasma potential $\overline{V_p}$ and the constant self bias $\overline{V_{dc}}$.

A radio frequency power cannot be applied without losses to the electrodes. Thus a matching network consisting of tunable capacitors and inductors is attached to the RF generator. With this matching network the power reflected and introduced into the plasma can be tuned. Furthermore, the attached generator can be protected from possible high

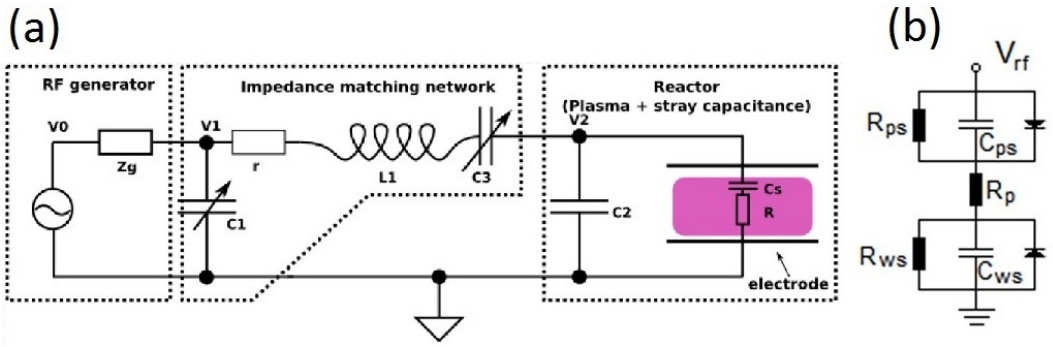

Figure 1.4: Sketch of the electrical network of a radio frequency driven plasma with the matching network (a), [214]. Panel (b) shows a more general electrical description of the plasma itself. In this the sheaths are equal to an array of a capacitor and a resistor whereas the bulk is represented by a resistor alone, [71].

currents. A scheme of the matching network as attached between a RF generator and a discharge chamber is displayed in figure 1.4(a), [214].

Electrically the plasma can be described as the neutral bulk plasma of almost infinite conductivity and two capacitors representing the sheaths. This is represented by the sketch in figure 1.4(a). Even if the electric plasma description displayed there might be correct for this special case, the description of the plasma (sheath and bulk) given in (b) is more general and accurate. The figures are reproduced from [214](a) and [71](b).

Another way of igniting a plasma is by using a coil wrapped around a gas filled volume. If a RF current is applied to the coil a magnetic field is induced. The magnetic field is then responsible for the ionization and acceleration of ions. Since this method induces electromagnetic fields a chamber operated in this way is called *inductively coupled*.

1.4 Plasma Chemistry

Depending on the neutral gas mixture and the plasma parameters a lot of different chemical reactions occur in plasmas. Some of these processes are endothermic, others exothermic. The energy delivered by the plasma enables all of these processes. Thus depending on the applied power the probability of a process and thereby the concentration of certain species can be influenced. It is important to note that some reactions are reversible while others cannot be undone. This is of special significance if a desired species shall be produced.

Two reactions have to be distinguished: those in the gas phase and those including the surfaces. In both cases dissociation, ionization, and attachment lead to new molecules. This is especially true if the plasma is not run by using a pure noble gas but in air or in a composition including portions of other gases such as acetylene or methane. Etching rate, occurring anisotropies, and composition depend on the concentration and energy distribution amongst the species in the plasma.

In the *gas phase* the main reactions are initialized by electron excitation, ionization,

and dissociation:

$$e^- + AB \rightarrow AB^+ + 2e^- \qquad \text{ion-electron pair production} \tag{1.12}$$

$$e^- + AB \rightarrow A + B^+ + 2e^- \qquad \text{dissociative ionization} \tag{1.13}$$

$$e^- + AB \rightarrow A^* + B^* + e^- \qquad \text{radical production} \tag{1.14}$$

$$e^- + AB \rightarrow A^- + B \qquad \text{negative ion production} \tag{1.15}$$

Due to vibrational and rotational modes auto dissociation

$$AB^+ \rightarrow A + B^+ \qquad \text{or} \qquad A^+ + B, \tag{1.16}$$

auto ionization

$$AB \rightarrow AB^+ + e^- \qquad \text{and} \tag{1.17}$$

auto detachment after endothermic negative ion production

$$A^- \rightarrow A + e^- \tag{1.18}$$

can occur. In case the ion production is exothermic the electron is not probable to detach from the ion again. Electrons can also be removed from negative ions by dissociation. The collision with another electron or any other particle can lead to detaching the electron from the negative ion leaving a neutral atom or a radical.

In addition, to the processes involving electrons chemical reactions in the gas phase are common:

$$A + B \rightleftharpoons C + D \tag{1.19}$$

These do not necessarily take place until the total amount of initial molecules (here: A and B) is transformed. According to the chemical energies necessary to produce either combination a chemical equilibrium will be reached in which usually all four components are present in the plasma.

Reactions including atoms from the surrounding *surfaces* are exclusively exothermic. Only if energy is delivered to the surface atoms can be released (etching / sputtering). The reversed reaction (deposition) may be endothermic, too.

$$A(gas) + S(surface) \rightleftharpoons A : S(gas). \tag{1.20}$$

Several consecutive reactions might be necessary for some of the very general reactions introduced above. In some cases even catalysts may be necessary. Similarly the presence of certain molecules or atoms may inhibit otherwise common reactions.

All of the chemical reactions given above are taken from Lieberman *et al.* [128]. In this book a more complete list of chemical reactions in the gas phase and on the surface including the thermodynamic properties and bond dissociation energies is given. According to the tables given there the probabilities of the occurrence of certain species can be calculated depending on the initial gas composition and supplied power.

1.5 Probing Plasmas

Gaining informations on what is going on in a plasma is very important with respect to controlling and reproducing certain conditions. In this section several probing methods will be introduced and discussed. The most preferable ones are the non-intrusive ones, but as it will be shown the information gained by these are not sufficient for complete plasma characterization.

As mentioned above the electron temperature and density strongly influence the plasma emission. Hence optical measurements are performed investigating the intensity and energy levels of the emission. This method does not deliver absolute values but provides comparative measurements. Here the change in electron temperature and density can be monitored instantly and without changing the plasma properties. In addition the composition can be estimated by monitoring the specific atomic excitation lines. As described in the section above the gas composition might strongly be affected over time. Thus, the surveillance by optical means provides a very effective way of controlling the ongoing chemical reactions. This can be supported by measurements with mass spectrometers both, before and behind the plasma volume.

Furthermore, light transmission and absorption spectra can be recorded. These are gained by mounting a laser of a specific wavelength and recording the transmitted and absorbed spectra. The changes in energy (i.e. frequency) and intensity carry informations on the plasma parameters.

Other, non-intrusive methods are external electric measurements. The applied voltage and the reflected portion can be monitored by means of oscilloscopes. In case of RF plasmas the self bias can be of interest, too. This is the continuous voltage formed at the powered electrode due to the presence of the plasma, see figure 1.3.

Getting absolute, but admittedly very rough, values for the plasma parameters (e.g. plasma potential, ion and electron density and temperature) intrusive probes have to be employed.

One of the easiest ways is to introduce artificial particles of known size and mass and monitor their behavior in the plasma [15, 135, 186]. In order to make optical observation of such particles levitated in a plasma as easy as possible the most common choice are plastic (usually Melamineformaldehyde) particles with radii of several micrometer. Their properties and other possible particle choices will be discussed in section 2.

Particles introduced into a plasma charge up. Being levitated in the sheath where the electric field balanced gravitation the thickness of the sheath can be probed by introducing particles with different radii and mass. Note, that the particle charge might substantially vary with sheath penetration depth. Next to the sheath thickness the dust plasma frequency, possible confinements, and electric fields can be probed by introduced particles. Please note, that an exact knowledge of the particle properties (size, mass, charge) are of crucial importance for any of these experiments. As it will be discussed in the following chapter the particles are not completely mono disperse and inherit thus a distribution in size and mass. Also, since they are subjected to a highly reactive environment, see subsection 1.4, their mass and radius might shrink or increase over time. Possibilities and

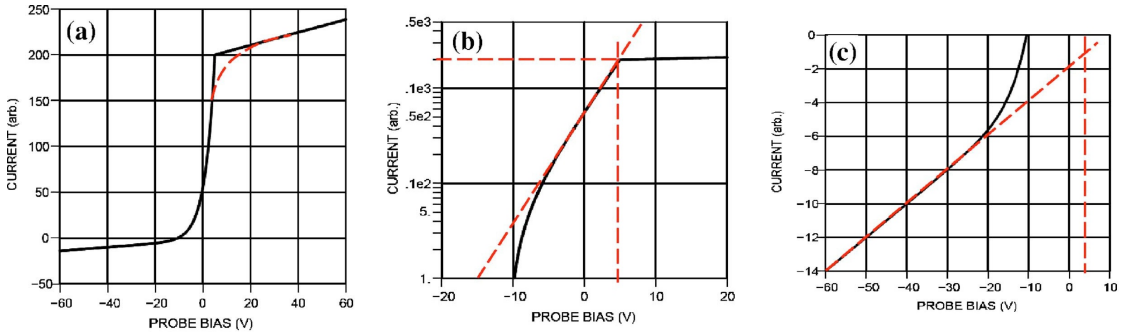

Figure 1.5: An ideal I-U characteristic for a low temperature plasma. (a) displays the total electron current towards the probe. The red dots indicate a rounding of the saturation current due to noise. Panels (b) and (c) show extended regions of special interest of this curve. From the plot shown in (b) the plasma potential and the ion saturation current can be deduced. From (c) the ion saturation current can be extrapolated. The figure is taken from [143]

limitations of calculating the particle charge will be discussed at length in the following sections. Further descriptions of the particles in question as well as their production, interactions, and applications in experimental studies will be discussed there, too.

Another intrusive measurement is the usage of so-called Langmuir probes [161]. In principle a Langmuir probe consists of a small wire to which a voltage is applied and the corresponding current is measured.

If the probe is introduced it is exposed to ion and electron fluxes. The theory describing the fluxes towards and the formation of a sheath around the probe are quite similar to the one for the charging of introduced particles (see section 2.2), [27, 43, 161]. But since the Langmuir probe is biased electrons and ions can be attracted or repelled depending on the applied voltage [143]. The resulting I-U characteristic is shown in figure 1.5.

In figure 1.5(a) the total electron current towards the probe is displayed. If the bias voltage on the probe is negative electrons are repelled. Thus the resulting current is negative. In figure 1.5(c) displays exactly this region. From the distribution there the ion saturation current can be gained.

As the bias voltage increases so does the electron current until a situation of electron saturation is reached. This is shown in the extended section displayed in figure 1.5(b). In experimental conditions the knee at which the current is saturated is smeared out, indicated in figure 1.5(a) by the dashed red line. The voltage corresponding to the electron saturation current is the plasma potential V_P.

From the saturation currents the ion and electron density can be obtained by

$$I_{i,e} = \frac{1}{4} e n_{i,e} v_{Ti,e} A_{probe}. \tag{1.21}$$

The slope of the curve leads to the electron temperature using

$$T_e = \frac{V_2 - V_1}{ln\left(\frac{I_2}{I_1}\right)}, \tag{1.22}$$

where $V_{1,2}$ are two voltages with $0 < V_1 < V_2 < V_p$ and the corresponding currents $I_{1,2}$, [143].

Langmuir probe measurements are mainly performed in the bulk plasma. In a situation of quasi neutrality the given equations provide values which are correct within an order of magnitude. This situation being already bad, it is worsened in the sheath where the electric field might be anisotropic leading to rather complicated electron and ion currents. Furthermore, particles and Langmuir probes alike change the plasma properties significantly.

Thus, probing plasmas is a big issue to which no very clear solution can yet be given.

1.6 Summary

Ionized gases are called plasmas. Plasmas occur in several environments next to which they are employed in laboratory setups for scientific, industrial, and medical purposes. They can be discriminated by the degree of ionization and the ion kinetic energy. Throughout the experiments conducted for this thesis low temperature plasmas have been employed. Likewise plasmas are usually produced by applying alternating or continuous voltages to a gas filled volume at pressures ranging from several Pascal up to atmospheric pressures. In the central part of the discharge ions and electrons are of almost equal density, leading to quasi-neutrality and thereby very high conductivity. Between this bulk plasma and the surrounding walls a strong electric field - the sheath - builds up. The fast electrons do not penetrate the sheath, whereas the ions slowly drift outwards. This accounts for the different density profiles. The resulting potentials can be probed by monitoring several different plasma parameters such as the emitted light, the electrical properties, or the chemical composition. As it is explained in the following chapters, particles can be employed as probes, too.

1.7 Résumé

Les gaz ionisés sont appelé Plasmas. Ils peuvent être rencontrés dans différentes conditions et utilisés tant dans le domaine scientifique de la recherche que dans les secteurs industriel et médical. Il est possible de les classer selon le degré d'ionisation ou la température électronique. Ainsi, dans le cadre du travail de recherche entrant dans le cadre de cette thèse nous avons mis en uvre un plasma froid. Les plasmas sont générés décharge électrique en appliquant aussi bien une tension continue qu'alternative à un gaz, contenu dans une enceinte de volume donné, à une pression pouvant aller de quelques Pascals à la pression atmosphérique. Dans le milieu plasma la densité des ions positifs est égale à celle des électrons assurant ainsi la condition de quasi-neutralité et une grande conductivité électrique. Entre le plasma et toutes les surfaces en contact s'établit un champ électrique (les gaines de charges d'espace) qui va confiner les électrons et permettre aux ions de dériver lentement vers les parois. Il en résulte ainsi une différence entre les profils des densités de

ces espèces dans les gaines. Il est par conséquent possible de sonder le potentiel dans ces zones en suivant l'évolution de certains paramètres tels que l'émission lumineuse, les propriétés électrique de la décharge ou la composition chimique du milieux. Comme expliqué dans les chapitres de la thèse il est possible d'utiliser les particules comme des sondes à cet effet.

1.8 Zusammenfassung

Ionisierte Gase werden Plasmen genannt. Neben den natürlichen Vorkommen werden Plasmen in Laboren zu wissenschaftlichen, industriellen und medizinischen Zwecken verwendet. Eine Klassifizierung kann anhand des Ionisationsgrades und der kinetischen Energie der Ionen vorgenommen werden. In der vorgestellten Arbeit wurden Experimente in Niedertemperaturplasmen durchgeführt. Solche Plasmen werden normalerweise in einer mit Gas gefüllten Kammer durch Anlegen von alternierendem oder konstantem Strom erzeugt. Im Zentrum der Entladung sind die Elektronen - und Ionendichte etwa gleich, was zu quasi-Neutralität und damit hoher Leitfähigkeit führt. In der Plasma Randschicht baut sich ein starkes elektrisches Feld auf. Die schnellen Elektronen dringen nicht in diese Randschicht ein, während die Ionen nach aussen driften. Das ist der Grund für die Dichteverteilungen. Der Potentialverlauf kann durch Messungen verschiedener Parameter, wie das emittierte Licht, die elektrischen Parameter, und die chemische Zusammensetzung, ermittelt werden. Wie in den folgenden Kapiteln dargestellt, können auch Teilchen zu diesem Zweck verwendet werden.

Chapter 2

Particles in Plasmas

2.1 Particles

Plasmas containing particles are called complex or dusty plasmas. Due to their interactions particles levitated in a plasma show a variety of different motions and arrangements that resemble in many cases the ones of bound atoms or other phenomena observed in nature. Hence complex plasmas provide a unique possibility for interdisciplinary studies as well as for fundamental research [68, 159, 196].

Particles can form in plasma environments either by introducing special gases such as acetylene and methane or by etching material previously introduced into the chamber, e.g. carbon-covered electrodes [8, 146] or particles from earlier experiments [28]. Pictures of grown particles are shown in figure 2.1, [19, 37]. One can clearly see the cauliflower like surface structure of the particle in figure 2.1(a) and the more even surface structure of the particle in figure 2.1(b). The grown structure depends on the composition of carbon, hydrogen, and oxygen. The non-diamond, diamond, and no growth regimes can be displayed by a C-H-O phase diagram, as it has been shown by S. C. Eaton and M. K. Sunkara [58]. The growth process and the different possible surface structures are described in greater detail in section 3.

Instead of growing particles one can introduce them artificially into the plasma. The most common material of the introduced particles is Melamineformaldehyde (MF). The mono disperse plastic spheres were originally used to calibrate scanning electron microscopes. A picture of MF particles is shown in figure 2.2(a). In some cases particles made from other materials are of use. Depending on the desired effects hollow glass spheres and particles made from Polystyrol (PS) are employed. The main reason to employ hollow glass spheres instead of plastic particles is their increased radius to mass ratio. Particles made from other materials, e. g. silica particles, are mainly employed due to their reduced etching rate or fluorescent properties. A picture of the hollow glass spheres is shown in figure 2.2(b). It can be seen that these particles are not quite as mono disperse as the MF particles in 2.2(a). To overcome this problem the particles are filtered by using several meshes of different grid sizes, refining the particle size distribution.

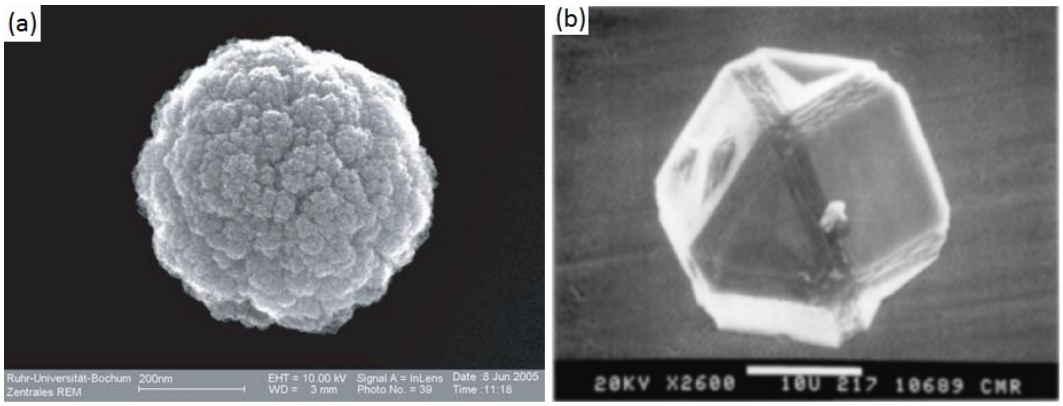

Figure 2.1: Two different grown particles. (a) Picture of a particle grown in a gas mixture of acetylene in argon. The surface shows the typical cauliflower structure, [19]. (b) Picture of diamond grown in a hydrogen / methane mixture, [37]

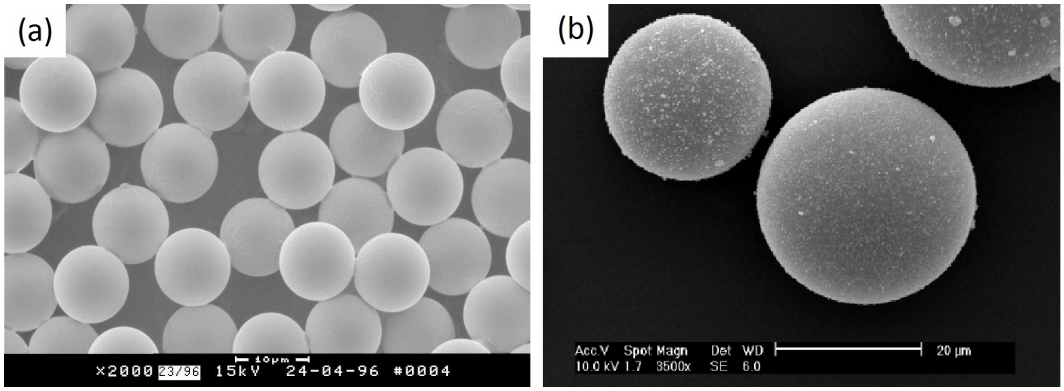

Figure 2.2: Pictures of two different kinds of artificial particles taken by means of a scanning electron microscope (SEM): Melaminformaldehyde (MF) particles (a), [83], and hollow glass spheres (b), [120]. Note, that the scales in both pictures are very similar.

Particles introduced into a plasma can get etched and material can be deposited on their surface. A picture of a MF particle with smaller particles grown on its destroyed surface as observed during the experiments on dust particle growth is shown in figure 2.3. The zoom allows to show only a small portion of the original MF particle. Thus, the whole field of view is basically showing a zoom on the particles surface. As it can be seen holes as well as additional bumps occur. The holes are a result of etching the particles surface under the influence of oxygen plasmas. The bumps are particles growing from acetylene. Note the difference in surface structure between the MF and the grown particles. Similar surface growth has been observed if employing a magnetron for sputtering aluminum [99].

However, the particle displayed in figure 2.3 is an exception. Usually deformations of the surface are very small compared to the particles diameter and of no importance in this and the following chapters.

A more serious problem is due to the etching rate. Particles introduced into a plasma

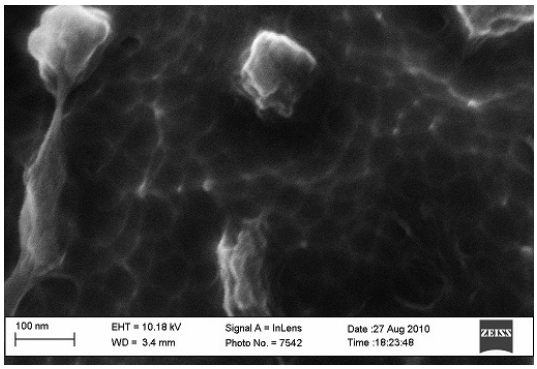

Figure 2.3: A picture of a MF particle which has been exposed to several plasma runs in a DC discharge. Due to the high zoom only a small fraction of the original particle can be seen (compare figure 2.2 for complete view on several MF particles). Some of the plasma runs were performed using oxygen. Hence the particles surface is being etched. During other runs acetylene was employed to trigger particle growth. It can be seen that on the disturbed surface some new particles grew.

are etched/sputtered. This depends strongly on their position and might even vary for particles being levitated at the same height. No further study on this matter has yet been performed and the effect will be neglected in the following discussions.

It has been shown that particles introduced into a vacuum loose mass due to out gassing of water [70]. This is especially true for particles introduced into a plasma. The loss due to the loss of water is substantial. In order to collect the least water amount possible outside the plasma the particles are kept in dry chambers. Also the particle dispensers later installed to introduce the particles are kept there if not in use. In order to reduce the impact of this effect on the experiments the particles are usually introduced into the plasma some time before the experiment is started. However, as mentioned above they are not to be left there too long due to the reduction caused by anisotropic etching.

For most experiments the initial distribution of mass and size among the introduced, almost mono disperse, particles is more prominent then any gain or loss during the experiment.

2.2 Charging

In *isotropic* plasmas, e.g. the bulk plasma, the electron thermal flux is higher than the one of ions. Once particles are subjected to a plasma their charge increases until the ion and the electron flux towards the particles are balanced. As a result a stationary surface potential Φ_s forms. This potential provides a barrier from which electrons are reflected. Thus, the negatively charged particles are surrounded by a region depleted of electrons.

The *orbital motion limited (OML)* approximation describes the charging of particles in collision-less plasmas. It is based on three assumptions [3, 68, 161]:

- The dust grains do not interfere with the electrons and ions in the vicinity of other

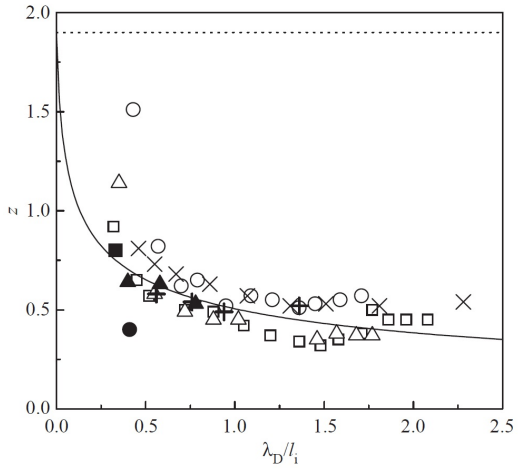

Figure 2.4: The prediction of OML, represented by the dotted line, compared to several simulation and measurements on the particle charge, [68].

dust grains: The dust grains are isolated.

- In the vicinity of the particles the electrons and ions are assumed to be collision-less.
- No barriers are present in the effective potential.

These three assumptions allow to calculate the cross section for electron and ion collection from the conservation of energy and the angular momentum. The cross section is independent from the plasma potential around the probe but depends on the surface potential Φ_s. With the Maxwell equations the fluxes towards the particle can be calculated. Once the fluxes towards the particle are equal the charge is constant. However small fluctuations around this value are to be expected [51, 156, 185, 208].

For small particles ($r \ll \lambda_D$) the vacuum relation

$$Ze = r\Phi_s \tag{2.1}$$

is a suited particle charge approximation [68].

As the OML theory is an assumption its compliance with real experiments has to be discussed. In figure 2.4 the result from different experiments and simulations are compared to the predictions of the OML theory (dotted line), [68].

Determine the charge experimentally is tricky, since the particles are bound by many electromagnetic forces and the interaction with other particles in the plasma. Furthermore, it has been shown, that the particle charge is affected by the particle levitation height as well as the interaction with other particles [41, 122].

However, several different methods exist to measure the charge including using hyper [18] and micro gravity environments [101, 220], particle collisions [67, 112], vertical resonances [39, 40, 41], oscillations [93], and the particle speed [65].

Some of the results from these determinations are displayed in figure 2.4. The actual values differ very much from the one predicted by OML. This is mainly due to three reasons:

1. Finite Dust Density
   The dust levitated in a complex plasma contributes to the quasi-neutrality of the system.
   $$n_i = n_e + |Z|\, n_d \tag{2.2}$$
   with n_d being the grain number density carrying an intermediate charge $|Z|$. Thus the ratio of ion to electron flux on the particle is increased leading to a reduced particle charge. This is described by the Havnes parameter [78]:
   $$P = |Z|\, \frac{n_d}{n_e}. \tag{2.3}$$
   The particle charge is the one of an individual particle for $P \ll 1$ and reduced for $P < 1$.

2. Barriers in the Effective Potential
   Ions streaming towards a negatively charged particle are attracted. However, the angular momentum of the ions leads to a repulsive centrifugal potential. The interplay between these forces can lead to a reflection of low energetic ions. Thus, the flow of ions towards the particle is reduced and the particle charge increases [95].

3. Collisions
   Ions collide with electrons and neutrals. While the electron-ion collisions can be neglected, ion-neutral collisions can lead to an ion energy reduction. These ions, being attracted by the negatively charged micro particles, are trapped in the vicinity of the particle or even fall onto their surface. In addition, further ions can be produced by ion-neutral collisions. This increases the ion flux towards the particle. The combination of these effects reduces the particle charge [176].In the collisional regimes the calculation of charge is different as for instance shown by Khrapak *et al.* [104].

Other effects such as thermionic emissions, photoelectric emissions and secondary electron emissions influence the particle charging [68].

Due to the limitations of OML theory several other charging models have been developed [2, 76, 224, 227] to solve the problems listed above.

In the *anisotropic* plasma regions, e.g. sheath, presheath, and striations, the electric fields dominate the plasma behavior. For this regime no self-consistent analytic solution exists. However, some approximations can be done. Due to the electric field the ion drift is large compared to the electron drift and the charge is determined by the ion velocity [7]. If approaching the electrode positive space charges build up in the sheath where
$$\frac{n_i}{n_e} > 1. \tag{2.4}$$
Thus, if particles penetrate deep into the sheath their particle charge approaches a maximum before it decreases. Very close to the electrode the ion flow becomes dominant and the particle charge should finally be positive [191]. Particles can then no longer be levitated and are accelerated towards the electrode.

2.3 Forces

Particles levitated in a plasma are influenced by several different forces. The different forces and the possibility of additional confinements will be discussed in the following.

In normal[1] ground based experiments *gravitation* is present at all times. For particles of certain mass[2] it dominates over all other forces in the bulk plasma.

$$F_G = m_d g \tag{2.5}$$

The particles are levitated in the sheath where gravitation and electric forces are in equilibrium. Hence the *electric force* is of high importance in ground based experiments

$$F_E = ZeE. \tag{2.6}$$

Due to the plasma polarization in the vicinity of a particle corrections to the electric field have to be introduced [53]. Close to the particles the magnitude of the electric field increases, leading to a dipole moment along the direction of the field. In contrast, the electric field is reduced due to plasma shielding in the Debye sphere. The effect of plasma polarization can thus be neglected for most of the experiments.

Several possibilities exist to overcome gravity. One can use small particles which will be kept levitated above the sheath. If however bigger particles are necessary in the experiments micro gravity conditions have to be employed. To dispose of gravity sounding rockets, drop towers, parabolic flights, and the International Space Station (ISS) are accessible.

Additionally the levitation of particles above the sheath can be achieved by heating or cooling the electrodes introducing a thermal gradient resulting in an asymmetry in the momentum transfer of the neutrals [182]. The *thermophoretic force* is always directed towards the lower gas temperature:

$$F_{th} = -\frac{4\sqrt{4\pi}}{15}\frac{r^2}{v_{Tn}}\kappa_n \nabla T_n, \tag{2.7}$$

with κ_n being the thermal conductivity coefficient and ∇T_n the temperature gradient [182].

The different temperatures introduce inhomogeneous flows into the plasma. Interesting phenomena such as shear flow [80] and thermal creep [153] are the consequence. Of course likewise inhomogeneities are disturbing experiments and cannot replace micro gravity environments.

[1] The term 'normal' is employed in this case to emphasize that the experiments in question are performed in a lab without any special means to reduce gravity such as parabolic flights or drop towers.

[2] The particle mass at which the levitation level and the behavior will not be dominated by gravitation anymore depends on the plasma parameters. In most cases the influence on particles with a diameter of less then 2 μm will be negligible. This is especially true for grown particles. To reduce the mass while increasing the particle radius glass hollow spheres are employed. However their mass is too big for them to stay levitated in multilayer systems without additional confinements. This will be discussed in sections 7 and 8.

Since plasmas are governed by ions and electrons the momentum transfer of both towards the particle have to be considered. Due to their small mass the *electron drag* is neglected in most cases.

$$F_{ed} = m_d \gamma_{de} u_e, \tag{2.8}$$

with γ_{de} being the momentum transfer rate from electrons to particles [68].

The *ion drag force* however, is considerable even though in usual low temperature plasmas the number density of ions is much lower than the number density of neutral gas atoms. The momentum transfer from ions to particles is mainly due to two processes [195]:

1. Direct Ion Impact or Collection of Ions
   In this case the ions hit the dust particles, transferring momentum by mechanical interaction. Assuming that the ion - dust cross section is equal to the cross section during charging the resulting transfer can be described by:

$$F_{id}^{coll} = \pi r_d^2 n_i m_i u_i \sqrt{v_i^2 + \frac{8 k_B T_i}{\pi m_i}} \left(1 - \frac{2e\Phi_s}{m_i u_i^2}\right). \tag{2.9}$$

2. Coulomb Interaction
   Here the momentum is transfered by electro - static ion - particle interactions. Ions with large drift speeds compared to the ion thermal speed cannot form a sheath around a negatively charged particle. The Debye sphere around a particle is therefore best described by a region of low electron density. Consequently the ion drag force due to Coulomb interactions can be calculated by:

$$F_{id}^{coul} = 2\pi r_d n_i m_i u_i \alpha \sqrt{u_i^2 + \frac{8 k_B T_i}{\pi m_i}} ln \left(\frac{(r_d\alpha)^2 + \lambda_{De}^2}{(r_d\alpha)^2 + (r_d\sqrt{1-2\alpha})^2}\right), \tag{2.10}$$

   with

$$\alpha = \frac{e\Phi_s}{m_i u_i^2}. \tag{2.11}$$

The complete ion drag force is a combination of the two processes:

$$F_{id} = F_{id}^{coll} + F_{id}^{coul}. \tag{2.12}$$

One of the most prominent examples of the ion drag force acting on the particles is the formation of the void in the bulk under micro gravity conditions [52, 77, 124, 129]. The void describes a dust free region in the center of the discharge. As it has been discussed in the previous chapter ions are moving towards the confining (grounded) walls. Thereby they introduce an outward acting force on the dust particles. An example of the void is shown in figure A.1.

The momentum transfer from neutrals to the dust leads to the *neutral drag force*:

$$F_{nd} = -m_d \gamma_n u_d. \tag{2.13}$$

It depends on the particle mass, the relative particle velocity u_d and the neutral damping (momentum exchange rate) [60]

$$\gamma_n = \delta \frac{8\sqrt{2\pi}}{3} \frac{m_n}{m_d} n_n v_{Tn} r_d^2. \tag{2.14}$$

The neutral damping rate depends on the mass, number density, and thermal velocity of the neutrals and the mass and radius of the dust particles. Dependant on the collision type the Epstein coefficient δ varies between 1 (specular reflection) and $1 + \pi$ / 8 (diffuse reflection) [60]. Several experiments have been performed determining the Epstein coefficient. In the following the results of measurements by Konopka [111], showing that $\delta = 1.48 \pm 0.05$ in case of MF particles levitated in an argon plasma at room temperature, are going to be used in the calculations.

Please note that these estimations of the neutral drag force are only valid if the mean free path of the neutrals is big compared to the particle radius and if the velocity of the particles is well below the thermal velocity of the neutrals. In the low temperature plasmas discussed throughout this thesis this can be assumed to be the case. If the particles move much faster than the neutrals the friction is in the form of Stokes friction [200].

In some cases the neutral gas friction can be neglected or easily subtracted while post processing the data. However, it can render certain experiments difficult or even impossible as well as being an important effect in others.

Additional forces, such as for instance magnetic or electric fields, can be applied to manipulate the plasma and the particles therein. The shape of the confinement resulting from the shape of the plasma chamber can be changed by introducing objects such as glass cylinders [92, 118, 110], metal bars or by drilling holes into the electrodes [112]. Especially additional confinements only influence the plasma and the particles in their close vicinity. But since in most cases the behavior under the changed conditions is of special interest the observation tools are usually adjusted to match the extension of the additional confinements.

2.4 Particle Interactions

As described above particles levitated in a plasma carry certain (usually negative) charges. Thus, they are entitled to interact with each other as well as with the surrounding plasma and potential additional electromagnetic forces. Since the particles are all like-charged they repulse each other[3].

Towards all particles a constant flow of ions is present. The ions approach a particle from all sides. If however two particles are fairly close to each other they disturb the ion flux and shadow each other from the streaming ions.

[3]Note, that in case of very small particles (≈1 nm) the charge fluctuations lead to a situation in which the mean overall charge can be assumed zero. In this case the particles repulse as well as attract each other.

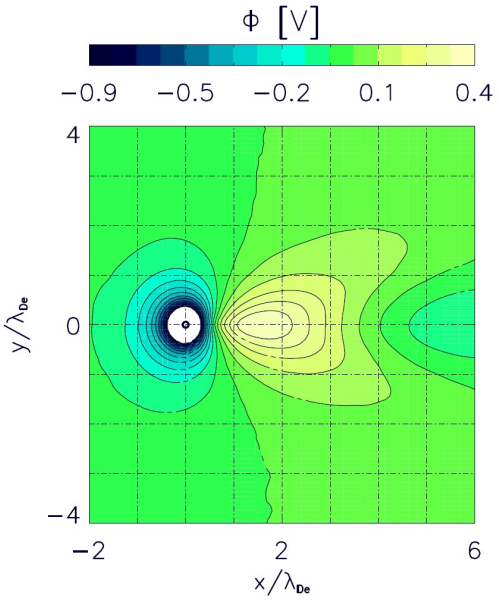

Figure 2.5: Wake field as it forms downstream a particle situated at (0,0). In this plot the ions stream from the left to the right. Downstream the negatively charged particle a positive potential forms. This is the so-called wake field which attracts other negatively charged particles and is responsible for string formation, [151].

Similar to the ion shadowing the neutrals can be shadowed by particles, as proposed by Fortov *et al.* [66]. If the gas temperature is smaller than the particle surface temperature the neutral shadowing force would be repulsive. In the opposite case the force is considered to be attractive. The proposed attractive shadowing force could then overcome the repulsive electrostatic force at large distances.

The particle charge is determined by the flux of electrons and ions towards it. Due to the higher electron mobility they usually carry negative charges in the order of several thousand electron charges depending on their size. Around each particle a positive space charge (Debye sphere, see figure 2.6(a)) with a radius of the ion Debye length builds up. Thus, the interaction of particles in the bulk plasma are best described by screened Coulomb (Yukawa) interaction [159, 196].

The most important inter particle interaction in this thesis besides the screened Coulomb (Yukawa, see equation (1.6)) interaction is the wake field potential. Ions streaming past the inserted particles deform the Debye sphere around the particle. Downstream the particle the ions are focused, introducing a positive wake potential [91, 122, 123, 151, 199]. The shape of the wake field is shown in figure 2.5 as it has been taken from [151]. This non-reciprocal positive potential does not comply with Newtons third law leading to a situation in which the system can no longer be described by a Hamilton equation [34, 98, 108].

The positive wake potential forms behind any negatively charged particle in a streaming plasma. But, it has also been observed if the particles move in the plasma. Thus, it can re-accelerate electrons in particle beam accelerators. In these facilities the plasma is ignited

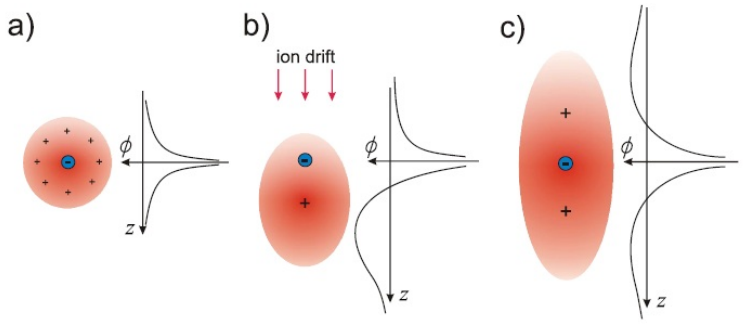

Figure 2.6: The potential distribution around a particle without any field (a), with the deformation due to the streaming ions (b) and in a time averaged reciprocal form due to an alternating electric field (c). This graphic is taken from [95]

either by strong lasers or by preceding electrons or ions [23].

The positive potential that forms downstream the particle attracts other negatively charged particles. Particle ensembles can form vertical strings [110, 122, 123], lanes [13, 95] or internal structures in clusters [92, 118] in response to the wake. Due to shadowing effects the charge of the lower particle is reduced. Thus, the focusing effect of the wake, depending on the particle charge, is reduced, too. This leads to an increase in the inner-string inter particle distance along a string. Charge depletion has been observed in particle clusters [22, 118] as well as in single strings [40, 41].

Since the wake field forms exclusively downstream the particle [22, 122, 139, 151] it is not reciprocal [107]. However, there exist possibilities to introduce a reciprocal deformation of the positive wake potential [33, 35, 95, 98]. In order to achieve this an alternating current with frequencies lower than the ion plasma frequency (see Equation 1.10) but higher than the dust plasma frequency[4] has to be applied. A like-wise alternating electric field will have an impact on the ions but does not change the particle positions [34].

The time averaged deformation of the wake field in response to an electric field is displayed in figure 2.6 (c), [95]. It is compared to the non - distorted Debye sphere (a), as it usually occurs in the bulk plasma, and the deformation as in response to ions streaming past a negatively charged particle (b), as it usually occurs in the sheath region where the electric fields are very strong, [95]. It can be seen that in difference to the usual deformation caused by ions streaming only in one direction past the particle the wake potential is symmetric in case of applying an (additional) alternating current.

If an alternating electric field is applied to a particle cloud an orientation along the electric field axis is observed [95, 98]. The resulting system is called an *'electrorheological plasma'*[5]. Similar situations have earlier been observed in colloids [192, 178, 217]. Next to the alternation of orientation by electric fields comparative results can be gained by applying magnetic fields. A corresponding system is called magnetorheological system

[4]The dust plasma frequency is defined analogue to the ion and electron plasma frequency given in Equation 1.10.

[5]A picture of an observed electrorheological plasma is displayed in figure 6.1

[211]. In line with the results from experiments on colloidal suspensions with electric fields alternating not only in one but in more dimensions (in-plane [133] and spherical rotating electric fields [170]) have been proposed.

Due to the tunable viscosity and electric and magnetic properties the advantages of likewise systems can be used in medical as well as in industrial applications[45, 171, 198, 222].

Electrorheological systems differ from other systems with orientated dipoles. For instance the magnetic dipoles in unordered ferro magnetic systems are stochastically orientated but present if no external field is applied. Once such a magnet is subjected to a magnetic field the internal dipoles are orientated along the external field axis. However, the dipoles are never as perfectly aligned as in electrorheological systems. Furthermore, the dipoles are introduced by the additional field and not present before [34].

In electrorheological plasmas a particle and the positive wake potential behind it form a dipole. These dipoles are, due to the additional electric field, perfectly aligned. Thus the isotropic interaction potential (usually Yukawa interaction) has to be extended by an anisotropic potential due to dipole-dipole interaction, leading to the time averaged potential [34]:

$$V(r,\theta) = \Phi_i - \xi\Phi_a P_2(cos\theta). \tag{2.15}$$

In this equation ξ gives the relative strength of the anisotropy. The anisotropic potential scales with

$$\Phi_a \propto \frac{M_T^2}{r^3}. \tag{2.16}$$

The angular distribution is best described by the Legendre polynomial

$$P_2(cos\theta) = \frac{3}{2}cos^2\theta - \frac{1}{2}. \tag{2.17}$$

It is an exact description if the dipoles are perfectly aligned along one well defined axis. If this is not the case Equation 2.15 will only describe the first approximation of the interaction potential.

As it has been shown by Kompaneets *et al.* [109] the isotropic interaction potential Φ_i changes depending on the thermal Mach number:

$$M_T = \frac{\text{Ion Drift Speed}}{\text{Ion Thermal Velocity}} = \frac{u_i}{v_{Ti}}, \tag{2.18}$$

Depending on the surrounding plasma the Mach number varies. In the bulk plasma, for instance, it is close to zero, whereas it increases in the sheath, where the ions are accelerated towards the electrode or the confining walls. If the thermal Mach number equals zero the isotropic potential is described by Yukawa interaction, if it equals one the best approximation is a Lennard-Jones potential:

$$\Phi_{LJ} \propto \left(\frac{\sigma}{r}\right)^n - \left(\frac{\sigma}{r}\right)^m, \tag{2.19}$$

with $\sigma \propto \lambda_D$. In figure 2.7 the particle interaction for increasing Mach numbers is given. To the curves displayed there a 6-12-Lennard-Jones potential (n = 12 and m = 6) has been

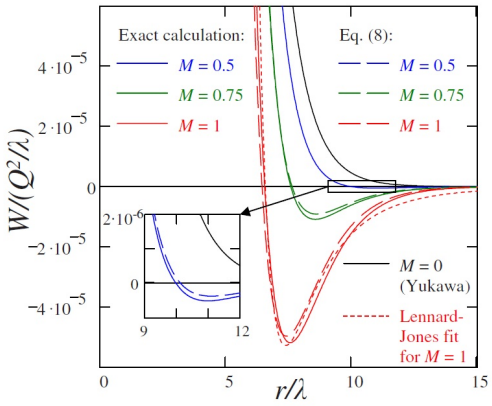

Figure 2.7: Isotropic interaction potential for different Mach numbers [109].

fitted. A like-wise potential is often employed to describe the interaction potential between two atoms. It can be seen that even the isotropic interaction potential has an attractive part if the thermal Mach number is high enough [13, 109].

In the horizontal plane, parallel to the electrodes, the interaction is not dominated by the wake field effect but by an interplay of attractive and repulsive forces. In ground based experiments negatively charged particles of sufficient mass[6] levitate in the sheath at the height where the electric field balances gravitation. Assuming that further introduced particles are of the same mass and size as the initial one they will all carry the same charge[7] and be therefore levitated at the same height in the plasma sheath. Due to their charge, the electrostatic confinement, and their interaction potential these particles tend to organize themselves in 2D lattices. To describe the particle behavior a coupling parameter describing the ratio of the interaction potential and the kinetic particle energy can be introduced [88, 209]. If the kinetic particle energy is samller than the potential energy the system is called strongly coupled. Furthermore the occurring patterns in the particle arrangement (phase transitions) can be predicted by the coupling parameter. The more the interaction potential of neighboring particles exceeds the kinetic energy, the higher is the ordering in the system. Such ordered systems (2D plasma crystals) have been observed by Thomas *et al.* [204, 205], Chu *et al.* [46], and Hayashi *et al.* [79]. In further studies different crystalline structures as well as phase transitions have been observed in 2D and in 3D systems [50, 86, 103, 106, 167]. If the wake field is not changed a particle downstream a layer of other particles is situated in the center of the particle configuration upstream. Thus, the most common 3D crystal arrangements are fcc (face centered cubic) and hcp (hexagonal closed packed) structures, [86].

[6]Very small (light) particles will be distributed homogeneously over the plasma. This behavior can be introduced also by using thermophoretic forces or by micro gravity experiments as for instance in drop tower experiments, parabolic flights, or on board the ISS.

[7]The charge and size distribution among the particles has at length been discussed above. However, for the following considerations particles of a certain parameter are assumed to have equal mass and size. If a situation is encountered in which the error made by this assumption is considerable this will be mentioned.

2.5 Summary

Several different types of particles can be formed or artificially introduced into a plasma. The resulting system is then called a dusty or complex plasma. In the plasma particles are subjected to electron and ion fluxes. Due to the higher electron mobility the particles tend to charge up negatively. Thus, the particles are subjected to several different forces caused by gravitation and electric fields as well as by impacts of neutrals, ions, and electrons. Furthermore, additional forces can be introduced such as thermal gradients or electromagnetic fields. Around each particle a positive space charge, the so-called Debye sphere, forms, leading to a screened coulomb inter-particle interaction. If positive ions stream past a negative particle they are focused depending on the ion velocity. This leads to a deformation of the Debye sphere. Furthermore, the Debye sphere and thereby the particle interaction potential can be manipulated by additional fields.

2.6 Résumé

Plusieurs types de particules peuvent être synthétisées ou injectées dans un plasma. Le système qui en résulte est dénommé "Plasma poussiéreux" ou "Plasma complexe". Dés leur formation ou injection, les particules sont soumises aux flux des électrons et des ions arrivant à leur surface. A cause de la grande mobilité des électrons, comparée à celle des ions plus massifs, la charge acquise par les particules est négative. Elles sont par conséquent soumises à différentes forces liées au champ gravitationnel, au champ électrique, aux collisions avec les espèces neutres, les ions et les électrons présents dans le milieu plasma. Il aussi possibles de les soumettre à d'autres forces telles celles liés à des champs électromagnétiques ou à des gradients de température (thermophorèse). Chaque particule est entourée d'une gaine de charges d'espace positives, appelée sphère de Debye, qui écrante le potentiel électrique généré par la charge qu'elle porte et ainsi affecte l'interaction entre particule. Selon leur vitesse, des ions positifs peuvent être déviés, et focalisés, par leur interaction avec les particules. Cela se traduit aussi par la déformation de la sphère de Debye. Ainsi, la sphère de Debye et par voie de conséquence l'interaction entre particule peut être modulée à l'aide de champs additionnels.

2.7 Zusammenfassung

Verschiedene Teilchen können in Plasmen erzeugt oder eingefügt werden. Das resultierende System wird als "komplexes" oder "staubiges" Plasma bezeichnet. Im Plasma sind die Teilchen einem Flußvon Elektronen und Ion- en ausgesetzt. Die höhere kinetische Energie der Elektronen führt zu einer negativen Ladung auf den Teilchen. Die geladenen Teilchen im Plasma sind verschiedenen Kräften, verursacht von Gravitation, elektrischen Feldern und dem Impulsübertrag von neutralen Teilchen, Ionen und Elektronen auf das Teilchen, ausgesetzt. Des Weiteren können zusätzliche Kräfte durch thermische Gradienten oder externe elektromagnetische Felder eingebracht werden. Um jedes negativ geladene Teilchen

baut sich eine positive Raumladung, die sogennante Debye - Kugel, auf. Das führt zu einer abeschirmten Coulomb - Wechselwirkung (Yukawa - Wechselwirkung) zwischen den Teilchen. Wenn die positiven Ionen an den Teilchen vorbeiströmen werden sie fokussiert. Dadurch verändert sich die Form der positiven Raumladung. Diese, und dadurch die Teilchenwechselwirkung, können durch externe Felder beeinflusst werden.

Chapter 3

Dust Particle Formation

3.1 Introduction

Dust particles in plasma environments have first been studied in astrophysical environments [156, 202, 215], explaining planetary and star formation in nebulae from dust forming in the surrounding plasma [57]. Later on particle formation has been discovered in plasma processing before it became a major field of research [28, 32, 62]. Especially during the production of silicon chips and solar cells, dust damages the processed material rendering it useless for the dedicated purpose. In addition, the presence of particles in fusion devices causes problems [218]. Much later the use of formed particles and their benefits have been discovered. Nowadays the controlled deposition of dust is a useful tool as for example in producing thin films [90, 219], nano-tubes [28], or super hard nano-composites [210].

To trigger particle formation certain molecular species are needed. Very common is the employment of carbon-rich molecules by either introducing a corresponding precursor gas (e.g. acetylene ore methane) or by etching previously introduced materials[1]. Growth has not only been observed from carbon based material but also from silane [19, 213] and from metallic materials, leading for instance to the deposition of titanium [99]. It has been shown that the three stepped growth process is independent from the initial material employed [19, 28, 31, 113, 114, 115].

The radial growth by accretion of molecules is considered to be linear [19]. Due to the usual experimental conditions particles reach a limited size before they are no longer confined at the initial place of formation and a new generation forms [28]. The new generation occurs at the initial point of formation [19]. Since the process and timing of the growth in each generation is the same for all the particles a very narrow size distribution is expected.

Growth has been observed in different plasma conditions such as RF (e.g. refs. [29, 149, 19]), DC (e.g. refs. [8, 163, 194]), arc (e.g. ref. [184]), and microwave plasmas (e.g. ref. [173]). The maximal observed particle sizes depend on the plasma parameters and the

[1] In the laboratory experiments these are mainly MF particles [148], but also electrodes made from carbon can be employed [145].

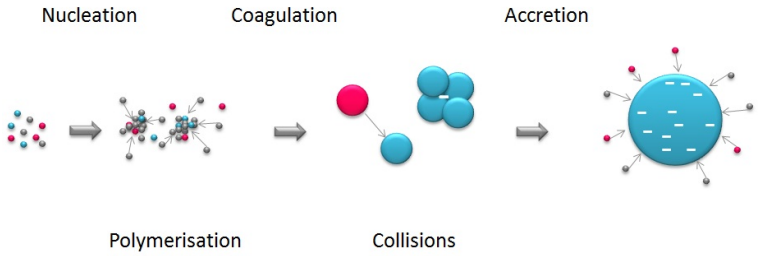

Figure 3.1: The different stages during particle growth.

plasma run time. The particle diameters vary from nanometers to micrometers.

The pressures in RF plasmas range from several Pascal up to atmospheric pressures. As in low pressures triggering the growth is the main challenge, igniting plasmas becomes problematic at atmospheric pressures, where delivering the necessary ionization energy is challening. In such conditions many experiments in air are performed, since for instance medical devices are operated in air. Particle formation in atmospheric pressure plasmas is therefore an interesting topic [155, 160, 221, 225].

Under micro gravity conditions experiments on the particle growth in plasmas have been performed, [148]. However, due to their low mass and the big particle amount (respectively density) grown particles tend to be homogeneously distributed among the plasma and behave in ground-based experiments quite similar to injected particles under micro gravity conditions. For instance the formation of a dust free region (void) in the central region can be observed. The void is not stable and shows different kinds of instabilities, such as periodic contractions [49, 149].

3.2 Growth Process

3.2.1 General

Particle growth is in principle divided into three stages: Nucleation, Coagulation and Accretion, [19, 28, 30]. A sketch to illustrate the three stages is shown in figure 3.1.

In addition to particle formation film production upon the surrounding surfaces has been observed. It has been found that the film production takes more time than the particle formation in the bulk plasma [19]. Films occur on surfaces and form due to the deposition of protoparticles on the surface [32, 90, 219].

3.2.2 Nucleation

The nucleation process describes a plasma chemical reaction during which the molecules inside the plasma are dissociated by electrons and polymerize afterwards [28, 75, 87, 164]. In general this can be divided into two steps: *initiation*, during which primary ions, excited molecules and radicals are formed, and *propagation*. In the second step the activated

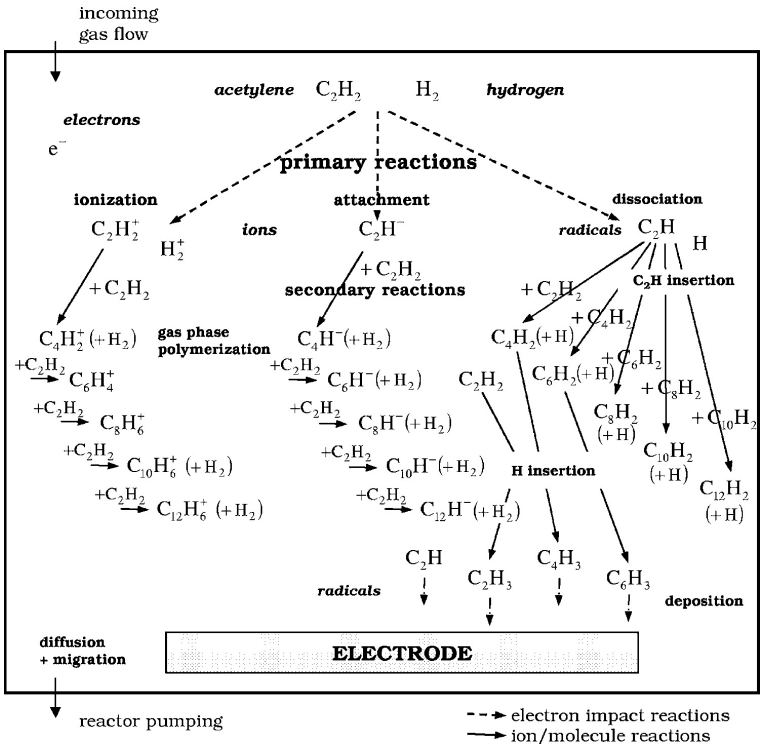

Figure 3.2: Chemical reactions during nucleation. They are caused by association, dissociation, ionization, and attachment, [54]. Further possible reactions leading to similar results can be found e.g. in ref. [54, 128, 201].

molecules[2] bond with other species (activated and not activated molecules) in the plasma. The newly formed bigger molecules than undergo the same process of initiation and propagation. This leads to the formation of so-called protoparticles [63, 201]. The nucleation of dust is due to avalanche condensation and can therefore also be triggered by introducing material into the plasma [116, 223].

During nucleation particles of several nanometer in diameter form. Since it is mainly a chemical reaction the particles are molecules of random charge. Positively, negatively charged molecules as well as neutral radicals exist. These protoparticles are chains as well as rings and are produced as long as the original species is present in the gas volume.

As discussed in section 1.4 several different ions and radicals form in the plasma. Their role during polymerization depends on their density and formation probability. Thus nucleation can be influenced by the plasma power, composition, gas temperature, and pressure. It has been found, that the most important role in triggering particle formation is due to negative ion production [19, 44, 54, 87]. Different possible chemical reactions are discussed e.g. in refs. [19, 28, 54, 116, 121, 201]. Possible reactions taking place due to dissociation, ionization, and attachment are displayed in figure 3.2, [54]. Note, that the reactions displayed here are only one possibility out of several (some of equal probability) that lead to

[2]Molecules in this context are described as activated if they are either ionized, excited or a radical.

comparable results.

3.2.3 Coagulation

In difference to nucleation coagulation is dominated not by chemical reactions but by physical effects. The protoparticles collide with each other forming mainly negatively charged particles of several tens of nanometers in diameter [28, 29, 168, 177, 201]. The coagulation can be described by the general dynamic equation for aerosols [19, 113]. From it the particle number density depending on the particle size and its development (loss and gain in density of particles with a certain size) due to coagulation can be deduced. It has been found that the coagulation process is much faster for charged particles than for neutrals [19]. As discussed in the previous section the protoparticles carry random charges. The collision probability is therefore increased with respect to a situation in which the particles carry the same charges. The growth rate during this phase is very high while the particle density is rapidly decreasing in time. Particles formed during the stage of coagulation are already negatively charged. Their size is of the order of several tens of nanometers in diameter.

3.2.4 Accretion

In the last step of the formation the particles grow in size by collecting positively charged ions and radicals from the plasma. The molecules attracted from the plasma are those produced during both steps of nucleation. The bigger the particles get the more negatively they tend to be charged. Assuming that the growth during this stage is mainly due to radicals the radial growth is considered to be linear [19].

$$\begin{aligned} \frac{dm_d}{dt} &\propto n_{radicals} r_d^2 \qquad \text{mass growth rate} \\ \frac{dr_d}{dt} &= const. \qquad \text{radial growth rate} \end{aligned} \tag{3.1}$$

If after this stage the particles are observed by means of a scanning electron microscope (SEM) a typical cauliflower structure for particles grown from carbon rich environments appears [116]. In addition the size distribution of the particles is almost mono disperse since the particle charging is as fast as the coagulation process [19]. The observed micro structures are seen as a hint that accretion of particles happens rather by ballistic deposition than by diffusion limited aggregation [72].

3.2.5 Generations

The grown particles are subject to the forces in the plasma. The growth always (re-) starts at one particular region in the plasma. This is where the active molecules can be trapped. If the particles reach a certain size they will be pushed away from the place of formation by (external) forces. As the charge carried by a particle scales with its radius the

particles are influenced by the ion drag. Thus, the ion drag, acting outwards, pushes the particles out of the center of the discharge. The resulting particle free region is called the void. It has especially been observed under micro gravity conditions, where the particles are distributed (almost) homogeneously among the bulk plasma. A picture of the void is shown in figure A.1. If the particles reached a size (charge) large enough to be pushed out of the central region of the chamber by the ion drag their mass is still relatively small. Thus, they act very much like particles under micro gravity conditions. Since the particles keep growing in size even after being removed from their initial place of formation they can reach a size (mass) at which they are affected strongly by gravity.

Depending on the geometry, plasma excitation mechanism, and gas composition the particles can then even fall out of the plasma instead of only being pushed away from the place of formation.

A second generation grows in the now empty place of initial formation until they are pushed out, too. This behavior is observed for any further particle generation. Thus, particle growth is (usually) periodic. However, under certain circumstances only a limited amount of generations (or even only a single one) are observed. This can be influenced by the choice of the carrier gas, power, pressure, and gas composition.

3.3 Influence on the Plasma

Besides changing the plasma chemistry (e.g. by depletion of certain gas components) the plasma parameters are strongly influenced during the formation process. The power absorption, the sheath properties, the density of excited states, the electron temperature and density, as well as their spatial distributions can change [9, 28, 31, 85, 214].

Particles in a plasma tend to charge up negatively. The negative charge is explained by the higher electron mobility. As it has been discussed the particle charge is constant once the electron and ion flux towards the particle are in equilibrium. If the particles carry mostly negative charges the plasma is depleted of electrons, which equals a reduction of the electron density. To compensate for these losses and to sustain the discharge the electron temperature increases[3]. Since the heating in the bulk plasma depends on the electron density this leads to an increased power consumption in the bulk and thereby to a change in the sheath size [55]. The plasma change has also been reported on in the case of introduced particles [6].

The correlation of the electron density and the dust particle growth in a Ar/C_2H_2 plasma is displayed in figure 3.3, [116]. The results of a Fourier transform infrared spectroscopy are correlated to the measured electron density. It can be seen that if the dust is present the electron density is rather low. If the particles are grown to a certain size the plasma is not capable to compensate for gravity anymore and the particles are removed

[3]The explanation of the resulting increase in the electron temperature can also be discussed the other way around: As the collision cross section of electrons and particles decreases with increasing electron energy mainly the low energetic electrons participate in the charging. Thus only the high energetic electrons remain in the vicinity of the particle.

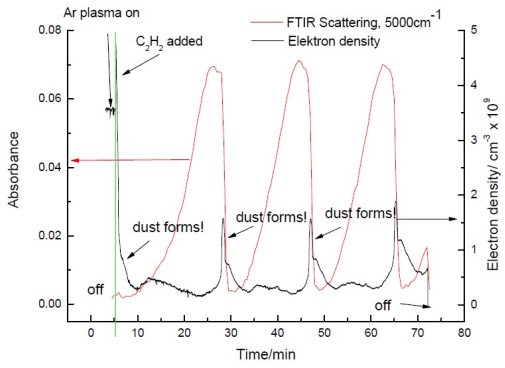

Figure 3.3: Electron density during particle formation in an Ar/C_2H_2 mixture. The green line marks the time the acetylene is added to the plasma resulting in immediate particle formation. The particle presence is seen both by the change in the absorbency of the plasma (red) and the drop in the electron density (black). Fourier transform infrared spectroscopy (FITR) is a very common method to observe particle formation. If the red curve increases the particles increase in size. As soon as it drops the particles have reached a critical size and are removed from the active volume, [116].

from the discharge. Once this happens the electron density increases, accompanied by a new generation of particles.

While new molecules are formed the initial ones are transformed. Thus, during the process of nucleation the precursor gas is depleted. Furthermore, the carrier gas is affected by the growth. In RF discharges an influence on atomic lines at the example of the Balmer alpha line of Hydrogen has been observed [55].

3.4 Influence on the Growth

As mentioned above particle growth can be triggered in many different environments. If portions of a highly electronegative gas such as oxygen are introduced into the plasma the particle formation can be inhibited. This is very useful for instance to clean the plasma chamber after having performed experiments. However the reactions of the particles and films consisting mainly of carbon or other inflammable components with the introduced oxygen may lead to undesired side effects.

Most of the experiments are performed by using noble gases as carrier gas. Due to the full outer shell the ionization energies of these are rather high. The growth characteristics differ depending on the carrier gas. For instance no periodicity in the growth has been observed if a He/C_2H_2 mixture is employed rather than a Ar/C_2H_2 mixture. A difference between the first and every further cycle has been observed in every gas composition. This is mainly due to the initial precursor gas (e.g. acetylene, methane, or silane) concentration. If the same precursor gas is introduced heavier molecules are found to be formed in argon-based mixtures than in helium-based ones. This combined with the observation of higher

amount of carbon double bonds in helium-based mixtures is the reason for the absence of further generations [116]. If no noble gas but for instance nitrogen is employed as carrier gas much faster growth has been observed. This is due to the difference in the ionization energy and might also indicate an alternate way of polymerization [116]. The observation of growth in nitrogen-based mixtures is of high interest since it also resembles the atmosphere of Titan [89].

In addition to the gas composition the temperature of the surrounding walls and thereby the neutral gas temperature can be changed. Changes in the neutral gas temperature can accelerate or inhibit the growth as it has been shown by refs. [17, 62]. Furthermore, also the structure and polymerization of the particles can be influenced by the temperature [201].

As mentioned above the surface structure can be influenced by the choice of the initial gas, see e.g. figure 2.1. Changing the surface structure can influence particle properties such as charging and interaction. Thus, the electrical as well as optical and mechanical particle properties can be manipulated by tuning the gas composition and the plasma parameters [28].

Several studies on the chemical properties of the particles indicate that the molecular structure is another property that can be addressed by the plasma parameters [116]. For example several experiments are conducted trying to grow diamond like structures and films from carbon based portions in the plasma [10, 12, 37, 90, 219].

3.5 Summary

Particle growth experiments have successfully been conducted in several different plasma environments. The formation process can be divided into three steps: nucleation, coagulation, and accretion. During the first stage proto-particles of several nanometer diameter are formed by ionization and polymerization. These proto-particles cluster due to collisions in the second step. They reach sizes of several tens of nanometers and carry mainly negative charges. Finally the particles acquire further molecules and positive ions from the plasma. Thereby sizes of up to several micrometers in diameter can be established. Even though the general process is independent of the origin of the initial molecules, the particle properties can be manipulated by plasma parameters such as power, pressure, and gas composition.

3.6 Résumé

Des expériences de croissance de particules ont été menées avec succès dans différents environnements plasmas. Le mécanisme de leur croissance s'effectue en trois phases: la nucléation, l'agglomération et l'accrétion. Dans la première phase, des particules primaires de quelques nanomètres de diamètre se forment grce à la dissociation et la polymérisation. Ces dernières s'agglomèrent par collisions durant la second phase pour atteindre une taille

moyenne de quelques dizaines de nanomètres et une charge électrique négative qui augmente avec leur taille. Puis, durant la troisième phase, elles continuent de grossir par dépt moléculaire et d'ions arrivant à leur surface. Ainsi leur taille moyenne peut atteindre quelques micromètres dans certaines conditions. Bien que le mécanisme général soit indépendant de la nature de la molécule du précurseur, les propriétés des particules formées peuvent être modulées en faisant varier la composition chimique des gaz, la pression et la puissance électrique injectée.

3.7 Zusammenfassung

Wachstumsexperimente wurden erfolgreich in verschiedenen Plasmen durchgeführt. Der Prozess kann in drei Stufen unterteilt werden: Nukleation, Koagulation und Akkretion. In der ersten Stufe werden Proto-Teilchen mit mehreren nanometern Durchmesser durch Ionisation und Polymerisation gebildet. Durch Stöße werden aus diesen Proto-Teilchen in der zweiten Stufe hauptsächlich negativ geladene Teilchen. Zuletzt wachsen diese Teilchen in der dritten Stufe durch Anlagerung weiterer Radikale und Ionen. Dadurch können Teilchen mit einem Durchmesser von mehreren Mikrometern entstehen. Obwohl der Wachstumsprozess unabhängig von den usprünglichen Bedingungen ist, können die Teilcheneigenschaften durch die Plasmaparameter wie Druck, Leistung und Neutralgaskomposition beeinflusst werden.

Chapter 4

Particle Formation in a DC Discharge

4.1 Previous Experiments

As discussed in the previous chapter growth can be triggered in various environments. To start formation a sufficient amount of certain molecules and ions are necessary. In this chapter the focus will be on particle formation in direct current (DC) discharges. These differ from RF discharges in some major respects as it has been discussed in chapter 1. The ion bombardment on the surfaces in DC discharges is not as intense as in RF discharges. This leads to a situation in which initial production of active molecules and their confinement at some place inside the discharge are not obvious.

If however carbon covered electrodes are employed the flux towards the electrode is high enough to trigger particle formation as demonstrated by C. Arnas *et al.* [8, 26, 144, 145, 146]. They reported on mono disperse particles with diameters of several hundred nanometers after exposure times of about 30 minutes. More common is to employ additives of carbon rich gases such as methane [163, 194] and acetylene [154]. In case of employing a mixture of 2 percent methane in argon nanometer sized particles up to 1000 nm diameter during an exposure time of several hours were reported [163].

The experiments by S. Mitic *et al.* [154] demonstrated the investigation of particle formation in the RF field of PK-4 using a premixed gas of argon and acetylene (4 percent) by means of Mie scattering[1]. In these experiments at low pressures and low flow rates particle sizes of several hundred nanometers have been accomplished.

In terms of this thesis the growth in PK-4 using acetylene and the influence of the neutral gas flow will be discussed. The results of these investigations are discussed in the following sections. Some of the results that will be discussed here have previously been published, [MY1].

[1]Mie scattering describes the angular dependent light scattering with wavelengths comparable to the objects radius, [147].

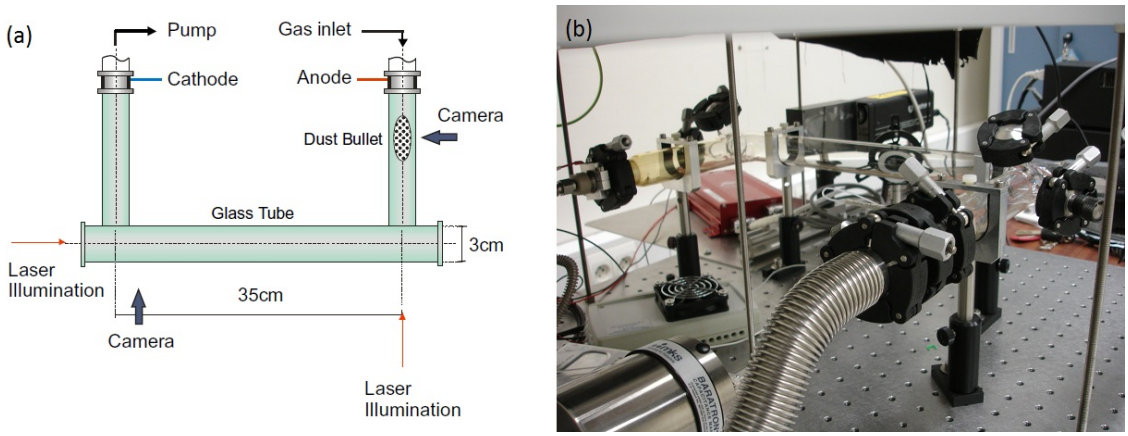

Figure 4.1: A sketch (a) and a picture (b) of the PK-4 setup as mounted at GREMI in Orléans.

4.2 Experimental Setup

The 'Plasma Kristall 4' (PK-4, [69]) experiment is the successor of PK-3 Plus [206] described in chapter 5. As such PK-4 will follow PK-3 Plus in operation on board the International Space Station (ISS) and allow experiments under micro gravity conditions.

PK-4 is a glass cylinder of 3 cm diameter and an overall length of about 71 cm. In order to save space it is bend into an u-shape. The sidearms have a length of 13 cm, the long central part has an overall length of 45 cm. At both ends hollow electrodes are mounted. Inside the electrodes small grids are installed. These grids prevent the plasma from penetrating into the gas line out of the observed volume. The grids are placed close enough to each other preventing a plasma to be ignited in between. Thus the distance is chosen according to the I-U characteristics which can be calculated by the so-called Paschen-curve [128].

One of the electrodes is grounded ('*passive electrode*') at all times whereas a constant current between +3 mA and -3 mA is applied to the other ('*active electrode*'). The maximal voltage reached is plus or minus 3 kV respectively. The current is set whereas the voltage arranges itself depending on the resistivity of the plasma. The gas is fed into the chamber through the active (powered) electrode and pumped out through the passive (grounded) electrode. A constant gas flow of up to 10 sccm[2] is possible. The pressures established during the experiments presented in this work range from 20 Pa to 150 Pa. Due to the hollow cathode design and the more fluid like behavior of the introduced particles[3] into PK-4 the growth in the DC field is triggered by using a premixed gas of argon and 2 % acetylene. In addition to the DC current an inductively coupled RF field can be applied by a coil wrapped around the cylinder. A sketch and a picture of the setup as used in

[2]Standard cubic centimeter per minute is a unit of flux. However, it does not give an estimate of the actual gas velocity which depends also on the tubes diameter, pressure, and the installed pump. The pump installed in Orléans is able to establish pressures of 20 Pa even at 10 sccm neutral gas flow, whereas the pump in Munich is not.

[3]For further experiments in PK-4 please see e.g. ref. [203]

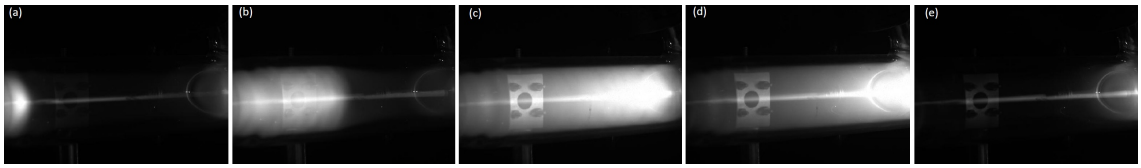

Figure 4.2: Growth as observed by a CCD camera. The particles emerge (a) from the anode (left hand side of the pictures) and move along the tube(b)-(e).

Orléans can be seen in figure 4.1.

During the preparation of this thesis particle growth in the pure DC field has been observed. The grown particles were illuminated by a laser (405 nm). The scattered laser light and the plasma glow has been recorded by a spectrometer and a CCD camera. In addition silicon wafers were introduced into the chamber to collect particles. The wafers are placed on the bottom of the glass tube and do not influence the plasma nor the particle growth. Particles re collected at three different positions: close to the active electrode, close to the passive electrode and in the central region of the tube. For the following discussions only the results gained from the wafer placed close to the anode are of interest. The collected particles are then investigated by means of a scanning electron microscope (SEM). As it will be discussed later the particles are kept in a sensitive equilibrium between the electric field and the neutral gas drag. If either one is removed the particles are transported along the other.

4.3 Results

4.3.1 Observation

The electron temperature and density are influenced by the formation of particles. An increase in electron temperature results in an increased intensity of the plasma emission. In figure 4.2 the change in the emission in the vicinity of the moving particle cloud is demonstrated. The particles are illuminated by a laser at 406 nm in the center region of the tube. If particles are present the laser light is scattered from the particles leading to a region of increased brightness in the center of the cloud. Note, that the particles are not illuminated by a laser sheet but only by a laser beam.

Another effect shown in figure 4.2 is the observed transport of particles along the tube after having reached a critical size. Note, that the particles move together in 'dust bullets'. This is an indicator for inter particle interactions, confinement of the cloud in itself, and mono disperse size distribution amongst the formed particles. It can be assumed that the particles keep growing while being transported along the tube. It is therefore preferable to collect particles not after the same time for the different settings discussed but at the same distance to the place of formation.

4.3.2 Particle Transport

The particle formation and transport can be manipulated by changing the neutral gas flow. If no flow is applied no particle growth has been observed. It seems that in this case the amount of acetylene is not sufficient to form particles that can be seen by the available means.

In case of low flow rates the particles grow in front of the active electrode (anode) and gain size without being swept along the tube. The neutral gas drag at these flow rates is not strong enough to overcome the electric field. Thus the particle radii increase linear in size as it is displayed in figure 4.7(a). Since in this regime no transport is observed it is going to be referred to as the *'static case'* throughout this chapter.

If increasing the flow the system passes into a regime of periodical behavior. In this case the formed particles are kept in balance between the electric field and the neutral gas drag and are transported along the tube if their size becomes too big to be captured in the equilibrium. Since the particle charge, and thereby the impact of an electric field, scales with the radius whereas the cross section of the neutral gas drag scales with the radius squared, the particles are transported along the neutral gas drag once they reach what is called a *'critical size'*. After the particles left the vicinity of the active electrode the next generation starts growing there. This regime, in which particles grow, reach a critical size and are transported away is called *'periodic case'*.

In between these two cases a transition occurs. In this transitional regime several growth cycles were observed before the growth stops. This is due to an insufficient amount of acetylene fed into the tube but a rather high flow. If switching on the discharge the initial acetylene amount in the chamber is high enough to trigger several growth cycles. But it is not enough acetylene delivered to the chamber to establish periodic growth. Thus, particle formation in this regime is neither static nor periodic.

At low flow rates possible turbulent flows and the confinement introduced by the glass walls may slow down the transport. This effect may also be responsible when it comes to the transition region in which some growth cycles have been observed before the amount of acetylene delivered to the chamber is too low to enhance further particle formation.

An example for each of the three cases is shown in figure 4.3. In all three plots the time evolution of the same three lines as observed by a spectrometer are shown: red (751 nm - plasma emission line), green (811 nm - plasma emission line), and blue (405 nm - scattered laser light). On the y-axis the measured intensity in arbitrary units is shown. Note, that while the y-axis is chosen to be the same, the time scales and the plasma on and off times are different in all three plots. In panel (a) the behavior at 2 sccm is displayed. After the initial growth the plasma emission and the scattered laser light stay constant over time. Panel (c) shows the periodic behavior as observed at 6 sccm neutral gas drag. In between the two the transitional case at 5 sccm is displayed. Several cycles occur before the growth stops and no further particle formation is observed.

The difference in the first peak observed in all cases is a very well known phenomena and is due to the higher initial amount of acetylene than provided during the later stages of the experiments [116].

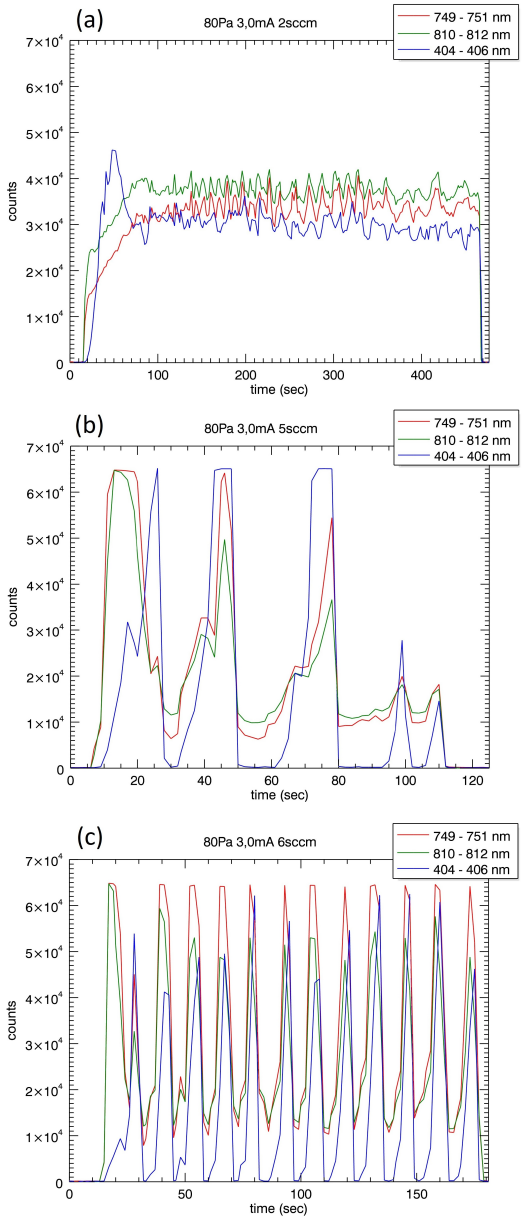

Figure 4.3: Three different behaviors of dust particle growth depending on the neutral gas flow. The particle presence is indicated by an increase in the scattered laser light (405 nm, blue line). It is set into relation to the emission intensity of two significant Argon lines (751 nm, red and 811 nm, green). (a) shows the static behavior at 2 sccm. (b) shows the transition stage at 5 sccm. (c) shows the periodic regime at a flow of 6 sccm. Please note that the switching on and off times are different at all four graphs shown here.

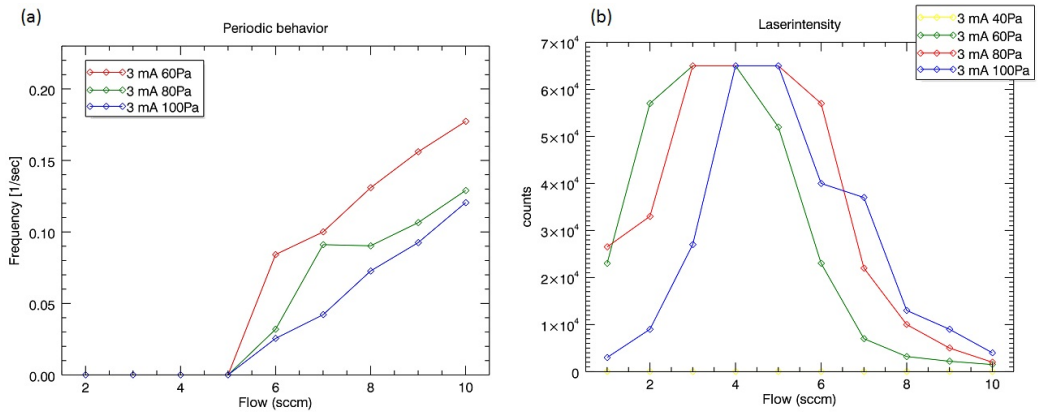

Figure 4.4: Growth cycle appearance frequency versus the neutral gas flow for three different pressures: 60 Pa (red), 80 Pa (green), and 100 Pa (blue) (a). The distribution of the scattered laser light intensity as a function of the applied neutral gas flow for four different pressures: 40 Pa (yellow), 60 Pa (red), 80 Pa (green), and 100 Pa (blue) (b).

To further illustrate this transition figure 4.4(a) shows the frequency of the growth cycles and is thereby also a measure of the growth rate. In this figure the frequencies as deduced from plots similar to those in figure 4.3(c) are shown for three different pressures. As the penetration depth of the inflowing gas increases with decreasing flow the transport velocity and thereby the frequency increases, too. Nevertheless, the *critical flow*, describing the flow at which the periodical behavior starts, is the same for all three pressures.

Even though some cycles appear at 5 sccm it is considered to have no frequency in the sense that the growth is not endlessly repeating itself. According to this argument all the measurements at lower flow rates are assumed to have zero growth frequency.

The higher the pressure the lower is the growth frequency. This is caused by the higher residence time and the increased neutral gas friction at higher pressures.

As it has been shown in figure 4.3 the intensity of the scattered light changes if the flow increases. It includes information about size, density and refractive indexes of the formed particles. The scattering cross section is proportional to the particle radius to the power of six [116]. To illustrate the change in the intensity figure 4.4(b) displays the distribution for all flow rates.

Starting from 1 sccm the intensity of the scattered laser light rises until the saturation of the spectrometer is reached before the periodic behavior starts at 5 sccm and the intensity decreases. It can be assumed that the particle size, being proportional to the scattered light intensity, first increases in the static case. As the spectrometer goes into saturation the information on further growth is lost. However, the particle size keeps increasing as long as the neutral gas flow stays below the critical flux. If the neutral gas flow exceeds the critical flow the particle size decreases. The higher neutral gas drag removes the particles at an earlier stage from the confinement in front of the active electrode. This is accounted for by the decrease of the scattered laser light intensity in figure 4.4(b). Again it can be seen that the situation depends on the pressure as well as on the gas flux. From the

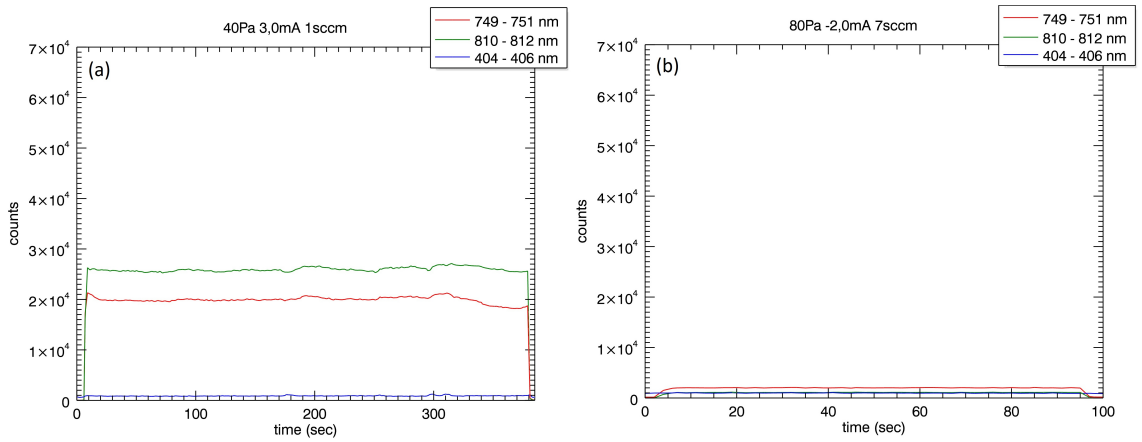

Figure 4.5: There are several situations under which no particle growth has been observed. One possibility is low pressure, as displayed in (a). The two plasma emission lines rise at the moment the plasma is turned on and decrease at the end when it is switched off. No change in the scattered laser light can be seen. In (b) the particle growth has been observed at 80 Pa. If compared with the earlier experiments (see figure 4.3) also the level of plasma intensity is low. This is a clear indicator that neither the plasma chemistry nor physics are influenced during the run. Hence no particle formation is triggered.

behavior of the scattered laser light it can be deduced that the particles have smaller radii at lower pressures. The reason for this is again the prolonged residence time and thus increased neutral gas friction at higher gas pressures. The lower the pressure the earlier the particles are transported along the tube by the neutral gas drag introduced by the constant gas flux.

4.3.3 Absence of Growth

Below 40 Pa no grown particles have been observed. A graph recorded during an experiment run at 40 Pa is shown in figure 4.5(a). The change in the plasma emission lines mark the plasma on time. But no change in the scattered laser light intensity occurs. Since also no observable change in the plasma emission is present it can be assumed that particles can form under the given conditions but that they are not kept in the discharge long enough to grow to a size noted by the spectrometer. These experiments have been repeated at different flow rates and powers. At higher flow rates a change in the plasma emission intensity can be measured indicating that growth in principle occurs the same way as in higher pressures.

If negative currents are applied to the active electrode no particle formation is observed. An example is shown in figure 4.5(b). The applied neutral gas flow in this case is 7 sccm. If applying a positive current to the active electrode periodic growth cycles have been observed. In addition, the intensity levels of the plasma emission lines stay very low. Therefore it can be assumed that the particle are not only too small to be seen (as in figure 4.5(a)), but that no particles are formed. Neither the plasma chemistry nor the

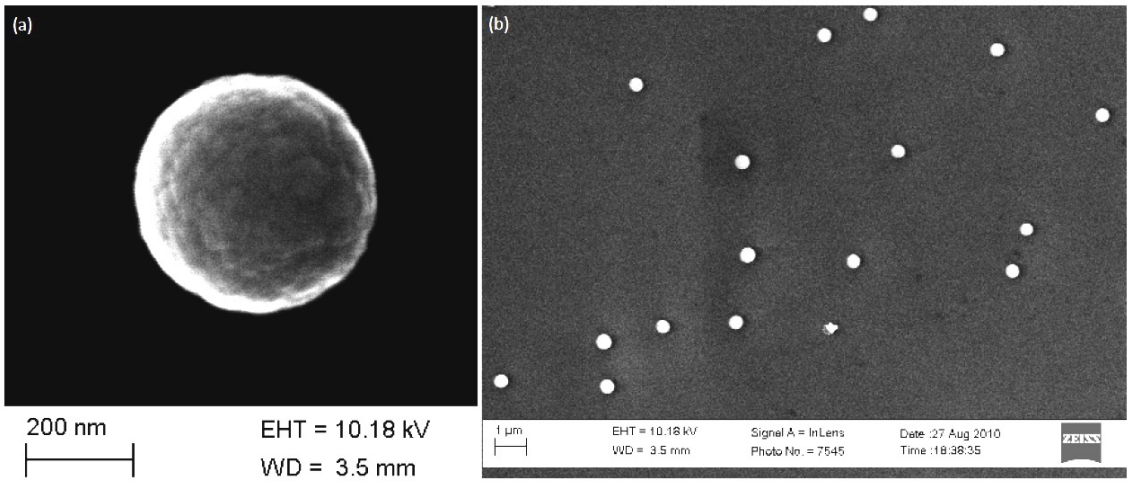

Figure 4.6: Two pictures taken by means of a scanning electron microscope (SEM). (a) is a single particle as grown at 80 Pa, 1 sccm, and 3 mA. Picture (b) demonstrates the mono disperse growth observed.

plasma physics are changed during the run, rendering the presence of dust very unlikely.

This can be explained by the force balance. In case of a negatively biased active electrode the electric field and the neutral drag force point along the same direction. Hence no place of trapping can be established. The molecules are not trapped and cannot form any protoparticles, the growth process cannot start.

Furthermore the trapping of molecules at the initial place of formation can be understood based on the lack of changes in the plasma emission, as displayed in figure 4.5. As shown in figure 1.1 a negative potential builds up in front of the anode. In this region the ion bombardment is higher than in any other region. Thus the acetylene molecules can be dissociated and kept there. If the pressure is too low too few and too small protoparticles are formed before being swept away. Thus the particles cannot be detected and no change in the scattered light intensity is observed. If negative currents are applied the molecules are not kept to be destroyed. Thus the plasma chemistry and therefore the emission does not change. Due to this argument it can be assumed that the particle growth starts in front of the powered electrode in case it is positively biased.

4.3.4 Scanning Electron Microscope Results

To follow on the periodic behavior as seen in figure 4.3 particle sizes at different flow rates were measured by means of a scanning electron microscope (SEM). Particles were collected on silicon wafers introduced into the glass tube. An example of collected particles can be seen in figure 4.6. The particle size distribution is mono disperse. A particle diameter of roughly 400 nm has been observed after running a plasma at 1 sccm, 80 Pa, and 3 mA. The exposure time in this case was 1 min. The cauliflower like surface structure resembles the commonly known structure of particles formed in carbon rich environments [116].

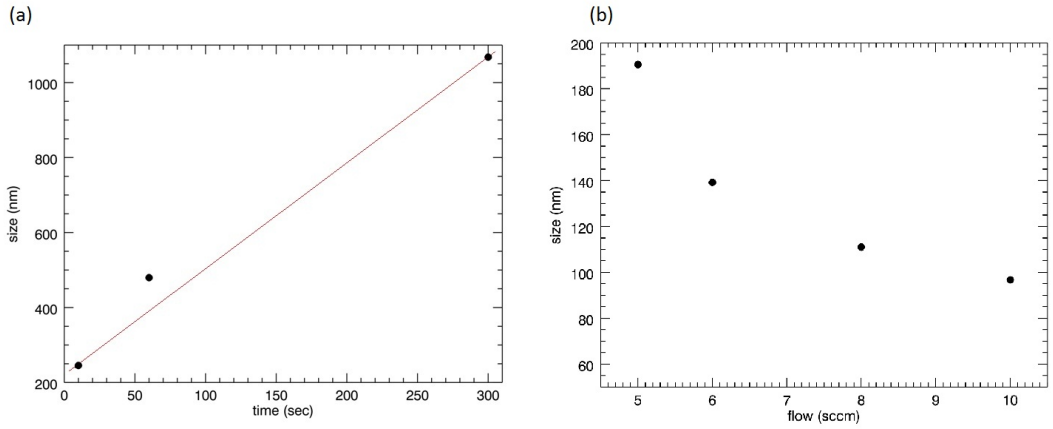

Figure 4.7: Dependence of the size on plasma run time (a) and neutral gas flow (b) as deduced from pictures made by means of a SEM. As suspected in figure 4.4 the particle radius decreases with increasing flow. The measurements were performed at 80 Pa, 1 sccm, and 3 mA. According to this picture a linear particle growth can be assumed.

Using this method the dependence of the particle size is demonstrated versus the flow in figure 4.7(b). As suspected from figure 4.4 the particle size decreases with increasing flow.

The main problem with this collection technique is due to the experimental procedure. A constant gas flow is kept throughout the whole experiment since no growth was observed without a constant flow of acetylene. This leads to a sensitive equilibrium between the electric field and the neutral gas drag in which the particles are kept. If removing either one the particles are transported along the other. Hence the particles falling onto the wafers might not be the biggest ones in the cloud. But the mono disperse size distribution which can be seen in figure 4.6(b) indicates that the results gained from the SEM measurements are reliable.

Figure 4.7(a) shows the growth of particles for different plasma run times. In difference to the critical size demonstrated in figure 4.7(b) the flow was kept at 1 sccm during these experiments to demonstrate the increase in size in the static case. It can be seen that the growth is linear. As mentioned before a linear particle growth can be assumed to be mainly due to radicals in the accretion phase [19, 28].

4.3.5 Transportation Time

If measured at different positions in the tube a delay in the transport can be seen. This is illustrated for the first cycle in figure 4.8. The characteristic argon emission lines appear in both figures ((a): close to the anode and (b): close to the cathode) in the moment the plasma is switched on. But it can be seen that the arrival of the first particle cloud is delayed in 4.8(b) with respect to 4.8(a). This clearly shows that the formation of particles starts close to the anode from where the particles are transported along the tube. In

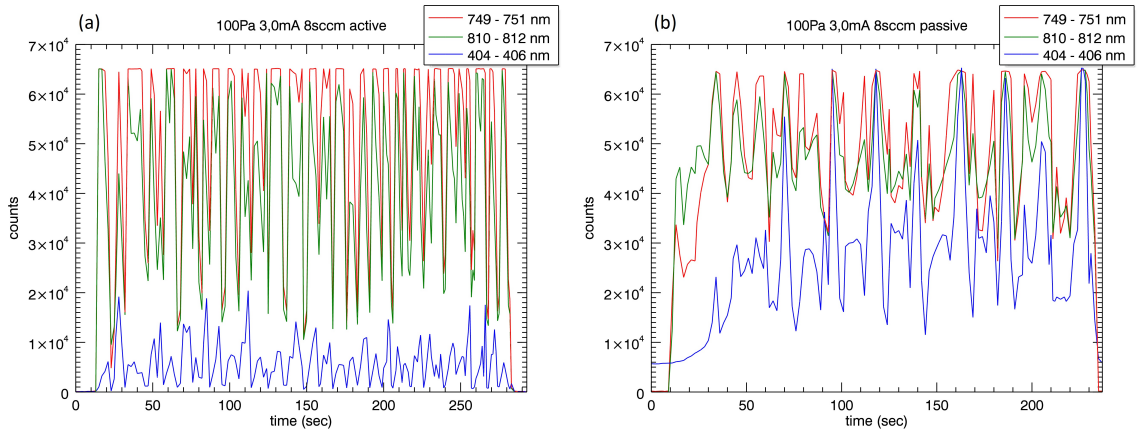

Figure 4.8: Two graphs displaying the data taken close to the anode (a) and close to the cathode (b). It can be seen that the appearance of the growth in (b) is delayed with respect to the plasma on time if compared to the behavior in (a). Please note that the zero line in (b) is no physical effect but caused by reflections of the laser at the electrode. In addition the time scales are not the same for the two graphs.

addition, the clearly pronounced cycles close to the anode merge into a more homogeneous cloud close to the cathode. This can be interpreted as a hint on the non-uniform transport along the tube. Especially if passing around the corners the cloud almost stops before being 'caught' by the next cycle.

4.3.6 Plasma Instabilities

As mentioned above the plasma changes when particles appear. In addition to the change in the electron temperature plasma instabilities comparable to the known phenomena of striations occur [64, 96, 100, 165, 180, 187]. The distribution of plasma emission intensity is not homogeneous in the vicinity of particles anymore but shows strong oscillations along the vertical and horizontal axis. Pictures of such phenomena are displayed in figure 4.9.

Panel (b) shows the striations that occur close to the grounded electrode. The same picture is shown in panel (a) with inverted colors and red circles to enhance the striations. An increased intensity in the center of the striations can be seen. This is due to particles kept in the striations where the confinement is enhanced [100].

Panel (c) shows a filamentation of the plasma. It is due to the increased particle density. As mentioned above the electron density increases if particles are confined in the plasma. If a situation is reached in which the particle density is so high the plasma cannot be sustained anymore first filamentations as displayed here occur before the plasma breaks down.

Further instabilities such as plasma contraction precede the filamentation. The phenomenon looks very similar to what has been observed by Mikikian *et al.* [150] in RF discharges. In his experiments the void in the center of the cloud contracts. This is accompanied by a change in the plasma emission. Due to the repetitive character of the in-

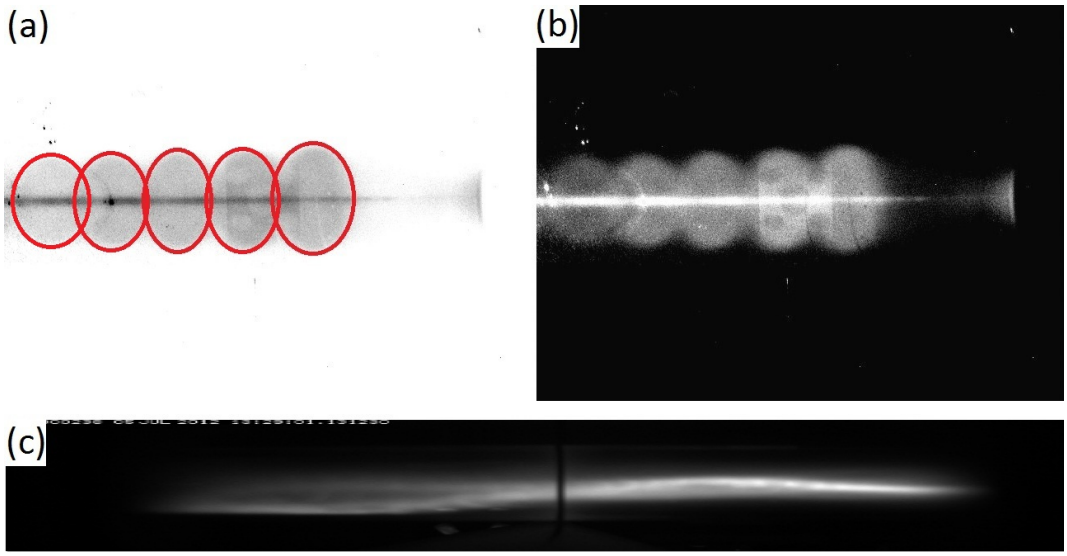

Figure 4.9: Instabilities as they occur in the vicinity of grown particles. (a) and (b): Striations close to the passive electrode. The picture (b) is shown again with inverted colors and red circles enhancing the striations in (a). (c) Plasma filamentation previous to the breakdown of the discharge. Note, that only in (a) and (b) the scattered laser light can be seen, while in (c) a filter is employed to show the plasma glow only.

stabilities observed they are called heartbeat instabilities. The decreasing electron density leads first to strong instabilities (as contractions and filamentations) before the discharge breaks down.

4.4 Possible further Experiments

As demonstrated by M. Mikikian *et al.* [148] growing particles under micro gravity conditions differ from experiments performed in ground based setups. Hence growth in the PK-4 setup in micro gravity will certainly be one of the future topics. The main problem then occurs due to the regulations on board of airplanes and the ISS. The inflammable gas used in the experiments described above is usually forbidden. Hence the growth has to be triggered from existing material. Unfortunately this has not yet worked out in ground based experiments. Thus a lot of time has to be invested into understanding the dust formation in PK-4. The knowledge gained in the process can then also be used to improve the cleaning process important for long time operation of the tube. It is crucial to be able to clean the tube without having to open it if several years of experimentation on board of the ISS are discussed.

The experiments performed with 2.2 percent of acetylene in argon showed a certain critical size at which the particles are swept away. The extension to these are experiments with a higher percentage of acetylene which should increase the growth rate. The flow at which the critical size is reached should be lowered and the frequency of periodicity

increased.

Next to acetylene experiments in methane are being discussed. The initial growth differs strongly for the two gases as it has been previously been reported on by J. Berndt *et al.* [20]. Establishing growth from methane in PK-4 turned out to be almost impossible. Only if an additional RF discharge is ignited growth from methane can be observed. The observed particles are much smaller than the ones observed in acetylene. And the distribution along the chamber differs, too. While particles in acetylene grow very fast filling the whole plasma, those growing in methane are divided by the streaming gas. At the borders of this formed channel turbulent and laminar flow phenomena can be observed. As however at this stage the quality of the data is insufficient further experiments are necessary before clear statements can be made.

The investigation of the film formation on the glass surfaces is another topic worth studying. So far a film has only been observed at high flow rates. The chemical and physical properties of this film as well as the formation rate and the destruction are very interesting. Not only can these experiments reveal the fundamental processes but they may also help in reducing film production in other environments.

As described above a transition from the static to periodic behavior occurred. The reason for the growth to stop after a few cycles is not yet understood and will certainly be subject to further studies in PK-4.

As mentioned above not only the chemical properties of the plasma but also the electrical properties change. Direct measurements of the electron density and temperature will have to be performed in order to gain a complete picture of the growth in this particular environment.

Changing the chemical properties also changes the resistivity of the plasma. Investigations of the voltage characteristics will therefore give an additional insight on the chemical growth processes.

Since the particle formation can be influenced by changing the gas temperature a parametric study in dependence on the gas temperature will be a future research topic.

In figure 2.3 a Melamine Formaldehyde (MF) particle is shown which was in the plasma during the growth process. The surface is strongly deformed. Parts of the particle have been etched, and particles have been grown on the surface. The properties and physical processes leading to this particular surface growth will surely trigger further investigations.

4.5 Summary

The experiments conducted on particle formation in a continuous discharge revealed a strong dependence of size and growth frequency on the neutral gas flux, the neutral gas pressure, and the applied power. If a certain 'critical' gas flow is applied the formed particles leave the initial place of formation and are transported along the tube. Above this critical flow a periodic growth has been found. Along with the increasing growth frequency and transport velocity the particle size decreases. Below the critical flow the particles grow in front of the electrode without being removed. In between this static and

the periodic regime a transitional regime occurs at which the particles are removed from the original place of formation but no periodicity has been found.

4.6 Résumé

Les travaux expérimentaux réalisés sur la formation de particules, dans une décharge continue, ont révélé une forte dépendance de la taille et de la fréquence de formation de la vitesse du flux de gaz neutre, de la pression et de la puissance appliquée. Au delà d'une valeur critique du flux de gaz, les particules formées quittent la zone initiale de leur croissance et sont transportées le long du tube à décharge. Pour des valeurs du flux supérieurs à la valeur critique la formation devient cyclique. Avec l'augmentation de la fréquence de formation et la vitesse de transport la taille des particules diminue. En dessous de la valeur critique, les particules restent piégées et localisées dans la zone de leur formation. Entre ces deux situations extrêmes, il existe un régime dans lequel les particules sont libérées de la zone de formation mais sans qu'aucune périodicité ne soit observée

4.7 Zusammenfassung

Die Experimente zum Teilchenwachstum in einer DC Entladung zeigten eine starke Abhängigkeit der Teilchengröße und der Wachstumsfrequenz von dem angelegten Neutralgasfluss, dem Druck und der angelegten Spannung. Sobald ein "kritischer" Fluss überstiegen ist, werden die Teilchen von dem ursprünglichen Wachstumsort weggeschwemmt und entlang der Röhre transportiert. Oberhald des kritischen Flusses wird periodisches Wachstum beobachtet. Mit zunehmendem Fluss nimmt die Transportgeschwindigkeit entlag der Röhre zu und die Teilchengröße ab. Unterhalb des kritischen Flusses verweilen die Teilchen vor der Elektrode. Zwischen diesem statischen und dem periodischen Verhalten wurden Teilchen geformt und weggeschwemmt, aber keine Periodizität trat auf.

Chapter 5

Decharging

5.1 Previous Experiments

The particle charge is one of the most important parameters in complex plasmas. Earlier experiments investigated the charge in the plasma by various methods [18, 41, 65, 67, 101, 112, 93, 220]. In this chapter the charge reduction in the plasma after glow will be discussed.

Particles injected into a plasma charge up negatively (see e.g. chapter 2). Once the plasma is switched off, and no energy is delivered anymore to the gas, the ions and electrons diffuse towards the confining walls [174] and recombine on the surface of the introduced particles [137, 207]. As a consequence the levitated dust particles loose their charge. They are decharged.

From earlier discussions by Ivlev *et al.* [94] it is known that for micrometer sized particles in a millibar plasma afterglow are expected to carry charges of about 10^{-2} z_0, with z_0 being their equilibrium charge in the plasma. However, if the plasma loss time scale is of the order of the charge fluctuations the charge can be frozen at values closer to the initial one.

As mentioned above the plasma is lost due to surface recombination and ambipolar diffusion to the walls. Thus, the time scales for ion and electron diffusion, relaxation, surface recombination, and attachment determine the remaining charge. Ions are mainly lost due to attachment to the negatively charged particles (in the order of 10 μs) while electrons are mainly lost due to diffusion (in the order of 0.1 μs) [73].

Unpublished 1D numerical simulations by Girshik *et al.* [73] show that the average charge of particles grown from silane (assumed diameter: 70 nm) in the plasma afterglow is +0.008 e[1] per particle. They found that 100 ms after switching off the discharge only about 21 % of the particles are neutral, whereas the rest carries positive and negative charges.

Particle decharging has been investigated in experiments on ground using grown particles [47, 48] and under micro gravity conditions on board the ISS [94]. In their experiments

[1] e in this case is the absolute value of the electron charge; $e = 1.602 \cdot 10^{-19}$ C [200].

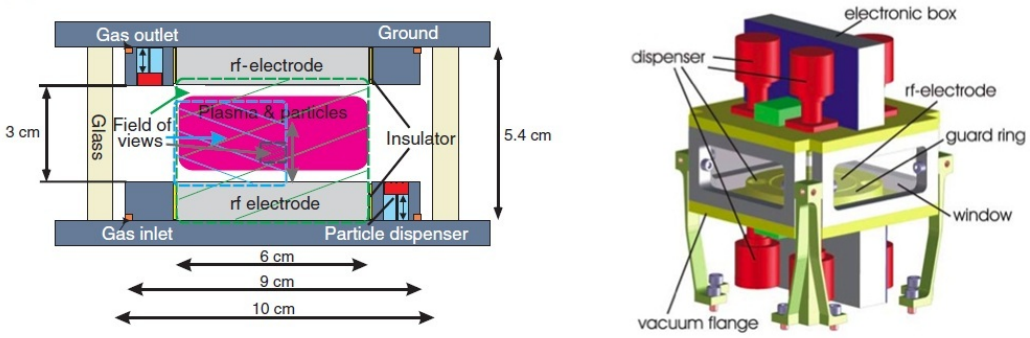

Figure 5.1: Sketch of the PK-3 plus chamber taken from [206]. One sketch shows the dimensions in 2D, whereas the second sketch is a 3D scheme of the setup.

they report on charges in the order of -20 e (for the smaller grown particles) and -150 e (in case of introduced particles) per particle. The difference between the observed charges and the predicted ones by Girshik *et al.* are mainly due to the particle sizes. The particle charges are expected to be distributed around zero, but the individual values depend on the particle size.

5.2 Experimental Setup

Experiments on the distribution of particle charges in the afterglow were investigated on board of the ISS (International Space Station) in a variety of plasma parameters. The experiments were conducted in a Plasma Kristall 3 Plus (PK-3 Plus) chamber. A sketch of the experimental setup is shown in figure 5.1.

PK-3 Plus is a capacitively coupled discharge chamber operated in push-pull mode. The diameter of the electrodes is 6 cm and their distance is 3 cm. They are surrounded by an insulated guard ring. In addition to the RF generator, function generators are attached to the electrodes. Particles of several different sizes can be injected into the chamber. The gas is not introduced by a constant gas flow but by indirect gas puffs. In order to reduce the disturbance to the system the gas is first introduced into a secondary volume. From there is streams slowly into the chamber.

To the chamber several optical and electrical survey systems are attached. Three cameras are recording the reflected light of a red laser. Since they are aligned on one optical translation stage scans through the active volume without having to readjust the cameras are possible. One additional camera is mounted to record the plasma glow.

During operation the chamber heats up due to the heat produced by the installed electronics. In this process one side heats up stronger than the other. To compensate for this the other electrode is heated after some time of operation. Throughout the experiments described here the thermal gradient is therefore of minor importance. However the impact of the gradient will be visible and discussed in the following sections.

The electrical properties and settings are monitored and saved to a log file for later

reference. The synchronization of the recorded pictures and the log files is explained in appendix A. A detailed description of the setup is given in ref. [206].

5.3 Experimental Procedure

In case of the experiments conducted here the pressure was adjusted to 20 Pa and 100 Pa. By the time the pressure is constant the plasma is ignited and the particles are injected. After having been given enough time for relaxation the plasma is switched off. The particles stay levitated in the central volume of the chamber. Afterwards an ac field with a frequency of 1 Hz is applied to the system. From the reaction of the particles to this field the residual particle charge can be deduced.

Since in earlier parabolic flight experiments a dependence of the particle charge on the moment of extinction of the plasma has been observed different switching off conditions were introduced. The three different conditions are displayed in figure 5.2.

In some cases a constant electric field is applied while the plasma is still in operation. Since this field is employed to remove electrons and ions from the active volume it will be called *'clearing field'* in the following.

1. No Clearing Field
   The plasma is switched off and followed by the alternating electric field at two different strengths. This configuration is displayed in figure 5.2(a)

2. Low Clearing Field (6.67 V/cm)
   While the plasma is still in operation, a DC electric field is applied. After the plasma is switched off the same alternating electric fields as in condition 1 are applied. This configuration is displayed in figure 5.2(b)

3. High Clearing Field (13.3 V/cm)
   The applied electric fields resemble those in condition 2. Only the electric field strength of the DC field is increased. This configuration is displayed in figure 5.2(c)

5.4 Analysis

In reaction to the field the particles perform a sinusoidal motion. The analysis of the motion is performed in four stages before the actual particle charge is calculated. The sinusoidal particle motion is overlayed by a thermal drift caused by thermal gradients introduced by the design of the experimental setup[4].To correct on the resulting linear upward drift of the particles a linear fit on the data is performed. The new particle track is then determined by the original track minus the individual linear drift. The intermediate track position in X and Y before correcting is kept for further display of the data. The linear fit however

[4]The physical processes, use, advantages and disadvantages of thermal gradients and the thereby introduced thermophoretic forces are explained in section 2.3

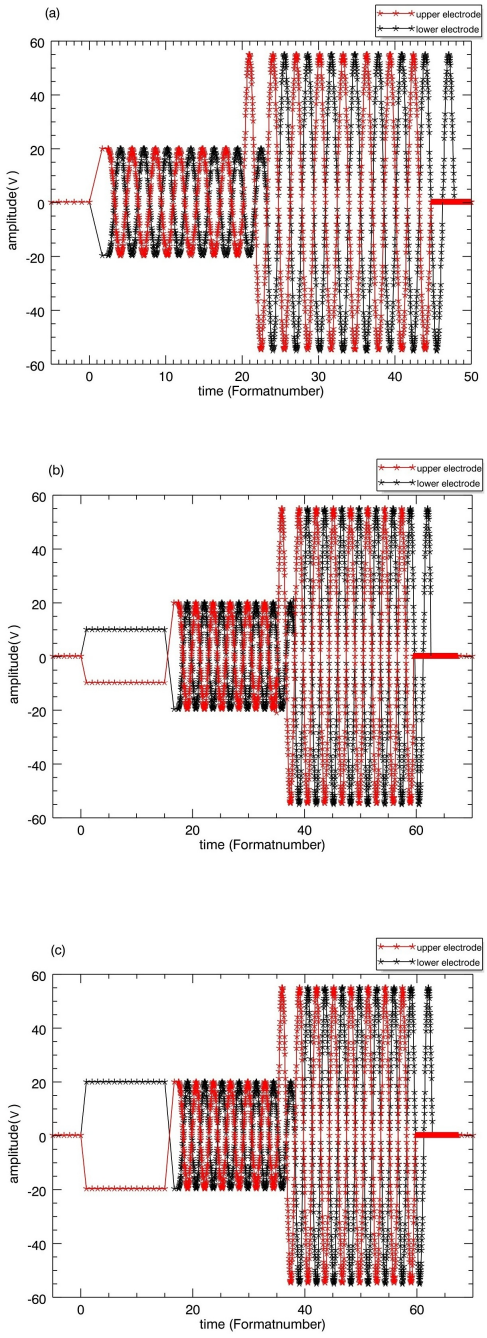

Figure 5.2: The three different switching off conditions. The voltages applied to the lower (black) and upper (red) electrode[3] are displayed. Three different conditions exist: no (a), a low (b), and a high (c) clearing field being applied before the plasma is switched off and the excitation starts.

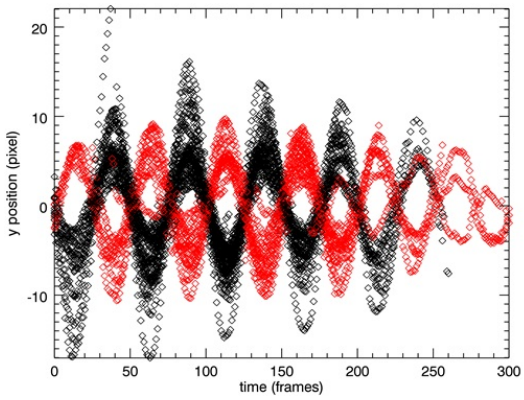

Figure 5.3: All tracks after correcting on the thermal gradient. The different colors indicate different behaviors of the particles in question. Between the motion of these particles a phase shift of 180 ° occurs. This clearly indicates that negatively as well as positively charged particles are observed. The amount of particles with opposite charges is approximately equal.

can cause severe problems. Since the particles move inside the cloud they are very likely to leave and reappear in the limited region illuminated by the laser. Hence the particle tracks are not visible at all times. This leads to a possible misfitting due to the starting and ending phase of the analyzed track. To correct on this possible misfit, a second function consisting of a sinusoidal and a linear part is fitted to the resulting data. Again the track is corrected by the second linear part. In the first step the linear slope dominates the sinusoidal motion leading to a situation in which the immediate fit with a sinusoidal and a linear part does not work properly.

As a result the reconstructed tracks are a sinusoidal motion around zero. This is displayed in figure 5.3. The different colored tracks underline the behavior of the tracks. There are only two kinds of tracks observed which have a phase shift of π between them. This shows the presence of positively and negatively charged particles only.

Now that the motion is purely sinusoidal the particle motion can be treated differently. With time the amplitude of the particle motion declines. This is due to a decline in the particle charge with time. Neglecting the thermal upward drift the particle motion is determined by the electric field F_{el}, the neutral gas drag F_{nd}, and the particle inertia F_{in}. The equation of motion can thus be written as:

$$F_{el} - F_{nd} = F_{in} \tag{5.1}$$

With the equations for the forces

$$\begin{aligned} F_{el} &= qE(t) = qE_0 sin(\omega_0 t) \\ F_{nd} &= m_d \gamma_n \dot{x} \\ F_{in} &= m_d \ddot{x} \end{aligned} \tag{5.2}$$

and the particle track

$$x(t) = A_0 sin(\omega_0 t + \phi) \tag{5.3}$$

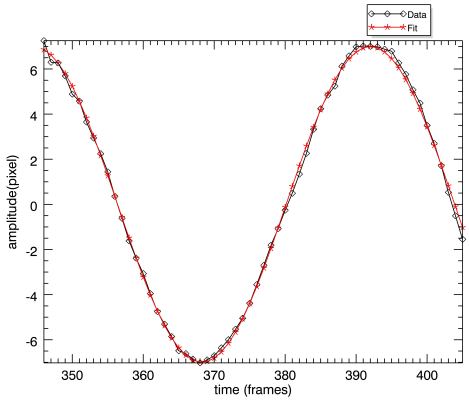

Figure 5.4: The result of the fit (red) to the corrected data (black) as given in equation 5.6.

the equations for the charge and the phase shift can be calculated [36]

$$q = \frac{A_0 \omega_0 m_d \sqrt{\omega_0 + \gamma_n}}{E_0} \tag{5.4}$$

$$\gamma_n = \left(\frac{\omega_0}{\phi} \right). \tag{5.5}$$

In these equations $\omega_0 = 2\pi \mathrm{f} = 2\pi$ Hz is the driving frequency, A_0 is the amplitude of the track, ϕ is a possible phase shift between the driver and the reaction of the particles, and γ_n describes the neutral gas damping according to Epstein [60].

The data is then fitted with equation 5.3. In a first step only the amplitude is fitted. This is to make sure that the resulting amplitude has the correct sign.

In the last step the amplitude and the phase shift as well as an additional exponential decrease are fitted.

$$x(t) = A_0 exp\left(-\frac{t}{\tau} \right) sin(\omega_0 t + \phi) \tag{5.6}$$

During the process of analyzing the data also fits of the frequency were performed. These revealed that the given frequency is almost kept by the fit. Hence removing this fit parameter granted a higher degree of accuracy. The result of the fit according to equation 5.6 is demonstrated by figure 5.4.

In red the fit to the black track is shown. It can be seen that the fit is very good and that irregularities occurring in the track[5] are corrected by the fit. Hence in the further considerations only the tracked amplitudes will be taken for calculation.

In principle the fit includes all the favored information:

- the particle charge, depending on the damping and the amplitude,

[5]Defects or irregularities in the track may be caused by 'pixel locking' or mistracking during the analysis. Additional effects caused by the reaction of the particle may also disturb the pure sinusoidal motion interesting in this analysis.

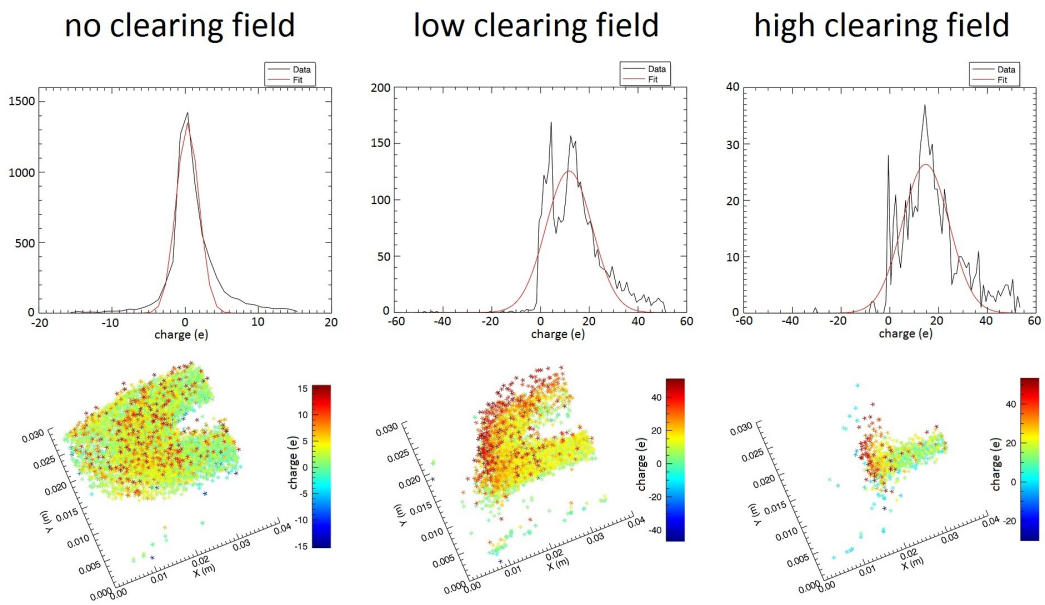

Figure 5.5: Charge distribution in the three switching off conditions displayed in figure 5.2. In the upper row the resulting charge distributions and an according Gaussian fit is displayed. In the lower row the charge distribution in the X-Y plane is demonstrated.

- the charge decline,
- and the spatial and time resolved damping, depending on the phase shift.

However accessing those informations in a sensible manner the synchronization between the excitation and the video files from which the particle tracks are gained has to be done properly. A detailed explanation on how the synchronization is performed and which problems still exist is given in Appendix A

5.5 Results

The particles exposed to the alternating electric field move in the observed volume. First the case without any clearing field applied will be discussed. The charge distribution for 6.8 μm particles at a pressure of 20 Pa is displayed in figure 5.5.

The charges in this case are distributed around +0.3 e per particle. Before switching off the particles carry negative charges in the order of several thousand electron charges per particle. The particle charge distribution in a plasma is Gaussian. After switching off the plasma the electrons and ions recombine on the surfaces of the particles. As discussed before the ions are drifting slower than the electrons. Even if no clearing field is applied the particles carry slightly more positively charge after switching off the plasma. This happens in dependence on the particle position in the volume.

The charge distributions as measured in the three different switching off conditions displayed in figure 5.2 are shown in figure 5.5. In the upper row the overall charge distribution is compared to a Gaussian fit. The particle charge is assumed to inherit a Gaussian distribution while the plasma is on. It is obvious that this is no longer the case if the plasma is switched off. Already in case of no clearing field the distribution is far from being Gaussian.

Please note, that the y-scales are very different for the three cases displayed. Even though the initial particle number is comparable for the three clouds observed the particle number entering into the main peak are very different.

If no clearing field is applied the original cloud shape is almost not disturbed. The upward drift observed is caused by the thermophoretic force induced by a thermal gradient introduced due to the stronger heating of one electrode by the electronics attached to the chamber. The particles carry residual charges distributed around a slightly positive value as it can be seen in the histogram. Thus the cloud is almost electrically neutral. This is the reason for the particle cloud shape to stay almost undisturbed.

Since it has been seen in earlier experiments that the switching off RF phase has an influence on the particle charge a series of dedicated experiments has been performed. For these experiments a constant electric field has been applied before the alternation of the voltage, the so-called '*clearing field*'. The distribution of the charges changes dramatically if the field is applied beforehand. This is illustrated as a histogram including a Gaussian fit and the distribution in the X/Y plane in figure 5.5.

The difference in the form of the cloud can clearly be seen. In case of the use of a clearing field the cloud is contracted and the more positively charged particles are on the upper side of the cloud. Without any clearing field the cloud stays rather the same and the particle charges are distributed uniformly. In the situation with clearing field the situation is the opposite. The charge is not distributed uniformly and not Gaussian distributed.

If a higher clearing field is applied this effect is even stronger. The upper particles situated in the upper part of the cloud get charged up in a manner that in the moment of excitation these particles are leaving the area of observation very quickly and are lost for analysis. This is why the upper part of the cloud is missing in the according graphs in figure 5.5. The effect is stronger the smaller the observed particles and the lower the neutral gas pressure.

Summarizing these findings the mean values of the charge distributions for all particle sizes observed at two different pressures (20 Pa and 100 Pa) are displayed for the three switching off conditions in figure 5.6.

As expected the particles carry overall higher charges if the pressure is higher. The charges rise along the particle size. The different clearing fields have different impacts at the two different pressures. At 20 Pa the strength of the clearing field is of no importance. In case of the higher pressure the situation is quite different. The particle charge is increased if a low clearing field is applied but not by the same strength as if the stronger field. Note, that particle with small radii and particles confined in low neutral gas pressures are very likely to be removed partly or completely from the observed volume as the AC field is applied. Thus, the observation of the change in particle charge as displayed in figure 5.6

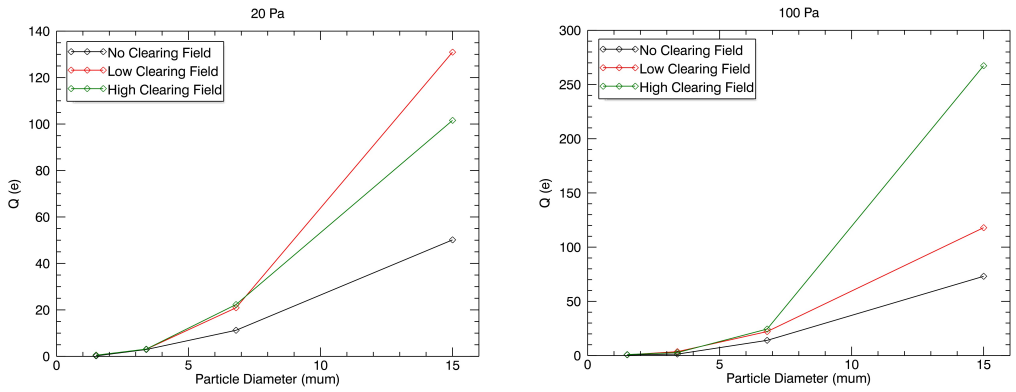

Figure 5.6: Charge distributions for all particle sizes depending on the pressure and switching off conditions.

does not show the accurate situation. However, it can be assumed that the trend displayed is correct: If no clearing field is applied the particle charge is distributed around zero with positive charges being slightly more probable. If a clearing field is applied the charge increases. Even though the upper part of the cloud, containing the particles carrying higher charges, is very likely to be lost in the moment the alternation is applied, the observed charges are higher than without the clearing field. furthermore, the particles are almost exclusively positively charged in case a clearing field has been applied prior to the observation of the particle motion.

In the moment the plasma is turned off the clearing field is still active. Ions, having lower mobility, traverse the active volume slower than the electrons. While doing so they pass through the whole cloud. Since the upper electrode is negatively biased, see figure 5.2, the ions move upwards. Therefore the upper more particles in the cloud are surrounded by the positively charged ions longer than the lower ones, leading to the more positively charged particles on the upper side of the cloud. The fact that the whole cloud is drifting downwards instead of following the thermophoretic force as discussed before is caused by the capacitive character of the chamber. The charges introduced during the on-time of the clearing field cannot be removed afterwards. A positive space charge builds up close to the upper electrode due to ions being attracted. The now positively charged particles recognize a repulsive electric force and move downwards. This is the reason for the disturbed cloud shape, as displayed for the low clearing field in figure 5.5, and the non-Gaussian charge distribution.

5.6 Possible further Experiments

Since the previously discussed PK-4 setup is going to be operated in micro gravity environments a similar series on the decharging properties in DC discharges might be nice for comparison. Especially since then the switching off phase will play no role on the devel-

opment of the charges. The experiments could then be compared to the results discussed above.

Another series with smaller clouds and different additional particles sizes will also be of advantage.

Furthermore the careful analysis of the remaining data has to be done.

5.7 Summary

Particles suspended in a plasma charge up negatively. The series of experiments described in this chapter are devoted to the duration of decharging in the plasma afterglow. It has been found that this process strongly depends on whether or not a constant field has been applied before the measurement was performed. If no field is employed the residual particle charges are distributed around zero. In case a field is applied, the charge per particle is increased and mainly positive. If the field is high enough the upper part of the cloud is even removed due to the high positive charging in the afterglow.

5.8 Résumé

Les particules piégées et en lévitation dans le plasma sont chargées négativement. Les expériences décrites dans ce chapitre ont été consacrées à la mesure du temps de décharge des particules dans la phase de post-décharge du plasma. Il a été démontré que ce paramètre dépend fortement de l'existence ou non d'un champ électrique constant entre les électrodes du réacteur avant l'extinction du plasma. En l'absence de champ électrique, la charge résiduelle des particules est distribuée autour de zéro. Par contre en présence de ce champ, cette charge augmente et est principalement positive. Si le champ est assez intense, une partie du nuage de particules peut être attiré vers l'électrode supérieure à cause de cette charge positive acquise en post-décharge.

5.9 Zusammenfassung

Teilchen in einem Plasma laden sich negativ auf. Die Experimentserie, die in diesem Kapitel beschrieben wurde, beschäftigt sich mit der Entladung der Teilchen im Nachglühen. Eine starke Abhängigkeit dieses Prozesses von der Präsenz eines konstanten elektrischen Feldes wurde gezeigt. Falls kein Feld angelegt wurde, sind die Ladungen der Teilchen um Null herum verteilt. Sobald ein Feld angelegt wurde, steigt die Ladung pro Teilchen stark an. Ist das angelegte Feld stark genug kann die obere Hälfte der Teilchenwolke entfernt werden.

Chapter 6

Confined Particle Clusters

As discussed at length in chapter 2 the interaction potential can be influenced by applying additional electric fields to the plasma. So far this has only been established along one axis leading to electrorheological plasmas [95, 97, 98]. A picture of the occurring phase transition of these string fluids in PK-3 Plus is displayed in figure 6.1.

It can be seen that, as the AC field increases the internal ordering in the system increases. This is caused by the character of the wake field interaction. In colloids these string fluids employing electric fields in higher dimensions have been observed [133, 170]. As predicted by Brandt *et al.*, [33, 34, 35] particle arrangements in plasmas subjected to 2D rotating electric fields should attract each other due to dipole-dipole interaction between neighboring particles and form discrete layers parallel to the rotational plane. The ion flux in this case is perpendicular to the rotational plane The results of these simulations are displayed in figure 6.2.

A rotating electric field perpendicular to the sheath electric field of sufficient strength results in time averaged 'donut'-like positive potential around the particle. Upstream and downstream the particle a time averaged attractive force forms [34]. Thus, once the applied electric field is strong enough layers along the ion flow direction are to be expected.

To apply a like-wise electric field configuration additional means have to be introduced into the plasma. In the following the rotating wall technique first utilized by Nosenko *et*

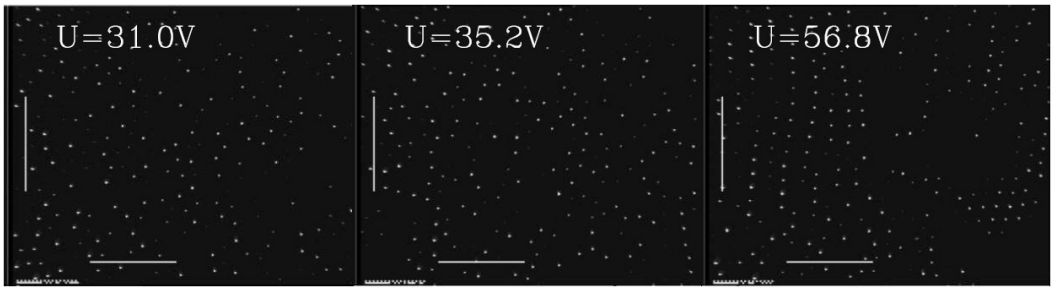

Figure 6.1: Phase transition as it occurs for increasing AC fields applied to a particle system levitated in PK-3 Plus [95].

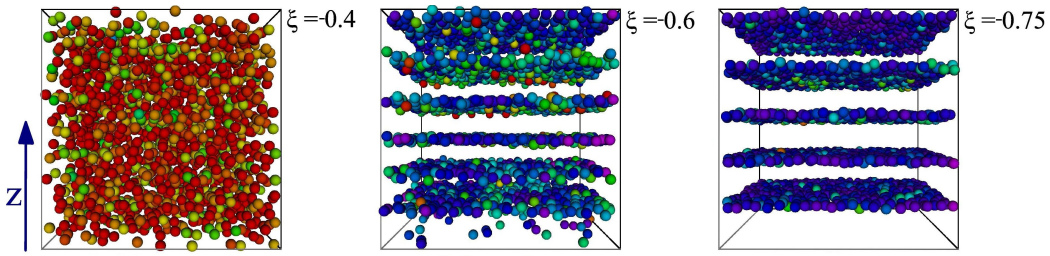

Figure 6.2: Layers in electrorheological plasmas as simulated by Brandt, [34]. The strength of the anisotropic interaction ξ increases from the unordered towards the ordered system. The different colors indicate the degree of order determined by the number of next neighbors.

al. [166] will be employed. In this case the electric field is applied by placing a glass box on the electrode. Each plate is covered with Indium Tin Oxide, providing a conductive surface on the inside of the box. They are insulated from each other allowing any electric field configuration inside the box.

Particles confined by additional means, such as conductive or non-conductive glass boxes, metallic rings, or holes drilled in the electrode, tend to form vertical strings [91, 110], zig-zag structures [110, 141, 142], 2D planar [166, 188], or 3D spherical clusters [4, 92, 142, 118]. Confined particles interact with each other due to the wake field introduced by the ions streaming past them. The usual internal structure that is found in such clusters are onion-like shells. The shell structure of a cluster as observed by Arp *et al.* [4] is displayed in figure 6.3. The particles in an undisturbed cluster tend to form spherical shells. Thus, if the radial particle position is plotted against the vertical position, disregarding the angular distribution, clear half-circles can be seen, figure 6.3(a). In panels (b) and (c) the particle positions in the bottom view for two different shells are displayed. It can be seen that the particles inherit a structural ordering on the surface of the shell. This ordering is indicated by the light gray (hexagons) and the dark gray (pentagons) shaded forms. The regular pattern in the cluster shell surface has been investigated further. It has been found that the pattern changes according to the plasma parameters [142] and the particle number [21]. Furthermore, competing structures as strings [118, 120], order transitions [16, 131, 21], and phase transitions [138, 189] in clusters have been observed. In addition instabilities as wave phenomena can be observed in confined particle clusters [183].

The electro static confinement provided by a non-conductive glass box has been simulated and probed by Arp *et al.* [5]. In principle the box provides a parabolic potential well in the center of the box. Figure 6.4(a) shows a superimposition of the simulation of all forces present in the box (gravity, electric field, ion and neutral drag). The potential energy of a sample particle, carrying about 2000 electron charges, is indicated by the contour lines. In figure 6.4(b) the resulting potential well (crosses: data, solid line: fit) inside the box is displayed. The dimensions of the simulated cluster are indicated by the vertical lines. The solid line shows the expected elongation if pure Coulomb interaction is assumed, the dotted line the one for Yukawa interaction with a Debye length of 0.5 mm. It can be seen that a cluster is confined in the center of the box. The screened interaction, producing

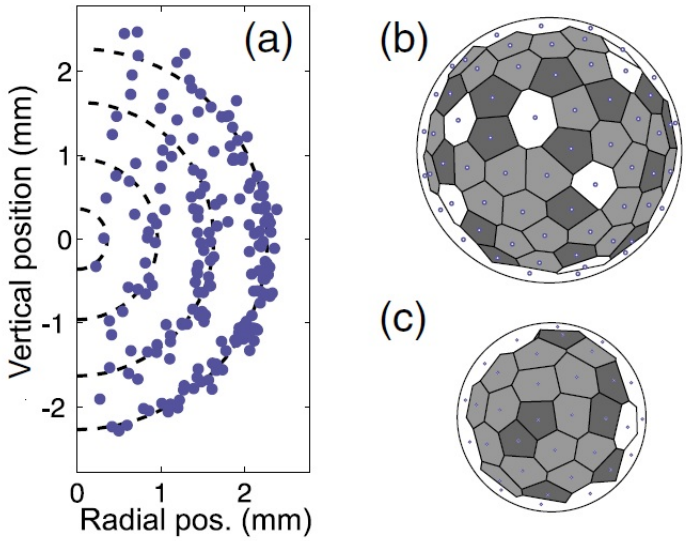

Figure 6.3: Spherical shell structure of a cluster containing 190 particles. (a) Projection of all particle positions in the rz- plane, disregarding their angular position. Panels (b) and (c) show a bottom view of the cluster for two different shells. The small circles indicate the particle positions; the cell coloring is according to the number of next neighbors, [4].

reduced repulsion, leads to a more compact cluster.

The presence of particles in a plasma decreases the electron density. To sustain the discharge the electron temperature has to be increased. This results in an increased plasma emission in the vicinity of the particles [6]. Thus, the number of free charges is reduced. If many particles are introduced the electron flux to each is reduced due to the presence of the others. This leads to a charge depletion in the plane. In response a particle cluster is reduced in size since the repulsion between the particles is reduced due to the lower particle charge.

Along the direction of the streaming ions a wake field is induced downstream the particles. This positive potential reduces the electron flux towards the particle and thereby the charge [40, 41, 134, 131, 151]. The charge reduction found by Carstensen *et al.* [40, 41] is in the order of 30 % for single strings composed of two particles.

In addition to the behavior of single particles, particle chains, and stationary clusters their motion has been a subject of investigation. Confined clusters show several internal modes of motion [92]. Especially rotation can be excited externally [38, 112, 166]. Since the particles carry negative charges they can be set into motion by additional electric and magnetic fields. Konopka *et al.* [112] demonstrated the rotation of confined particle clusters in response to magnetic fields. Another possibility to set a cluster in motion is by exciting the neutral gas [38, 39]. In this case a rotating electrode was employed. The neutral gas rotating then sets the cluster in motion.

The excitation of 2D layers by rotating electric fields has been shown by Nosenko *et al.* [166]. In this case an electric field is introduced to the confined particle cloud by using

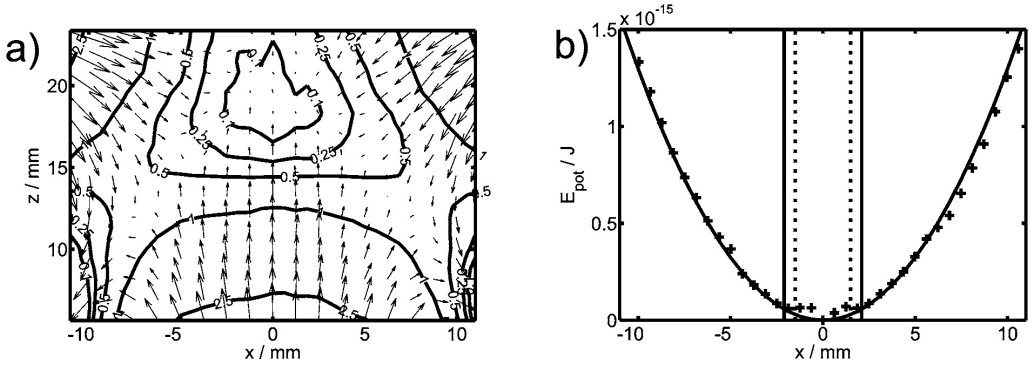

Figure 6.4: Simulations and measurements on the confinement in a non-conductive glass box. (a) Distribution of all present forces (gravity, electric field, ion and neutral drag) superimposed. The contour lines describe the energy potential to a test particle with q = 2000 e in 10^{-15} J. (b) Resulting potential well. The crosses show the data points fitted with a parabolic function (solid line). A cluster (200 particles, each with q = 2000 e) suspended in this confinement would have the extensions given by the solid (pure Coulomb) and the dotted (Yukawa) vertical lines, [5]

a box consisting of four conductive yet transparent plated. Note, that the confinement shown in figure 6.4 is strongly affected in this situation. It further varies depending on the potential applied to the individual plates. Nosenko *et al.* reported that the particle cloud does not always show rotation in direction of the applied field. To describe the situation inside of the box they introduced two main rotation mechanisms: torque due to the ion drag and due to the electric field. The rotation against the direction of the electric field is due to an introduced dipole on the cluster in the box, whereas the rotation in direction of the field is explained by the ion drag force. Only if the charging of the cloud by the additional electric field is asymmetric the dipole can result in a rotation. Depending on the orientation of the dipole with respect to the electric field the cluster rotates with or against the electric field. In order to gain further insight into the asymmetric charging they probed the plasma shielding. Therefore a single particle was levitated inside of the box. To one electrode a constant voltage is applied while the others are grounded. They found the asymmetric plasma shielding explaining the reversed rotation direction. Experiments following this procedure will also be discussed throughout the following chapter. Even though a lot of effort has been put into these investigations no conclusive results can be given on the origin of the asymmetry at this point.

Particles confined by additional means tend to form spherical clusters. The excitation of such clusters is predicted to result in layering perpendicular to the applied field. However, the past results mainly demonstrated the rotation induced by magnetic and electric fields as well as by rotation of the neutral gas.

Les particules piégées par des moyens additionnels, aux effets du plasma, tendent à former des clusters sphériques. Il a été prédit que l'excitation de ce type de cluster conduit à un arrangement en couches perpendiculaires à la direction du champ appliqué. Cependant, les résultats précédents avaient montré l'induction de mouvements de rotation dus à un

champ magnétique, un champ électrique et même à la rotation du gaz neutre.

Teilchen, die in einem zusätzlichen Konfinement eingefangen werden neigen dazu spherische Wolken zu formen. Die Anregung solcher Wolken sollte zu der Formation von einzelnen Schichten führen. Frühere Experimente zeigten aber die Anregung von Rotation durch externe elektrische oder magnetische Felder sowie durch Anregung des umgebenden Gases.

In the following two chapters the work of Nosenko *et al.* [166] will be extended. The main goal of the performed experiments is to tune the interaction potential in a way to introduce the layer structure predicted by Brandt [34]. Since this requires to apply a rotating electric field to the cluster the rotation is the first observation. The results will be discussed in chapter 7. Please note, that these are published in [MY1]. Afterwards the results on smaller clusters investigated by stereoscopic digital in-line holography in a collaboration with the colleagues from Kiel will be discussed. The main results shown here are to be published [MY3][1].

[1]Please note that this very paper has been edited while this thesis has been written. Thus, chapter 8 and the draft of [MY3] will be very similar or even equal in parts. This is true in some extend also for chapter 4 / ref. [MY2] and chapter 7 / ref. [MY1].

Chapter 7

Cluster Rotation

7.1 Experimental Setup

The experiments described in the following were performed in a modified Gaseous Electronics Conference (GEC) RF reference cell. The original properties of this cell are described in [169]. In difference to that setup the employed one has a bigger electrode of 22 cm diameter. 3 cm above the electrode a grounded guard ring is mounted. Glass windows placed in three flanges (two sides and on top) allow the observation of particles from the sides as well as from the top. Three CCD cameras are employed for optical particle observation. One of these is a high resolution camera allowing recording with up to 1250 frames per second (Photron FASTCAM 1024 PCI). The particles are illuminated by two red lasers which are not powerful enough to disturb the particles. The electrode is powered by a RF generator with up to 20 W_{rf}. The experiments described in the following were carried out at neutral gas pressures of 4 and 6 Pa and 1 W_{rf} power, which corresponds to a peak-to-peak voltage of about 200 V. A picture and a sketch of the GEC are displayed in figure 7.1. On the photo the chamber is illuminated by the green manipulation laser. Since during the experiments described in the following the particle manipulation is introduced by electric fields this laser is not employed throughout the experiments.

The plasma parameters were measured by a Langmuir probe. From these measurements the electron density $n_e = 3 \cdot 10^{-8}$ cm^{-1}, the electron temperature $T_e = 3.4$ eV, and the plasma potential $V_p = 21$ V can be estimated for the parameter region of interest.

Water is fed through the electrode. By changing its temperature the electrode temperature can be changed. With respect to the particle behavior temperatures of 60°, 75°, and 90° C have been established. Direct measurements of the electrode temperature show that its temperature remains lower than the one of the water. It has been shown that the self bias is strongly affected by the water and its temperature and therefore resistivity change. The self bias determines the particle levitation height [125]. In later experiments the water was therefore exchanged by a non-conductive silica oil. The effect on the particle levitation height is substantial. If left alone for about an hour, the system reaches an equilibrium state in which the self bias does not change any longer.

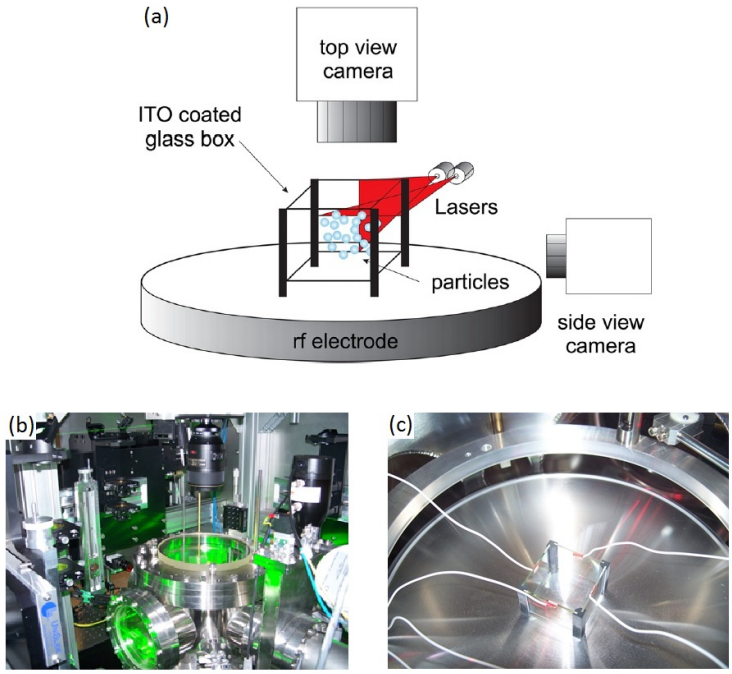

Figure 7.1: Sketch of the GEC setup with the glass box and the illumination system (a), ref. [MY1]. Picture of the chamber illuminated by the strong green laser (b) and the glass box mounted on the electrode (c). Both pictures are courtesy of V. Nosenko.

On top of the electrode a glass box is placed. A sketch of the setup including the glass box and the illumination system is displayed in figure 7.1(a). The glass box consists of four ITO (Indium Tin Oxide) covered plates. Each plate is 3 cm long, 2 cm high, and 0.1 cm thick. The glass plates are electrically insulated from each other by plastic poles allowing the introduction of an additional electric field. It is mounted in a way that the inside of the box is conductive and can supply any wished electric field configuration. The poles are attached to the plates in a way that a gap of about 0.4 cm is kept between the lower edge of the plates and the electrode. Each plate is connected to a function generator. To sustain a rotating electric field a sinusoidal voltage is applied to each plate keeping a constant phase shift of $\pi/2$ between the alternation of two neighboring plates. The plates are powered with a peak-to-peak voltage of $V_{pp} = 20$ V at frequencies between 0.1 and 1000 kHz. A cluster being introduced into this field can start to rotate. The first time this 'rotating wall' technique has been reported by Nosenko *et al.* [166]. A picture of the glass box as mounted in the GEC is shown in figure 7.1(c).

7.2 Observation

The confined cluster consists of about 1500 particles and has a radius of roughly 5 mm. The introduced particles are MF micro spheres with a diameter of 8.77 ± 0.14 μm. In response

to the temperature gradient applied to the chamber the cluster position and shape changes. The higher the temperature the higher the levitation height of the cluster. Additionally the initial spherical cluster deforms with increasing temperature and becomes more cigar-like. Images of the cluster at the three temperatures (60° C top, 75° C center, and 90° C bottom) are displayed in figure 7.2. The vertical position of the illuminated horizontal cross sections (left hand side) are indicated by the arrows in figure 7.7. On the right hand side the vertical cross section at each temperature is displayed. The deformation of the cluster can be seen in this projection. Note, that the very same cluster is discussed throughout this chapter. It has been shown that this is very important regarding the comparability of the results. Even a small variation in particle number can change the cluster [142].

In response to the applied electric field the cluster contracts. The additional confinement introduced by the electric field changes the potentials inside the box. The potentials in a non-conductive box have been discussed by Arp *et al.* [5]. Their estimation on the parabolic confinement is displayed in figure 6.4.

As demonstrated by Nosenko *et al.* [166] 2D clusters show rotation in and against the direction of the electric field depending on the applied frequency. For the 3D clusters discussed in the following rotation has been observed only in direction of the field. The reaction of the cluster depends on the frequency:

- Low frequency ($< \sim 50$ Hz)
  The cluster shows a sloshing motion inside the glass box following the electric field.
- ~ 50 Hz - ~ 500 Hz
  The cluster remains static in the center of the glass box. No rotation has been observed.
- ~ 500 Hz - ~ 1 MHz
  The cluster remains in the center of the glass box. The rotation shown by the cluster has always been observed in direction of the field.
- High frequency ($> \sim 1$ MHz)
  The cluster rotation stops. It remains, beside some residual rotation, stationary in the center of the box.

In this chapter the frequency and height dependence of the rotation will be discussed. Furthermore, the results on plasma shielding and vertical dust resonance frequency will be shown.

7.3 Analysis

In figure 7.3 the analysis of the recorded data is displayed. The distributions of the velocities in x and y are plotted versus the particle position in y and x, respectively. In case of rigid body rotation the plots would show straight lines. Since real data are regarded here a certain distribution is observed. Since the particle cluster behavior is mainly fluid-like,

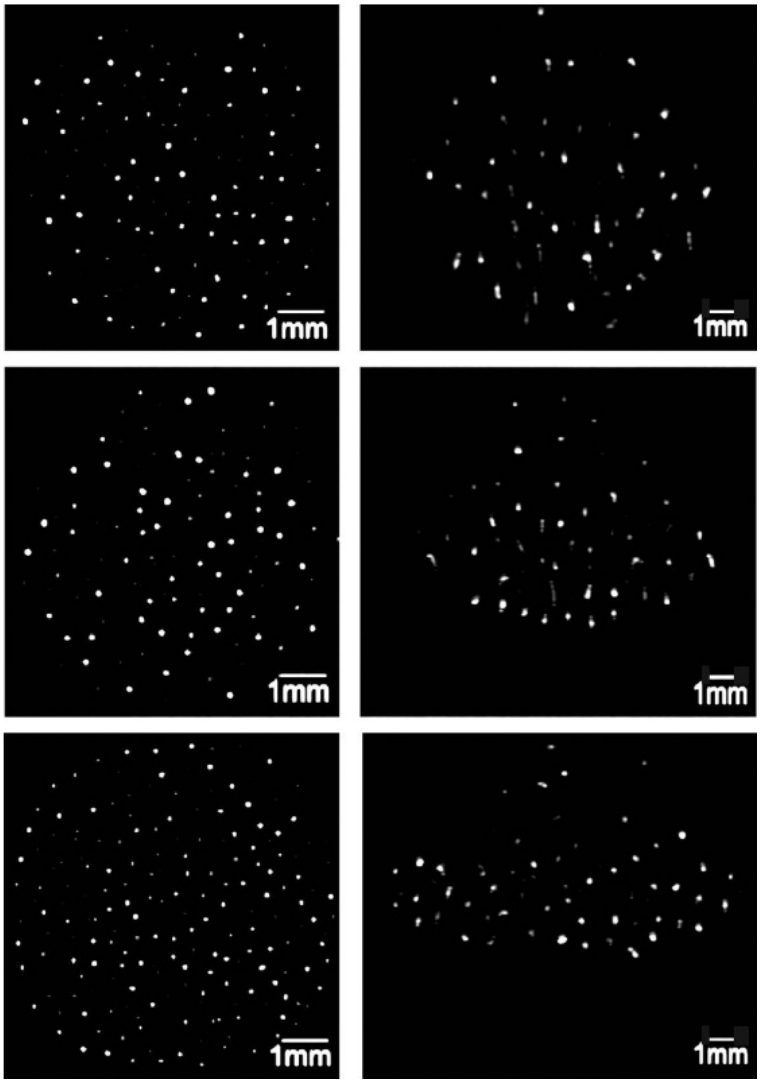

Figure 7.2: A sequence of side (right) and top view (left) images of the cluster as confined in the box. From top to bottom the temperature increases (60° C top, 75° C center, and 90° C bottom). In all three cases the same cluster is used. The displayed horizontal cross section of cluster is illuminated at the equatorial level (marked by the arrows in figure 7.7). Please note the change of the cluster shape in the side view images, [MY1].

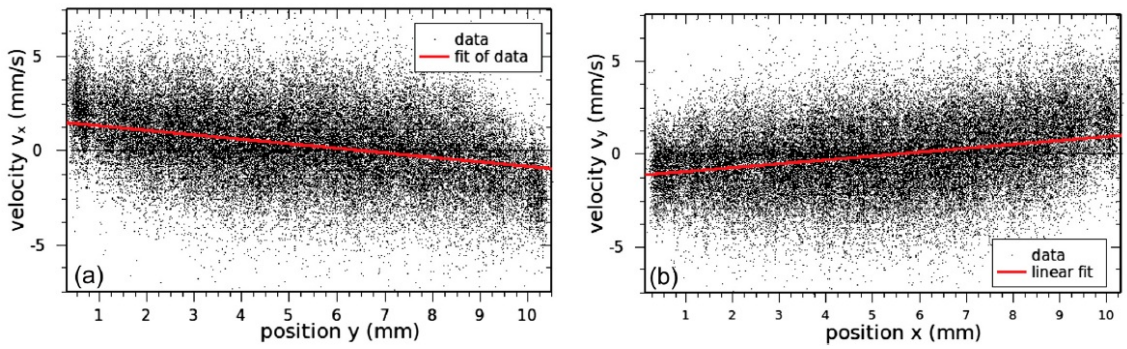

Figure 7.3: The fit (red) of the $v_{x,y}$ vs y, x distribution. The black points are the particle positions. The picture is taken from ref. [MY1].

the rotation is not completely rigid. Due to the high number of particles in the cluster (≈ 5000) the statistics in the central area is very good. Hence, the linear fit results in the mean rotation speed of the illuminated layer. For a more detailed description of this method please see ref. [228]

The slope of the linear fit is used to calculate the rotation speed. With the 2D observation method only one horizontal layer can be illuminated at a time. For the frequency scan the equatorial plane is chosen as representative for the cluster rotation. For a chosen frequency more horizontal slices of the particle cluster are recorded. The rotation speed is calculated for each slice. By this a height distribution of the rotation speed is gained.

7.4 Results

7.4.1 Frequency Dependence

As discussed above the cluster reaction changes depending on the applied frequency. At low excitation frequencies in the order of 10 Hz the cluster follows the excitation and moves around inside the glass box (*'sloshing'*). If the electric field frequency is too fast for the cluster to be able to follow the motion the rotation stops and the cluster remains static in the center of the box. Using thermophoretic forces the *cluster rotation* starts at about 500 Hz. The distribution of rotation speed for the three different electrode temperatures is shown in figure 7.4(a).

The cluster rotates in direction of the field at all times. At about 5 kHz the rotation speed is maximal. Note, that even the maximal rotation speed is much lower than the excitation frequency. At higher frequencies the rotation speed declines. Above frequencies of about 1 MHz the cluster rotation stops almost completely and only a residual rotation remains. The direction of the residual rotation is independent of the direction of rotation of the electric field. This residual rotation can be observed at all frequencies. To display this the measured rotation speeds are summed up considering clockwise rotation as negative. The result is displayed in figure 7.4(b). This residual rotation is driven by the neutral drag

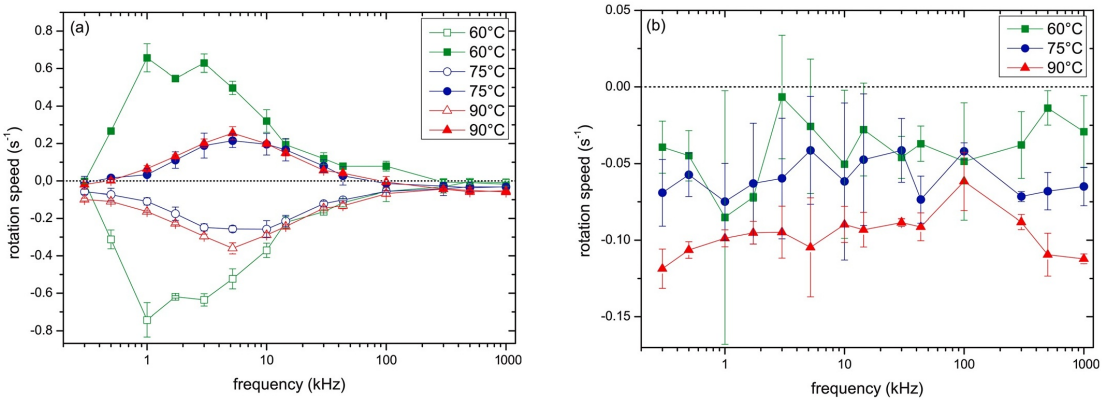

Figure 7.4: The rotation of the cluster in response to the applied electric field (a). A residual rotation has been observed. (b) displays the sum of clockwise (cw) and counter clockwise (ccw) rotation speeds. The picture is taken from ref. [MY1].

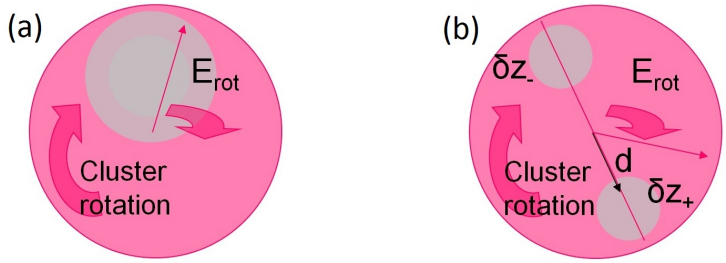

Figure 7.5: Schematic pictures to illustrate the ion drag force (a) and the electric force (b) as it occurs in the box. Due to the depletion of Ions by the walls the center-of-mass of the ion cloud is shifted. Following the electric field the Ions set the cluster into rotation in direction of the field. Due to the delayed charging the charge variation on the positive region is more positive than in the negative region. Hence a dipole moment d almost parallel to the field occurs which causes the cluster to rotate in direction of the field.

and the magnetic field of the Earth.

The electric field is introduced by four function generators which can provide a maximal peak-to-peak voltage of 20 V. If the amplitude of the electric field is reduced the cluster rotations slows down until the cluster is completely at rest. The electric field affects not only the particles but also the plasma. Thus, if the electric field amplitude would be much higher, the plasma would be strongly disturbed and the particle cluster would be lost. Even though higher electric field amplitudes would be possible without loosing the cluster the rotation is clearly pronounced with the accessible means.

7.4.2 Driving Mechanisms

As described by Nosenko *et al.* [166], the rotation is mainly driven by two different mechanisms: the ion drag and the electric force.

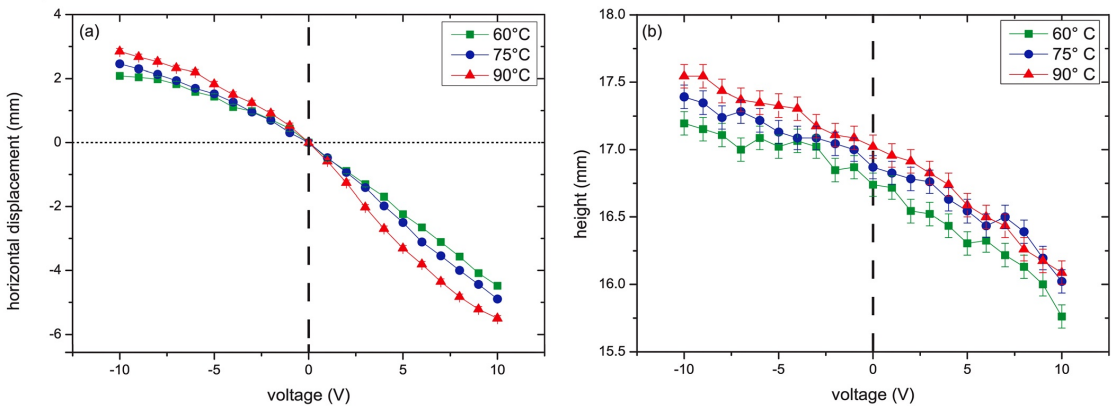

Figure 7.6: The horizontal (a) and vertical (b) displacement of a single particle as response to a constant electric inside the box. The zero in (a) is set as all four plates are grounded. The picture is taken from ref. [MY1].

- Ion Drag Force
  Ions streaming trough the glass box are affected by the sheath and the applied rotating electric field. The depletion of ions close to the glass box walls leads to a horizontal shift in the ion density. The non-homogeneous ion density distribution leads to an ion drag force which depends on the rotational phase. By this ion drag force acting on the particles a rotation in direction of the field is induced. The mechanism is demonstrated in figure 7.5(a).

- Electric Field Force
  The electric field rotating with frequencies in the order of several kHz induces a dipole moment on the particle cloud as indicated in figure 7.5(b). The charging of the cloud is delayed with respect to the electric field frequency. The plasma shielding inside the box is asymmetric, [166]. This asymmetric shielding leads to an asymmetry in the charging and thereby to a non-zero torque.
  To probe the confinement and the electric field penetration inside the box a single particle is introduced. Three of the four glass plates are grounded whereas a constant voltage ranging from -10 V to +10 Vis applied to the last plate. The displacement of this is displayed for the three different temperatures in figure 7.6 for both the horizontal and the vertical direction. Along the remaining axis no displacement was observed. The particle always stayed in the laser illumination sheet. An asymmetry as displayed in figure 7.6(a) leads to a delayed charging of the cluster and a dipole moment as sketched in figure 7.5(b). The dipole moment is hence induced parallel to the electric field. Thus the particle rotation caused by the electric field is in direction of the field.

Due to the time of flight of ions in the box the ion torque peaks at about 30 - 60 kHz. As shown in figure 7.4 the observed rotation peaks at 5 kHz. This is the frequency range is associated with the charging time. In contrast to the previous experiments by Nosenko

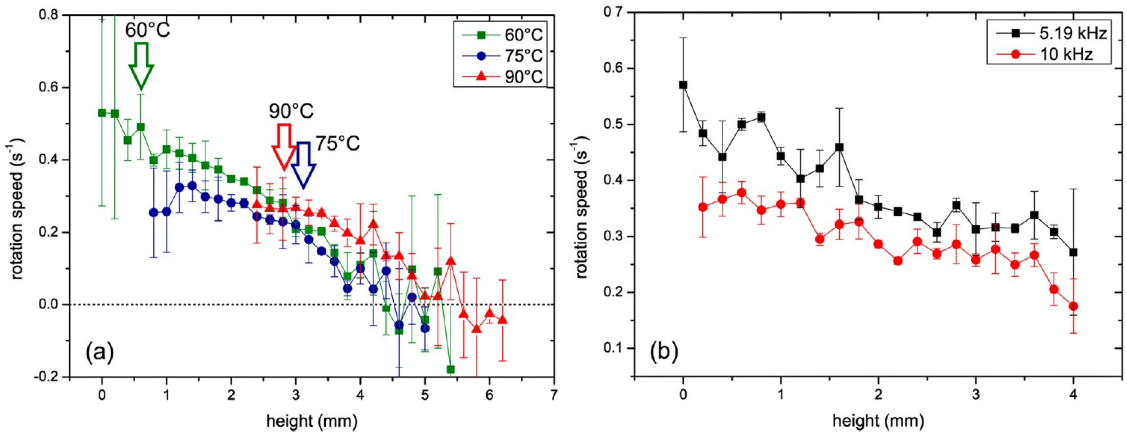

Figure 7.7: The distribution of rotation speeds along the clusters height for two different clusters. The height distribution of the cluster described in figure 7.4 is displayed in panel (a). It can be seen that the cluster rotates at different speeds on the upper and the lower portion. The pictures are taken from ref. [MY1].

et al. [166] no rotation has been observed at high frequencies. In the earlier studies the ion drag force has been found responsible for the rotation at these frequencies. Thus, the electric field is considered to be the main rotation mechanism throughout the observations.

With increasing temperature the particle levitation height is increased. At the higher position in the sheath the charging time is reduced. In addition, the ion time of flight is shorter. This results in an increased rotation frequency.

7.4.3 Height Dependence

In addition to the observation of the rotation speed in dependence on the driving frequency height scans at 5.19 kHz have been performed. The height scan reveals a differential rotation which decreases with height. The measurements have been performed for two different clusters displayed in figure 7.7(a) and (b). The decline in the rotation speed is similar in both clusters and for all temperatures. Thus, it can be assumed that the height distribution of the rotation is dominated by the difference in levitation height of the cluster.

The increase in the rotation speed is due to the energy gain of the ions penetrating deeper into the sheath and the increased effect of the delayed charging. Moving a cluster through the plasma sheath by means of thermophoretic forces can thus be used to probe the sheath.

7.4.4 Vertical Resonance Frequency

In addition to the response to an electric field a single particle captured can be used to probe the vertical dust resonance frequency of the plasma. Therefore an additional generator is attached to the electrode. It supplies a low voltage alternation. The vertical resonance is

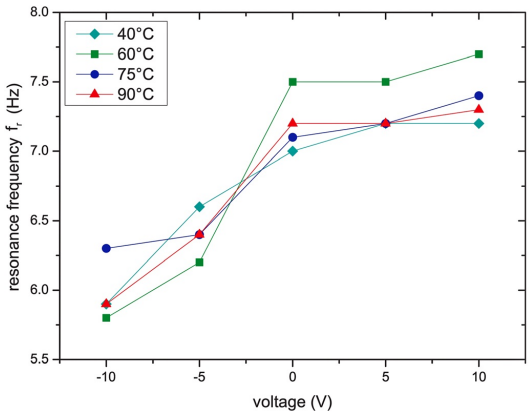

Figure 7.8: The vertical resonance frequency as depending on the applied voltage. The picture is taken from ref. [MY1].

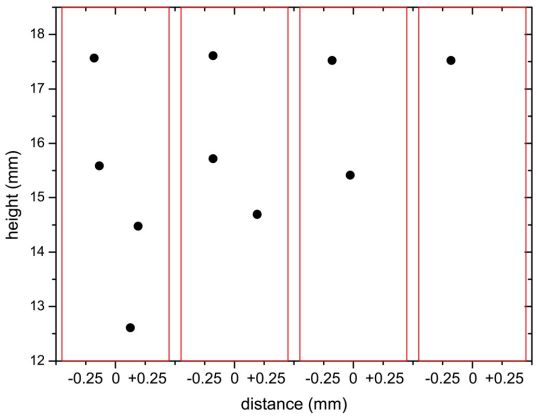

Figure 7.9: A sequence showing the positions of a particle string as the lowest particles are dropped one by one. The picture is taken from ref. [MY1].

then taken from the particles response. The outcome of the measurement as dependent on the voltage applied to one plate is displayed in figure 7.8. The change in the resonance is linked to the vertical and horizontal position of the particles. Thus the penetration depth in the sheath changes the particle behavior.

7.4.5 Suspending a Single Particle

It is necessary to suspend a single particle in the glass box in order to perform the experiments discussed above. As it is possible to introduced only a particle cloud and not a single one the experimental procedure is described here. Starting with small particle numbers simplifies the procedure. Once a small particle cloud is suspended the plasma confinement is weakened by de-matching the the RF power.

Once very few particles are suspended they will levitate above one another due to the attractive wake field potential. By de-matching the power further one can drop the

particles one by one. After dropping one particle the original matching is reestablished. The remaining particles will then regain their original position. A sequence of this behavior is shown in figure 7.9.

7.5 Possible further Experiments

Further experiments on the cluster rotation and behavior in response to other excitations such as e.g. dipoles or quadrupole are of interest. In addition the shell and vertical string rotation as suspected from the data will be in the center of interest. Also the initial phase of the cluster rotation has to be investigated in order to distinguish between the two driving mechanisms.

Experiments on the shielding of the box will also be conducted. A series of such experiments has already been performed at a wide range of parameters but no conclusive outcome can yet be reported.

7.6 Summary

A particle cluster suspended inside a conductive box has been set into rotation by applying a rotating electric field. The rotation has found to be always in the direction of the applied electric field. This is caused by the ion drag and a dipole moment induced due to delayed charging. The latter has been investigated by steady state single particle measurements. Furthermore, the height dependence of the rotation has been discussed. It has been found that the cluster is rotating faster on the lower than on the upper edge. This is due to the acceleration of ions along their path through the box.

7.7 Résumé

Un cluster de particules piégées dans une boites conductrice a été mis en rotation grâce à un champ électrique tournant. Il a été démontré que la rotation s'effectue toujours dans le sens que le champ électrice. Ceci est d à la force de poussée des ions et au diple induit. Ce dernier phénomène a été étudié par des mesures effectuées dans des conditions d'état d'équilibre d'une particule seule. De plus, la dépendance de la rotation avec la hauteur a été étudiée et est présentée. Il a été ainsi montré que la partie basse du cluster tourne plus vite que sa partie supérieure. Ceci est d à l'accélération des ions le long de leur trajet dans la boite.

7.8 Zusammenfassung

Eine Teilchenwolke wurde durch ein elektrisches Feld in Rotation versetzt. Die Wolke drehte sich immer in der gleichen Richtung wie das angelegte rotierende elektrische Feld.

Die Rotation wird durch Impulsübertragung der Ionen und durch Entstehung eines Dipols in der Wolke getrieben. Letzteres wurde durch Versuche mit einzelnen Teilchen untersucht. Des Weiteren wurde die Höhenabhängigkeit der Rotation bestimmt. Die Rotationsgeschwindigkeit ist am unteren Ende der Wolke höher als am oberen. Das wird durch den Zuwachs der Ionenenergie entlang des Weges durch die Wolke verursacht.

Chapter 8

Competing Cluster Symmetries

8.1 Experimental Setup

To get further information on a cluster 3D diagnostics are employed. During these experiments the particle cluster is investigated by the digital in-line holography at the University in Kiel. In this setup the region of interest is illuminated by a laser and the interference patterns of the scattered light are collected by a CCD camera. The resulting image contains information about the x, y and z position of each particle which can be extracted by careful Fourier analysis. A picture and a sketch of the experimental setup with the chamber mounted in the center of an optical table is shown in figure 8.1

The particle positions are reconstructed from the interference patterns observed on the camera chip. Figure 8.2(a) shows an image of a cluster as taken by the cameras. In panel (b) the interference pattern corresponding to a single particle is displayed. The depth information is artificially gained by introducing slices along the laser beam direction in the analysis. This is displayed in figure 8.2(c). The two cameras are synchronized. From each camera the full 3D analysis can be gained. However, the depth information gets

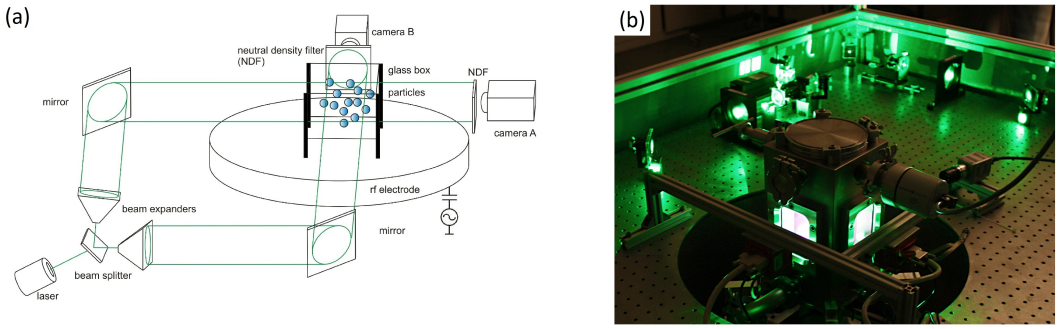

Figure 8.1: Picture (b) and sketch (a) of the chamber and the illuminations system as mounted in Kiel. The green illumination laser is in operation. In front the chamber surrounded by the two cameras can be seen. In the back the illumination system is mounted. The picture is courtesy of J. Schablinski.

more accurate if it can be compared to the reconstruction from a second camera. This recording method requires big particles. To increase the radius while keeping the mass as low as possible hollow glass spheres are employed. Given the physical and geometrical parameters of the hollow glass spheres provided by the manufacturer [132] (Scotchlite S22 glass with a density ρ=2.5 g/cm^3 and a wall thickness of s$\approx$0.3 μm, which are sorted later to get a mostly monodisperse particle size distribution with a diameter of d=22$\pm$2 μm.), it is straightforward to estimate the particle mass:

$$M = \frac{4}{3}\pi\rho\left[\left(\frac{d}{2}\right)^3 - \left(\frac{d}{2} - s\right)^3\right] \approx 1.11 \pm 0.23\ ng, \tag{8.1}$$

and the gas drag friction coefficient. Obtaining the value of the gas drag coefficient one has to take into account that the particle is hollow, compared to that suggested in [60]. The generalization shown in text is rather straightforward. At 4 Pa argon gas pressure it is:

$$\gamma_{eff} = \gamma_n \frac{d^3}{d^3 - (d-2s)^3} = 17.5\ s^{-1}. \tag{8.2}$$

A picture of these particles has been shown in figure 2.2(b).

Due to the limitations of the recording system the chamber has to be rather small if compared to the GEC cell used in the experiments at the MPE in Munich. The inner dimensions of the chamber are 14 cm x 14 cm x 26 cm [117, 119, 120]. The lower electrode diameter is 7 cm. The upper electrode is mounted at a distance of 7.2 cm. Its diameter is 9.6 cm. The lower electrode is powered by a RF generator at 13.56 MHz at 120 V_{pp}. The upper electrode and the surrounding walls are grounded. In the center of the upper electrode a grid is installed through which particles can be transfered into the chamber.

In the center of the electrode a smaller glass box is placed. Its side length is reduced to 2 cm due to the smaller electrode diameter. Besides, the box is the same as the one employed in Munich. In Kiel two experimental series have been performed. During the first series the connectors to the function generators were fixed to the center of the glass box. During the second series the connectors were attached at the poles. In combination with the finite conductivity of the ITO glass plates an asymmetry in the rotating electric field is introduced. This results in an asymmetry in the cluster reaction as it is displayed in figure 8.4.

In difference to the experiments discussed in chapter 7 the usage of thermophoretic forces led to a non spherical shape of the cluster. If the lower electrode was heated the particles moves upward at the edges of the box rather than form a spherical cloud in the center of the box.

Even though the confined cluster is of roughly the same spacial size it is composed of less than 100 particles. Since the particles are much bigger than the ones employed in the experiment described in the previous section the inter particle spacing is higher.

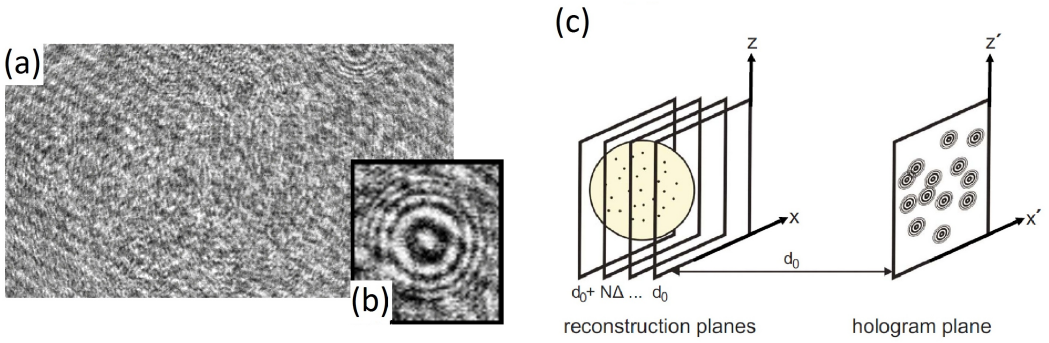

Figure 8.2: Sketch to explain the particle identification method. In plane the particles are recognized by the interference patterns of a cluster as shown in (a). In panel (b) the interference pattern of a single particle is displayed. To gain the particle positions along the laser beam imaginary slices are introduced to the cluster. This is displayed in panel (c), [118].

8.2 Parameters

For the given discharge settings (118 V peak-to-peak voltage applied to electrode; 32°C bottom electrode temperature; 20 V peak-to-peak voltage applied to each ITO plate, controlled by function generators) in the performed experiments the plasma parameters have been estimated as follows[1]: the electron temperature is T_e ≈3 eV, the electron-to-ion temperature ratio T_e/T_i ≈100, the plasma density n≈10^9 cm^{-3}. Subsequently, one can estimate the electron Debye (screening) length to be of the order of λ_{De} ≈400 μm and the ion mean free path λ_{ia} ≈770 μm [2].

The particle charge is expected to be of the order of Z=(40000-50000) elementary charges, as 'standard' theoretical approximations, OML [25], DML [158], or 'modified' OML [102], allows to estimate. Note that in the presented conditions the ratio N_d/Z∼2-3 is not that big. (N_d is the 'standard' number of electrons inside the Debye sphere). Therefore, due to depletion [1], the real charges can be expectedly smaller.

In experiments with small clusters, constituted by 2-3 charged particles, the particle charge and the damping rate can be measured directly by exploring the reaction of the clusters (actually the single particle strings) to the harmonic excitation applied to the lower electrode [40, 41]. The measurements are based on the well-known vertical resonance method testing the phase resolved reaction of the particles to the excitation. In this very setup a series of such measurements has been performed with a single particle, two particles and three particles confined in the box. Based on the estimated plasma parameters the experiments allow to determine the charge of the particles. The upper particle charge is in the order of the 40000 electrical charges, while the charge of the lower particle is reduced by 30%. As discussed in chapter 6 the situation might be quite different for the confined particle cluster.

[1]Note that those are normally the typical bulk plasma parameters obtained, see, e.g. [161].
[2]ion-atom charge-exchange collisions [181, 174] are assumed to be dominant

The effective damping ($\sim$10 s^{-1}) was calculated to be in a fairly good agreement with the predictions in relationship (8.2).

8.3 Rotation

The resulting particle positions in the clockwise or counter clockwise rotating cluster as observed during the first, symmetric sequence at 5 kHz are displayed in figure 8.3(a) and (c). The two rotation directions differ a bit which is caused by the neutral gas drag, the magnetic field of the earth and other possible forces acting on the particles. A similar asymmetry has been observed in the previous chapter.

The complete information on the particle positions at all times helps to understand the internal mechanisms of the cluster. This revealed a shell rotation which has not been observed this way in the previous experiments.

Throughout this chapter the three cases displayed in figure 8.3 are discussed. The two rotating clusters (top and bottom) are compared to a static case. In this case a rotating electric field with a frequency of 1 kHz is applied. The cluster does not rotate in response to this field. Thus, it is referred to as the 'static' or 'non-rotating' case. The rotation speed for the cluster subjected to a frequency of 5 kHz is calculated to about 0.2 s^{-1}. This is in good agreement with the results displayed in figure 7.4.

In figure 8.4 the rotation of a cluster recorded during the second, asymmetric sequence is displayed for different electric field rotation frequencies. The cluster is subjected to electric fields rotating clockise (left hand side, figure 8.4) and counter clockwise (right hand side, figure 8.4). It can be seen that the cluster rotates in discrete shells. As the frequency increases the inner particles of clockwise rotating clusters are more and more at rest. However if the frequency is increased further and the cluster rotation behavior flips. If applying a counter clockwise rotating field at this frequency the cluster is static.

In difference to the earlier experiments in Munich a stronger asymmetry on the cluster reaction can be observed. This is be due to the asymmetric wiring of the glass box. The function generators were attached to the corners of the box. Since the conductivity of the ITO coating is finite the distribution of the voltage above the plate is decreasing.

Furthermore, the plasma and the confined cluster are different to the cluster observed at Munich. The observed behavior is quite similar to the observations of Nosenko *et al.* [166] where the rotation direction flips at a certain frequency. Above this frequency the cluster is considered to be mainly driven by the ion drag. That the rotation reversal is not observed for the two rotation directions at the same frequency is due to the asymmetric wiring of the box. It can be concluded, that the asymmetric wiring suppresses the effect of the delayed charging and thereby the torque due to the electric field force.

As discussed in the previous chapter the rotation speed varies depending on the height. The results displayed in figure 7.7 indicate that the liquid-like cluster suspended in the glass box at Munich rotates faster on the lower edge than on the upper one. In the situation displayed in figure 8.4 is quite opposite. The lower particles move slower than the upper more ones. It has also been found that the motion of the lowest particles is rather chaotic.

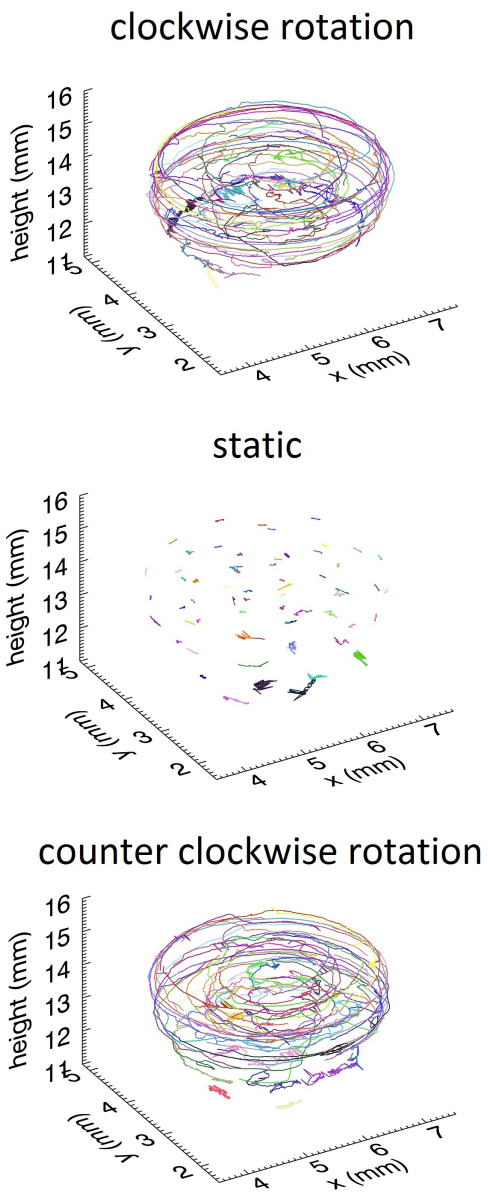

Figure 8.3: A spherical cluster as recorded and analyzed during a collaboration with the group in Kiel. It is subjected to a clockwise (upper most graph) and a counter clockwise (bottom) rotating electric field at 5 kHz. In the middle the same cluster is presented. In this case the applied electric field is rotating at a frequency of 1 kHz. This rotation frequency is too low for the cluster to rotate in response. Each line represents the track of an individual particle.

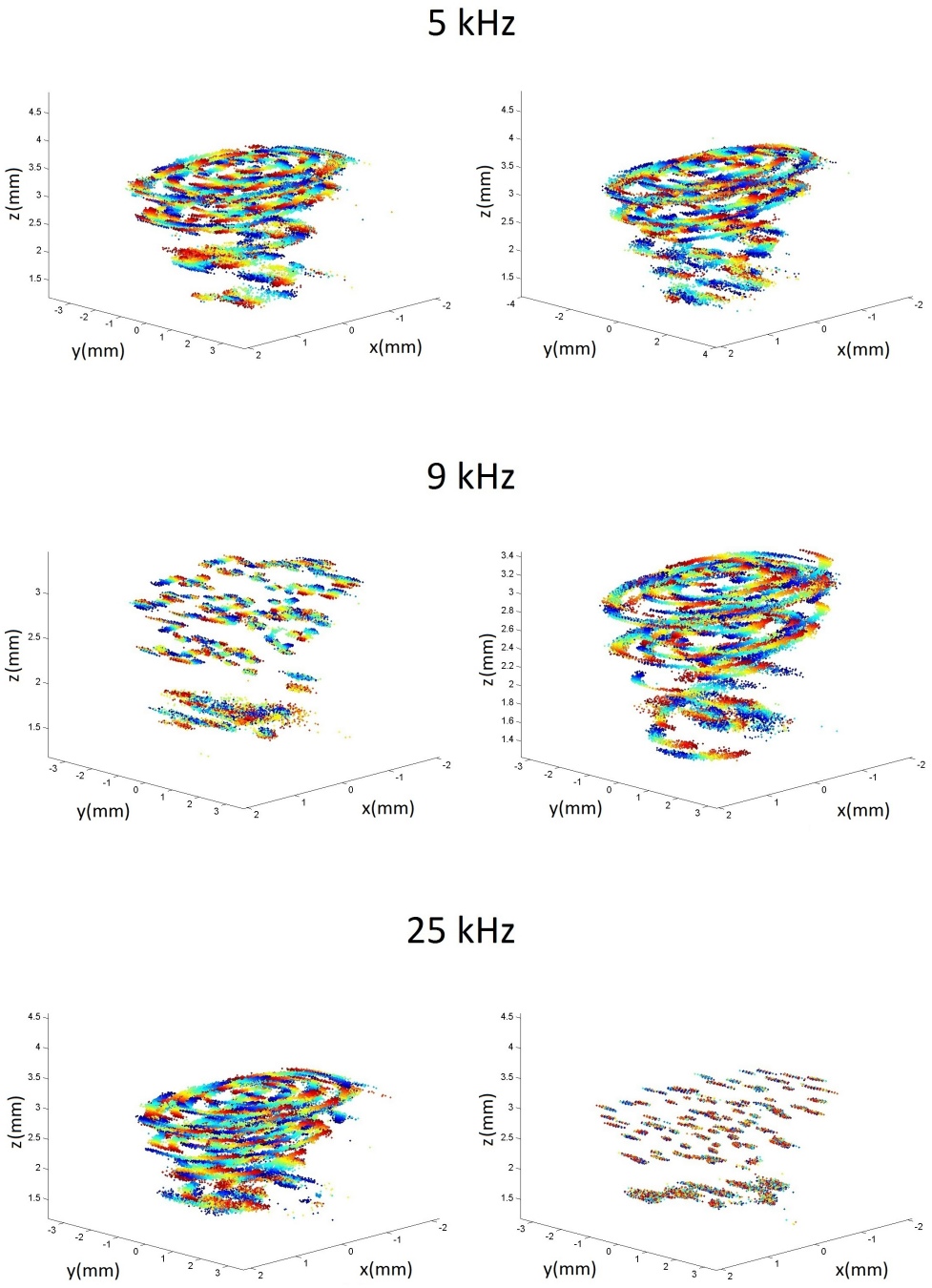

Figure 8.4: Shell rotation as seen in a cluster for different excitation electric field frequencies (Right hand side: clockwise rotation, left hand side: counter clockwise rotation). The time is displayed by the color coding. Early particle positions are given by blue, later by red colors.

This is not surprising, but, as the cluster is very small and the particles are very big the portion of particles showing this motion rather than following the electric field is relatively high. Nevertheless, the differential rotation observed in the displayed cases is also caused by the dragging effect.

In the following only the cluster displayed in figure 8.3 will be discussed.

8.4 String Analysis

8.4.1 Spatial Correlation

The particle ordering is studied by using the procedure schematically sketched in figure 8.5(a). Two different coordinate systems are introduced to describe the particle positions. The center of mass system (CMS) of the cluster is calculated by averaging over all particle positions at all frames. Therefore the origin of this coordinates system remains immobile while the actual position of the center of mass might deviate from one frame to the next. The radial distance of each particle to the origin of this coordinate system is calculated. Around each particle a vertical cylinder with radius of r_{cyl}=200 μm is placed as shown in figure 8.5(a). If a second particle is found inside this cylinder it is considered to be in pair with the first one. By this method the particle pairs and combinations with higher particle numbers can be identified. In figure 8.5(b) some examples taken from the experimental data are displayed. The strings are composed of two, three, and four particles and are elongated mainly along the z-axis.

The cylinder radius r_{cyl}=200 μm introduces a geometric limitation to the strings. The particle strings are considered ruptured once a particle moves out of the cylinder. To emphasize this limitation the actual radius of the cylinder (r) is plotted versus the polar angle ($\theta \cdot r$) for the three discussed cases, see figure 8.6. The geometric limits to the analysis are indicated by the red and the blue lines in these plots. However, considering interacting strings rather than only accidentally paired ones the geometric limit is sufficient. According to the vertical ordering parameter as introduced by refs. [105, 131] a particle combination with a polar angle θ of less than 10° is considered a string. Thus, an interacting particle string is expected to be within the set limitations. The angular distributions will be discussed later.

The criteria of counting several particles as a string are illustrated in figure 8.7. First the distances between all particles in the xy-projection (top view) are calculated, resulting in a distance matrix. Two particles are considered to be in a string if their distance is below threshold. Every black dot in figure 8.7(a) indicates that the distance between the two particles i and j is below the threshold introduced by the cylinder radius, see Fig. 8.5. The maximal distance (threshold) is indicated by the radius of the cylinder r_{cyl} shown in figure 8.5. In what follows, r_{cyl} is chosen to be 200 μm, that is about half of the Debye radius, see section 8.2.

Figure 8.7(b) shows a top view of the actual particle positions. If the distance between two or more particles is below threshold they are marked red. The shown circle

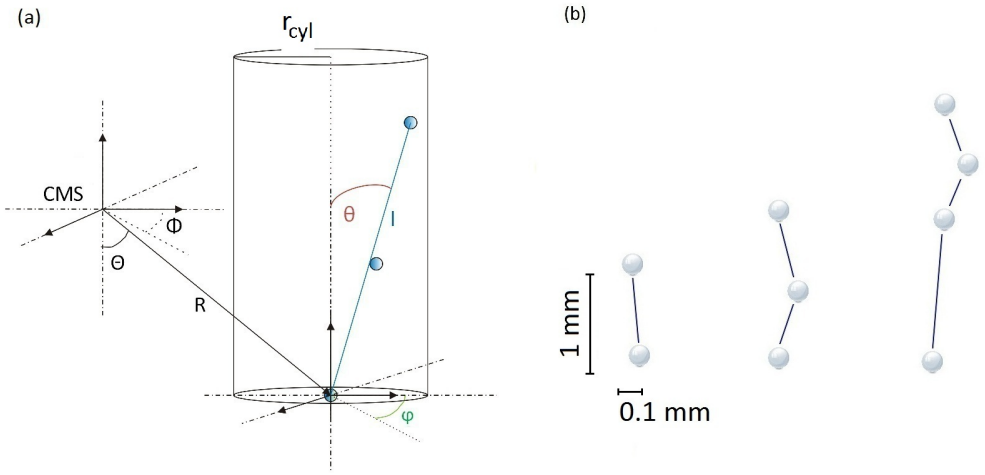

Figure 8.5: (a) Coordinate systems together with a sketch illustrating the string identification procedure. The center of mass system (CMS) has been obtained by 'global' averaging over all frames and all particle positions. It is used as a convenient 'bench mark' to describe the particle positions (the corresponding spherical coordinate system is introduced by the capital letters as R, Θ, and Φ). To analyze the vertical particle arrangement, around every particle comprising the cluster (filled circles in the figure), a cylinder is centered around its position (with a radius r_{cyl}=200 μm well below the inter-particle distance). Everything within that cylinder is considered to be a string. To describe the strings interior structure an additional internal coordinate system (conventionally originated at the lowest particle of the string, and designated as l, θ, and φ) is introduced. (b) Three examples of the strings composed from two, three, and four particles tracked by the procedure described above. The strings scaled spatially as indicated in the figure.

demonstrates the radius of the cylinder employed in the analysis as introduced in figure 8.5. Importantly, the circle diameter is way below the mean inter particle distance in the xy-plane.

The top view of the cluster in figure 8.7(b) shows that basically all particles are organized in vertical strings. Only very few particles remain alone. Furthermore, the space in-between two strings is larger than the usual horizontal elongation of a string. Thus, most of the particles are well aligned in vertical direction (along the z-axis).

8.4.2 Temporal Correlations

Another important criterion is the life time of a particle string. Studying the lifetime of particle associations one can easily distinguish *particle pairs*, which only occasionally happened to be close to each other, from *persistent particle pairs* or *strings* which are interacting with each other by wake field attraction. The easiest way to distinguish the two is via the time the particle distance is below threshold. If two or more particles are fairly close for a considerable amount of time and follow the motion of the applied electric field, they can be assumed to be a string.

Examples of three particles (A, B, and C) being part of different identified strings are

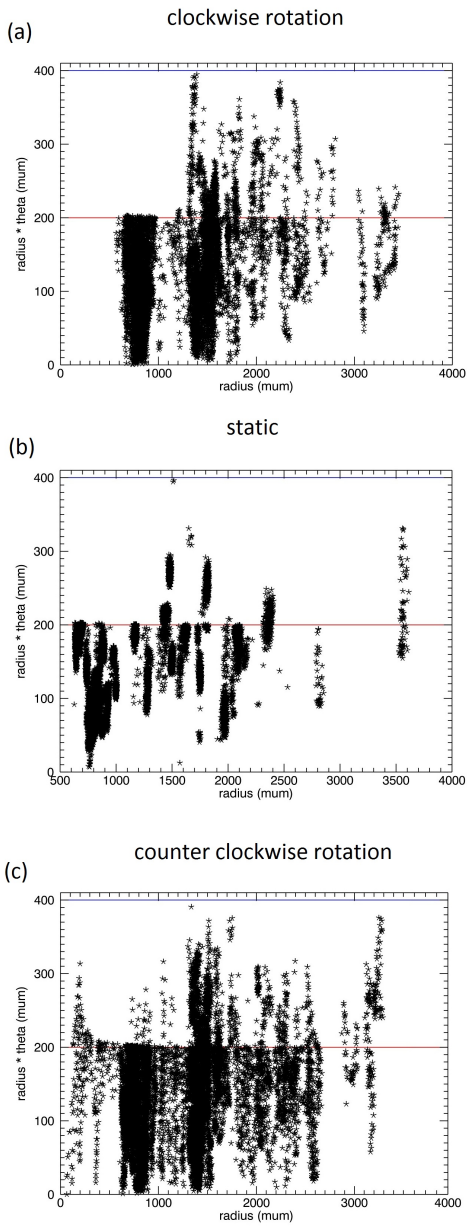

Figure 8.6: Geometric limitations are displayed for three cluster rotations: (a) clockwise rotation, (b) static, (c) counter clockwise rotation. The red and the blue lines indicate the geometric string limitation.

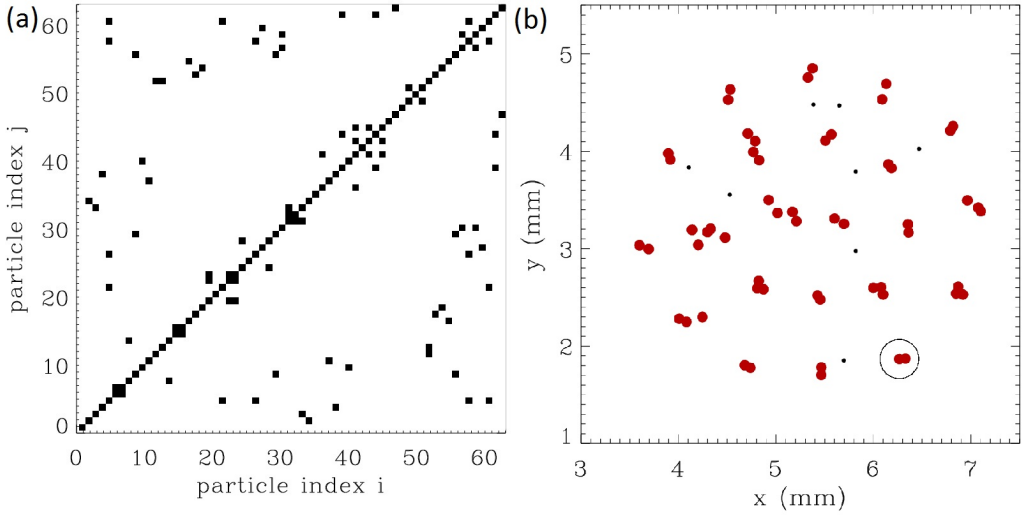

Figure 8.7: (a) Below threshold distances between all particles and (b) a top view of the cluster consisting of 64 particles in a single frame. The black entries in the distance matrix in panel (a) indicate a distance below threshold. The particles having a distance below the threshold are considered to be combined. Thus the black points in panel (a) result in the strings displayed in panel (b). The red colored particles are those being in combination with at least one other particle at the chosen frame. In addition to the vertical alignment a structuring in the xy - plane can be seen. The strings tend to be organized in a lattice with certain symmetry, see figure 8.13. The circle in panel (b) indicates the chosen threshold. It has a radius of 200 μm, that is about half of the Debye length λ_D. The mean inter-string distance, being determined by the Debye screening length, is about two times larger, see section 8.5.3.

displayed in figure 8.8. Those three examples show typical behaviors of strings and serve well to understand the analysis as well as the string recognition procedure.

Particle A is coupled to another particle all the time, forming a string. The corresponding string length is almost constant. Particle B shows how a particle can interact with two different strings. For quite some time it is alone, traversing from the inner to the outer shell. Particle C stays in the same shell at all times but the composition and length of the corresponding string changes with time.

8.5 Description of Strings

8.5.1 String Identification

The main results are the identification and analysis of the structural and temporal particle string characteristics within 3D clusters during their rotation. In figure 8.9(a) the histogram of the coupling time intervals is shown. The cluster (clockwise rotating) consists of 64 particles. The coupling time interval is introduced as the time duration at which any particle is combined (coupled) to at least one other particle.

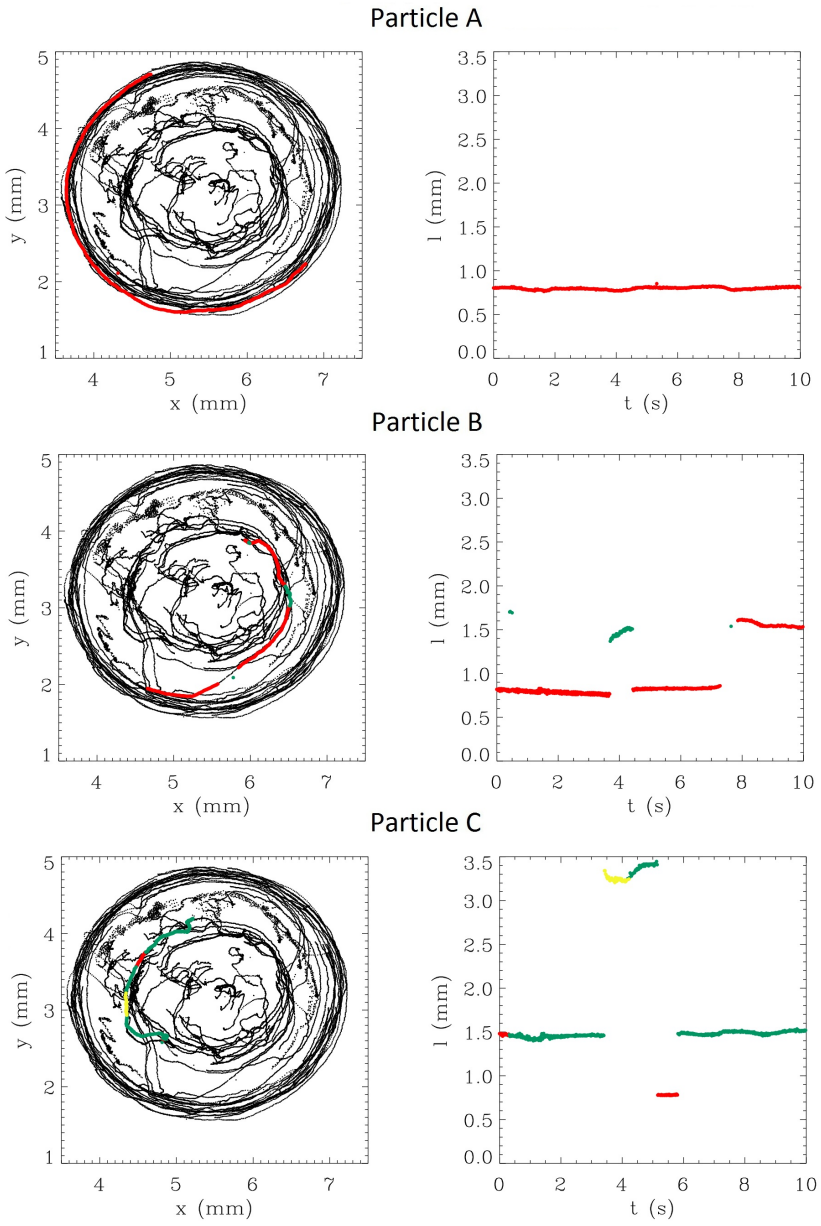

Figure 8.8: String formation and dynamics. Three representative examples of the evolution of the particles labeled as A, B, and C and their trajectories illustrate the string formation discussed in the text. The particle A is in a 2-particle string which remains stable all over the observation time. Particle B during evolution interacts (collides) with two different strings along time. Particle C contributes to one string which is composed from two, three, and four particles. The panels on the left: Top view of the cluster with the superimposed (over all 500 frames) particle positions. The panels on the right: Time evolution of the string length and the particle associations. The particle positions and the association to other particles are highlighted by color: (black) single, (red) two, (green) three, and (yellow) four particles.

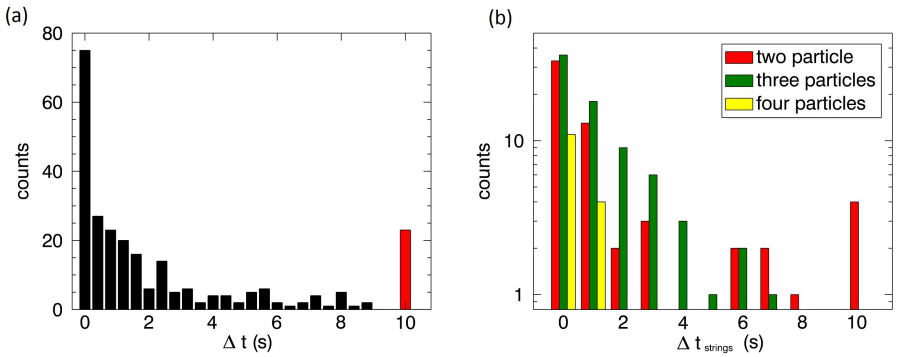

Figure 8.9: Life times and string composition demonstrated at the example of a clockwise rotating cluster at 5 kHz (20 V peak-to-peak on each plate) electric field rotation. (a) Histogram (bin size = 0.4 s) of the coupling time intervals Δt (irrespective to the string composition number): (black bars) all entries with the time intervals shorter than 10 s, (red bar) the 23 entries corresponding to the long-term coupling, Δt=10 s. Every particle is counted as many times as it appeared to be coupled. The most of strings are apparently short-living, 0-0.4 s. (b) Histogram (bin size = 1 s) of the time intervals $\Delta t_{strings}$ computed exclusively for the particles the entire time coupled (comprising the red bar in the panel (a)). The strings composing of 2, 3, or 4 particles are shown only. $\Delta t_{strings}$ is calculated in the same manner as Δt in (a), see text for details.

It is worth noting that, to understand the composition of the histograms shown in figure 8.9 better, figure 8.8 helps a lot. The key point is to explain the differences between the number of entries per particle. For instance, particle A (the upper two panels in figure 8.8) evidently contributes to both histograms (a) and (b) in figure 8.9 since it was coupled to exactly one particle for all 500 frames (equals 10 s). Particle C (two bottom panels in figure 8.8), making only one entry in panel (a), being an element of a few strings having different composition numbers, makes several entries in panel (b). Whereas particle B (two middle panels in figure 8.8) would make no entry in panel (b), because only the entries marked 'red' in (a) were taken into account. Note also that the integral of the entries shown in panel (b) gives the total number of realizations (23·500) in the red bar in (a). The strings considered are composed from two, three or four particles.

The black bars in figure 8.9(a) indicate particle pairs, at the most not coupled, whereas the red bar represents the particles remaining combined with another one during the whole observation time, for all possible string composition numbers. (The string composition number is introduced as the number of the particle comprising the string.) It can be seen that many particles stay in combination with another particle for very short times only [the short-time peak in figure 8.9(a), Δt<2 s], or merely 'fly-by' with Δt=0-0.4 s. Importantly, there is another peak of the long-living coupling events at Δt=10 s. In between the two peaks basically no entries are observed. Thus particles are either combined throughout the whole observation time or for very short time intervals only. Note that during the 10 s of observation the cluster performs a little more than half a turn, leading to a rotation period of about 14.9 s.

The histogram of the time intervals for the long-time coupled particles is displayed in figure 8.9(b). Included into this plot are only the particles which are coupled all times. The distribution of strings with different composition numbers is displayed. It can be seen that the fly-by phenomenon is present in this case, too. Especially long strings composed of four or more particles tend to exist for only very short times. Furthermore, the most probable and most stable composition of particles is a doublet – a coupled pair of particles. One can see that the particle strings dissociated and recaptured particles along their path.

8.5.2 String Lifetimes

One of the unexpected results of this study is the fact that the system of strings formed in the clockwise or counter clockwise rotating clusters are differently stable. The three left panels in figure 8.10 show the histograms of the observation time Δt of certain string compositions observed in the experiments with the same 64-particle cluster but at different frequencies of the driving electric field. The single particle 'lifetimes' are also present to emphasize the role of the inter-string association and dissociation processes.

In case of the clockwise rotating cluster the two-particle strings observed the entire time existing (figure 8.10, upper left plot). In case of the counter clockwise rotation the longer strings happened to be less stable (figure 8.10, lower left plot). The system might be considered to be more disordered, 'fluid-like' as compared to the case of clockwise rotation. However short-living longer strings still formed. In addition the non-rotating cluster statistics is displayed (figure 8.10, central left plot).

Histograms of the number of particles per string is shown in the plots on the right hand side in figure 8.10. It can be seen that doublets strings are the most probable string configuration. This is true especially for the 'static case'[3] , where the associated particles mainly form doublets. This might be interpreted as the self-organization of the particles in a system of spherical shells as it has been observed for example by Arp *et al.* [4] and Ivanov and Melzer [92]. For static configurations an interplay between string and spherical structures has been shown by Kroll *et al.* [118] and Block *et al.* [22]. Due to the way the analysis works particles orientated in spherical shells will not be recognized as such but be occurring mainly as singlets or doublets. If the cluster rotates it restructures. The spherical shell symmetry breaks and is replaced by a cylindrical one. Consequently, the vertical string interactions becomes dominant which is indicated by higher percentage of occurring triplets, quartets and quintets.

8.5.3 Individual String Geometry

The individual strings are dominated by wake field interaction. In the driven systems the internal ordering increases. If the driving frequency is in the right regime the cluster starts

[3]Note that what is referred to as the 'static' or non rotating case only describes the absence of observed cluster rotation. In the case discussed here a counter clockwise rotating electric field with a frequency of 1 kHz has been applied. Furthermore, the behavior of the cluster is not completely static but dominated by particle fluctuations. The electric field applied contracts the cluster.

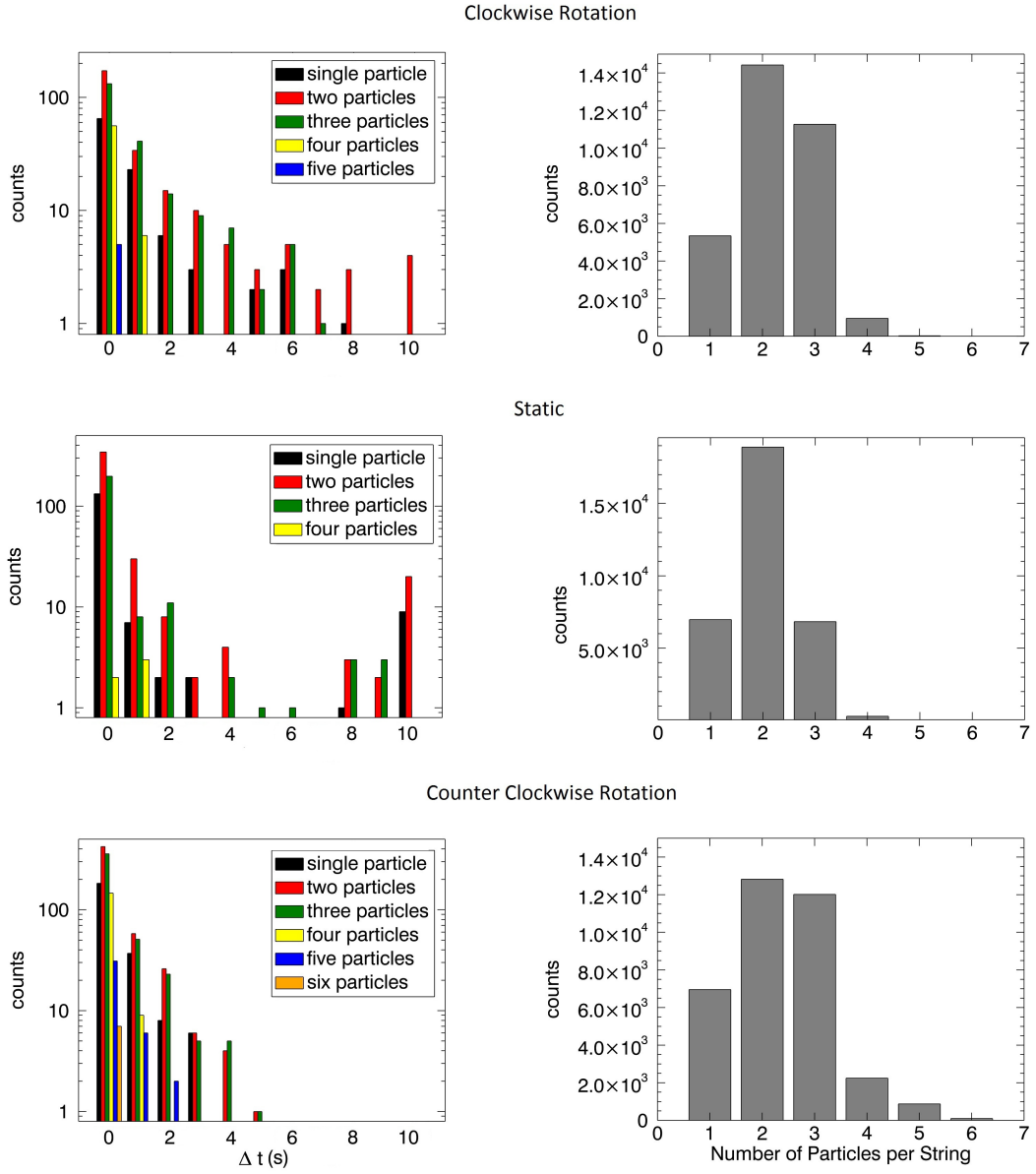

Figure 8.10: Histograms of the string lifetimes obtained with: (top panels) a 5 kHz ac rotating electric field, the clockwise rotating cluster, (middle panels) a 1 kHz ac rotating electric field, the non-rotating cluster, and (bottom panels) a 5 kHz ac rotating electric field, the counter clockwise rotating cluster. The left panels: The lifetime histograms of the strings with a range of the composition numbers from 1 to 6 (if occurring). The associations with the single particles are indicated as well. The right panels: The occurrence plots of the number of particles per string. The doublets and the triplets are the most probable composition of the strings in the rotating complex plasma, whereas the non-rotating cluster is dominated only by doublets. All three experiments were performed with the same 64-particle cluster.

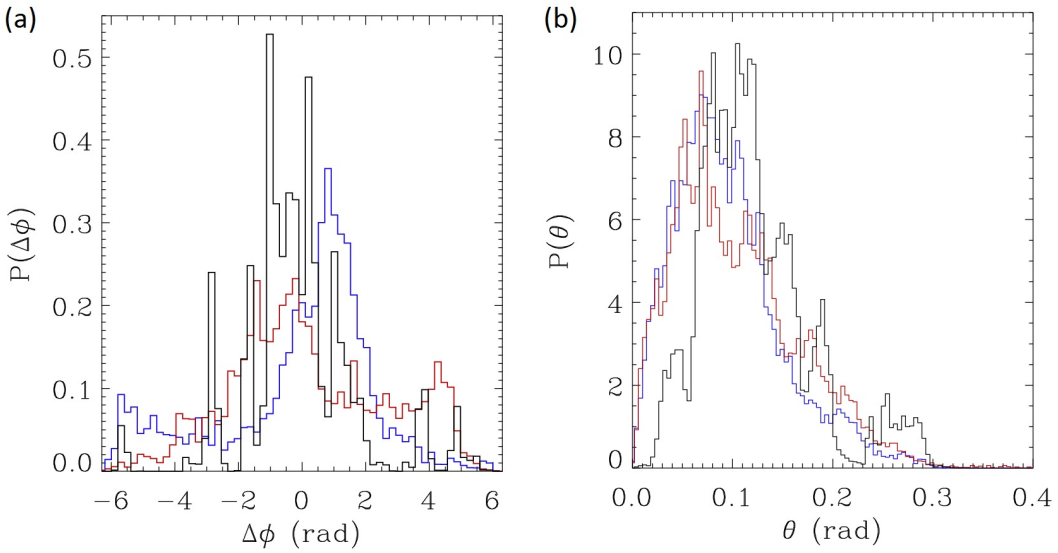

Figure 8.11: Azimuthal $\Delta\phi = \Phi - \phi$ (a) and polar θ (b) angle probability density for all particle strings as introduced in figure 8.5. The probability density is calculated from the distribution by normalizing the area under the curve. It is displayed for three situations: counter clockwise rotation (red), clockwise rotation (blue), and no rotation (black). The azimuthal probability distribution in the static case the main peak is located at zero, whereas the main peak is shifted towards $\pi/2$ (-$\pi/2$) for clockwise (counter clockwise) rotation. This can be interpreted as the lower particle being towed behind the upper more one. For the polar angle the way the analysis works on the data a upper limit at about 0.3 rad (≈20°) of the angular distribution is introduced. The absence of entries at θ=0 is due to the carousel effect caused by the rotation. Furthermore, it can be seen that in the static case the most probable polar angle is much higher than in the rotating ones. It seems that the introduction of additional forces leads to a more straight orientation of strings.

to rotate. As it will be described in this section this leads to a more vertical orientation of the strings (polar angle $\theta \approx 10°$), see figure 8.11(a). The rotation has another effect on the string structure. As wake field interaction is supposed to be dominant the lower particle is connected to the upper one at all times leading to a dragging of the lower particle. Thus the azimuthal angle $\Delta\phi = \Phi - \phi$ of the strings is shifted towards $\pi/2$ $(-\pi/2)$ for clockwise (counter clockwise) rotation, see figure 8.11(b).

The distribution of strings along the radius of the cluster varies. According to their position in the cluster the probability of particles being combined with another varies as well. Due to the spherical shape of the cloud more layers of particles exist in the central region. Thus, the string length is expected to be longer at the cluster center. As it can be seen in figure 8.12(a) the string lengths distribution is discrete. Furthermore, it can be seen that the longest strings do not occur in the center but at an intermediate position of the cluster. This is due to the fact that the particles in the cluster do not inherit the inner most position but rather a cylindrical shell a little space apart, as it can be seen for

instance in figure 8.8. The color coding in figure 8.12(a) is the same as in figures 8.8, 8.9, 8.10: Strings composed of two particles are marked red. Those composed of three particles are green. Four particle strings are yellow and those with five blue. As it can be seen the discrete particle string length is not only linked to the radial position but also to the number of particles in the string. In case of the rotating clusters strings with a certain number of particles mostly have the same length. Thus, it can be assumed that the inter particle distance along the particle string is nearly always constant. This is enhanced by the fact that the layers are equidistant. Hence any additional particle elongates the string by the same length. This is due to the distance of the wake interaction being responsible for the vertical confinement.

Since the particle strings have discrete lengths an inter particle distance Δl_{part} in a string can be calculated from them:

$$\Delta l_{part} = \frac{l}{n-1}. \tag{8.3}$$

With l being the length of the string and $n \geq 2$ the number of particles in the string. The resulting distributions are displayed in figures 8.12(a) for clockwise rotation, (b) for the non-rotating cluster, and (c) for counter clockwise rotation. From these distributions it can be seen that the length of the string increases with the string composition number while the inner inter-particle distance shrinks (i.e. the string shrinks when further particles are added to it). Furthermore, the presence of rotation leads to a drastic change in the distributions. While very broad in the non-rotating case, clear peaks in the distributions appear if the cluster is set into rotation. This can be accounted for by the change in the effective potential induced by the rotation. The mean inter particle distances for the three cases are shown in table 8.1. It is about 0.9±0.1 mm if all events are taken into account. It increases a bit if only doublets are concerned and shrinks for triplets. In this table no error bars are given since the distributions of the inter particle distances are quite broad, see figure 8.12. Hence no reasonable error estimations for the mean inter particle distances for the values given in table 8.1 corresponding to strings containing more than three particles can be given. The overall length of a string composed, e.g. from three particles, may be longer than the one composed of only two particles, but on average, three-particle strings are internally more compact. The shrinkage of particle strings with higher particle numbers is of the order of 30 % if compared to doublets. Note, that 2D plasma crystals are nearly incompressible in the elasticity sense [226].

From the angular distributions the vertical particle interaction can be proven. In figure 8.11(a) the development of the azimuthal angle $\Delta\phi = \Phi - \phi$ in all three cases are displayed. This angular distribution describes the orientation of the lower particle with respect to the upper one. Remember, that the capital Φ describes the azimuthal angle of the projection in the center of mass system, while ϕ describes this angle in the inner string system, see figure 8.5. In figure 8.11(a) it can be seen that the main peak for the rotating clusters is slightly different from zero. Dependent on the rotation direction the asymmetry in the distribution changes. If two particles would be perfectly aligned, and the upper would always precede the lower particle, the azimuthal angle $\Delta\phi$ would display a phase shift

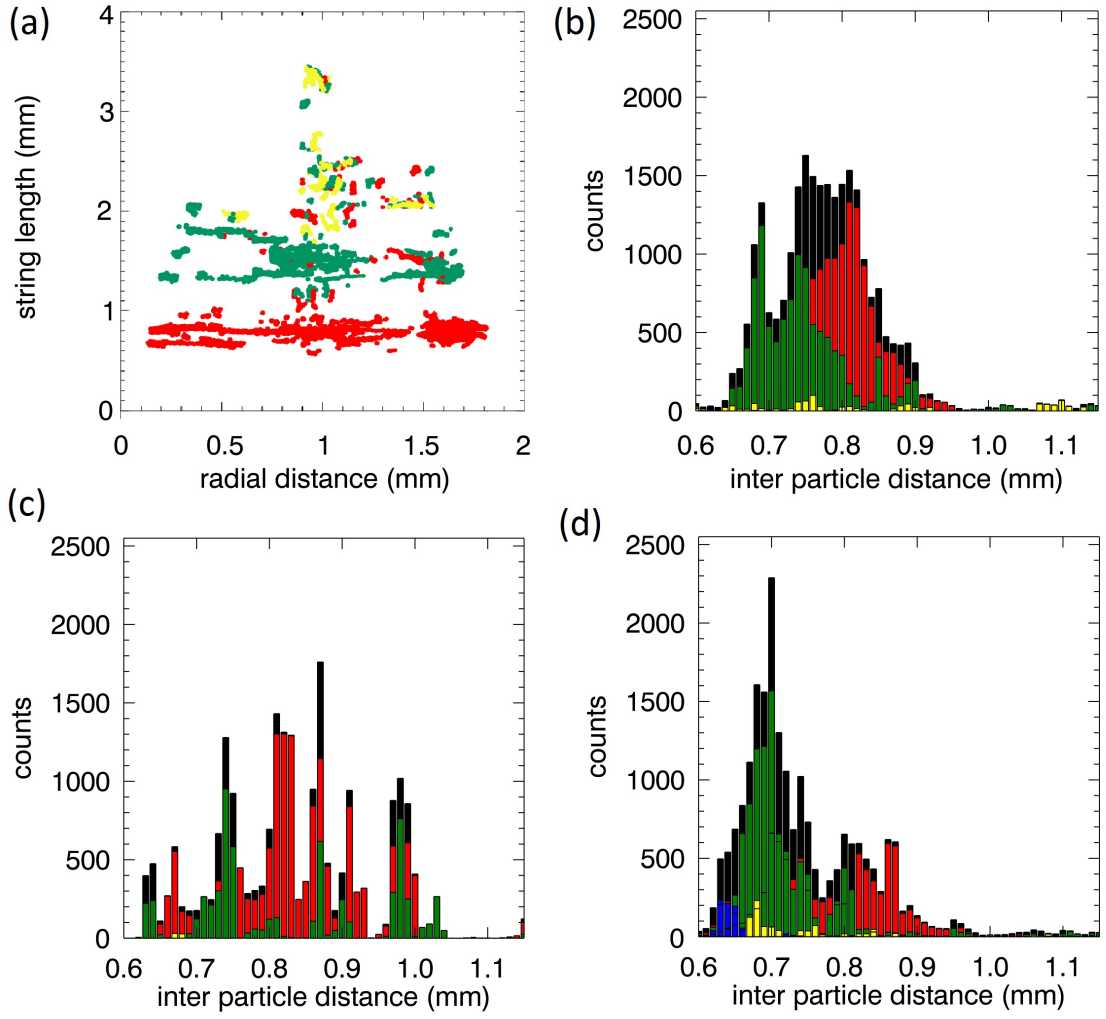

Figure 8.12: String length and in-string inter-particle distance. Distribution of the length of the strings vs. radial (XY-projected) distance to the CMS, shown for the clockwise rotating cluster (a). Two main effects can be seen immediately:(i) the discreteness of the string length distribution is well pronounced and (ii) surprisingly, the longer strings are located dominantly not in the middle of the cluster. (b, c, d) Histograms of the in-string inter particle distance Δl_{part} computed for: (b) the cw-rotating cluster, 5 kHz driving ac-field [same as in (a)], (c) non-rotating cluster,1 kHz driving ac-field, (d) ccw-rotation, 5 kHz driving ac-field. Note that statistically the triplets are relatively more compact 'constructed' than the doublets, for all cases $\left\langle \Delta l_{part}^{doublet} \right\rangle > \left\langle \Delta l_{part}^{triplet} \right\rangle$. For longer strings the statistics is poor. Color coding: (black) all events, (red) doublets, (green) triplets, (yellow) quartets, (blue) quintets, and (orange) sextets

Table 8.1: Mean inner-string inter-particle distances expressed in mm for the cases: clockwise rotation (cw), no rotation (nr), counter clockwise rotation (ccw). The mean distances calculated: (i) for all strings irrespective to their length, and (ii) separately for the strings consisting only of two, three, four, five, and six particles (if available). As it is shown in figure 8.12 the distributions of the inter particle distances are quite broad. For any string consisting of more than three particles the distribution even gets too broad to determine any reasonable width. This is also true for the static case. Thus, no error bar will be given in these cases. Taking into account all events, only doublets, or only triplets the width of the main peak is in the order of 0.2 mm. Thus, the error in these cases can be estimated to about ±0.1 mm. For the other cases the error is quite large as is can be seen in figure 8.12.

case	all events	doublets	triplets	quartets	quintets	sextets
cw	0.83	0.87	0.78	0.85	0.64	–
nr	0.96	0.99	0.86	1.09	–	–
ccw	0.84	0.99	0.74	0.62	0.64	0.51

of plus or minus $\pi/2$, depending on the rotation direction. It can be deduced that the rotation is due to 'towing' of lower particles in contrast to previous experiments. In these experiments the cluster was almost liquid-like. Thus the vertical coupling of the particles is limited and the rotation is driven on each layer. Hence the ion energy gain while traversing the cluster is responsible for higher rotation velocities on the lower edge of the cluster.

In the experimental series reported here the vertical coupling is determined by the wake field interaction. The lower particles are attracted by the positive wake potential downstream the upper particles. Thus the motion of the lower particles is not driven individually but dominated by the rotation of the upper ones. This is described as the 'dragging effect'.

Due to the rotation the lower particles inherits a position a little different than in the static case. This is shown in figure 8.11(b). The particles are drawn inwards as the cluster rotates with respect to the static case (black curve). The maximal angle displayed shows the rupturing of strings and is below the geometric limitations. The overall 10° degrees difference, as observed for the rotating clusters, are way below the string rupture angle discussed in ref. [151]. According to refs. [105, 131] a vertical ordering parameter (VOP) is introduced. It describes the ratio of strings with a polar angle of less than 10° to all observed particle pairs. According to this almost the entire particle cloud shows a high vertical order.

In addition to the mentioned dragging effect a string constant could be calculated. The estimations of this constant rely on inner-string oscillations. Due to very strong pixel-locking, for a review see e.g. Feng *et al.* [61], in the reconstructed particle positions no value for it can be given at this point. Further investigations and refining of the experimental method as well as of the reconstruction are necessary to gain insight into the inner-string interactions.

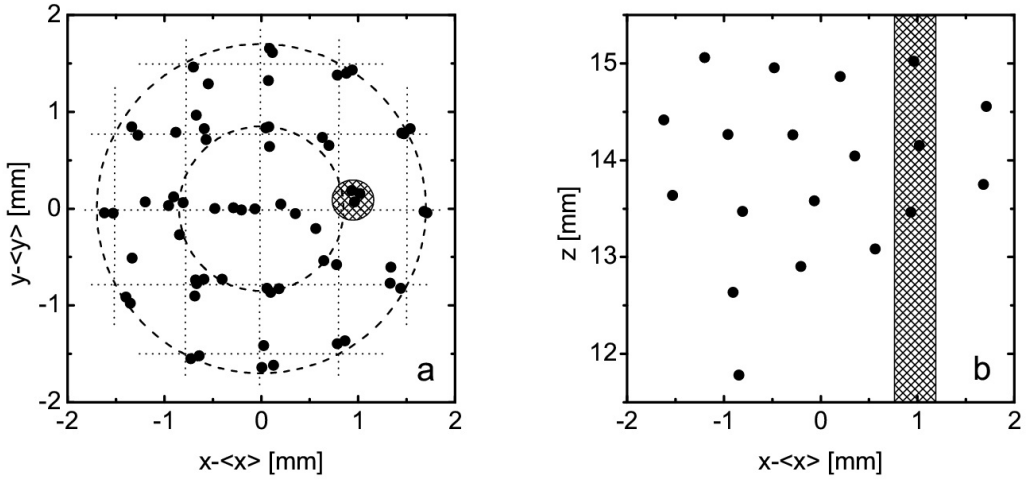

[ht]

Figure 8.13: Competing symmetries in a rotating cluster. (a) X,Y projected particle positions (black dots) are structured either as a system of cylindrical shells (dashed lines) or squares (dotted lines). The dotted and dashed lines are included to guide the eye and are not calculated from the cluster symmetry. The inner dashed circle has a radius of 850 μm, the outer of 1700 μm. The dotted lines grid has a box side length of 770 μm. Both symmetries are meta-stable, the resulting symmetry alternates from shells to squares while the cluster rotates. (b) The wall of the string in the cluster center (Side-view is taken for: -500 μm<(y-$\langle y \rangle$)<500 μm). The shadowed circle (of 0.4 mm diameter) in (a) and the shadowed rectangle (of 0.4 mm width)in (b) indicate position of the tracked three-element particle string.

8.6 Global Cluster Symmetry

Global symmetry in the cluster has been observed. In the top view displayed in figure 8.7 it can be seen that the particles are organized. Several different structures can be seen. The most striking is a cylindrical shell structure which is emphasized in figure 8.13(a) by the dashed circles. Next to it the strings tend to organize themselves in squares while the cluster rotates. These are indicated by the dotted lines. Both structures are meta-stable and the symmetry of the cluster changes from one to the other while it rotates. A behavior like this, where two interactions are constantly in competition which each other forming structures, can also be found in colloids [192, 178, 217] and in quantum states in superconductors [197].

In figure 8.13(b) the central section of the cluster along the z-axis is displayed. The vertical strings are very obvious. But in addition to the strings secondary structure occur. The organization of particles in hexagons in this plane can be seen. This competition of structures resembles the phase transitions observed in electrohereological plasmas [95].

The observed cylindrical shells are very similar to the predictions by Brandt [34], see figure 6.2. The layers are cylindrical due to the additional confinement. The separation of the cylindrical layers is also in quite good agreement with the predictions.

Thus, it can be concluded that the structure of a rotating system is dominated by

cylindrical rather than spherical shells leading to the observation of longer strings than in the non-rotating but driven system. In contrast to this a non-driven system is dominated by the spherical shells [4]. Furthermore, it can be assumed that the rotating electric field introduces an anisotropic electric field of sufficient strength. Thus, an attractive dipole-dipole interaction as described in equation (2.15) with $\xi < 0$ may be responsible for the cylindrical shell structure.

As predicted, the interaction potential responsible for the ordering in cylindrical shells and vertical strings can be tuned by the rotation frequency. The larger the difference between the optimal and the applied frequency the stronger the spherical shell structure is pronounced. Furthermore, the vertical string alignment is less straight for lower frequencies. This has been displayed for 1 kHz in comparison to an excitation frequency of 5 kHz. In subsequent experiments this trend has been observed, too. If a rotating electric field with a frequency of only 500 Hz is employed the cluster structure is almost not affected[4]. The distribution of the polar angle θ has shown to be completely homogeneous inside the possible range[5].

8.7 Possible further Experiments

The purpose of the experiments was to determine the particles at all times gaining more information on the driving mechanism. Besides the string configurations found some hints on this have also been found. However experiments dedicated to the rotation have to be repeated. Therefore the initial moment of excitation is of great interest.

In addition different kinds of sloshing modes are interesting. The response of the cluster to dipole and quadrupole excitation has thus already been measured. But as mentioned above the analysis of the data is rather complicated. Thus no results from these measurements can be given yet.

Furthermore the confinement inside of the box is not fully understood. Further experiments on this employing particles as probes are therefore preferable.

Another frequency scan increasing the dipole-dipole interaction has to be performed. In this series the ordering in vertical layers and the phase transition could be investigated.

8.8 Summary

As it has been shown in the previous chapter, a confined cluster can be set into rotation by rotating electric fields. If the electric field frequency is adjusted an increased order in the particle cluster can be observed. To do so a rather small cluster has been recorded by means of stereoscopic digital in-line holography. The reconstructed particle positions have been searched for vertical strings. Therefore a cylinder has been placed around each particle.

[4]Since this cluster behavior has been observed with another cluster it is not shown in this discussion. However, the description of the cluster structure by the discussed properties is complete.

[5]The range is determined by the cylinder introduced in the analysis.

All the other particles inside the cylinder are then considered to by in a string with the first one. The strings have then be characterized according to their lifetime. Furthermore, it has been found, that if set into motion the lower particles are dragged along due to the wake field interaction. This is in difference to what has been found previously, where the upper particles moved slower than the lower ones.

Overall it can be concluded, that the structural properties of a cluster can be changed by subjecting it to an additional electric field. Thus, the glass box can be a useful tool to investigate the simulations done by Brandt et al., even though the predicted order transitions have not yet been found.

8.9 Résumé

Comme il a été démontré dans le chapitre précédent, un cluster de particules peut être mis en mouvement de rotation à l'aide de champs électriques rotatifs. Lorsque la fréquence du champ électrique est ajustée à une certaine valeur on observe une augmentation de l'ordre du cluster de particules. Afin d'effectuer cette observation, le mouvement d'un cluster de petite taille a été enregistré par holographie stéréoscopique. La reconstruction des positions des particules a été réalisée de faon à avoir des alignements verticaux. Par conséquent, un cylindre a été placé autour de chaque particule. Toutes les particules se trouvant dans le cylindre qui entoure la particule seront considérée comme faisant parties de l'alignement de celle-ci. Ces alignements ont été caractérisés selon leur durée de vie. De plus, il a été montré que si les particules sont mises en mouvement alors elles sont entrainées le long de ces alignements à cause de la interaction dans le sillage du champ. Ceci est différent par rapport à ce qui avait été observé auparavant o les particules du dessus se déplaaient plus lentement que celles du bas.

Nous pouvons conclure que les propriétés structurales d'un cluster de particules peuvent être modifiées par l'action d'un champ électrique additionnel. Ainsi une boite de verre dans laquelle est formé le cluster peut être utilisée pour étudier expérimentalement les résultats théorique de Brandt et al. obtenus par simulation même si les transitions d'ordre prédites n'ont pas été observées.

8.10 Zusammenfassung

Wie zuvor gezeigt kann eine Teilchenwolke durch externe elektrische rotierende Felder in Rotation versetzt werden. In einem bestimmten Frequenzbereich kann eine höhere Ordnung im System festgestellt werden. Dafür wurde eine relativ kleine Teilchenwolke mit Hilfe von Holographie beobachtet. Die rekonstruierten Teilchenpositionen wurden auf Strings untersucht. Dazu wurde um jedes Teilchen ein Zylinder mit festem Radius gelegt. Alle weiteren Teilchen innerhalb dieses Zylinders gehören zu einem String mit dem Ersten. Die gefundenen Strings wurden dann anhand der Zeit während derer sie existieren charakterisiert. Des Weiteren zeigte sich, dass die unteren Teilchen von den Oberen gezogen

werden. Das steht im Gegensatz zu den Erkenntnissen des vorigen Kapitels, in dem der untere Teil der Wolke schneller rotierte als der Obere.

Insgesammt kann zusammengefasst werden, dass die Struktur einer Teilchenwolke durch externe Felder beeinflusst werden kann. Daher ist die Glassbox ein gutes Mittel um die Simulationen von P. Brandt et al. experimentell zu untersuchen, auch wenn bisher die vorhergesagten Übergänge nicht beobachtet werden konnten.

Summary

Throughout this thesis experiments in a wide variety of setups has been performed. The main aim was to tune and describe the particle interaction potential. After showing the basic plasma concepts and particle formation experiments on a main parameter, the particle charge, are discussed. In the final three chapters the interaction potential has been addressed.

During this thesis first some basic plasma concepts have been discussed. This was followed by a detailed discussion about the dust particle formation and the behavior at different flows. The dependence on the applied flow has been shown. Possible reasons for the observed behavior were discussed. In addition the plasma behavior has been investigated.

As the charge is a major parameter the de-charging of particles in the plasma afterglow has been described. The influence of a clearing field has been conclusively shown. In addition the charge dependence on the particle size and position has been a topic of investigation.

Afterwards the impact on the interaction potential by electric fields has been discussed. The concept of experiments on electric fields applied along direction of the electric field in the sheath and simulations on perpendicular rotating electric fields have been introduced. In order to apply a comparable rotating electric field the usage of a glass box has been proposed. The observed structures of clusters confined in such boxes has been discussed.

The first attempts on applying rotating electric fields to a confined cluster led to cluster rotation. The dependence of the rotation velocity on the electric field frequency has been shown.

In a further experimental series a stereoscopic digital in-line holography was used. The 3D data includes vertical strings and can hold for understanding the initial driving mechanism. Furthermore, a higher internal order of the cluster in cylindrical rather than spherical shells has been observed. The experimental observations have been compared to the predictions of earlier simulations.

Résumé

Dans les plasmas plusieurs expériences différentes peuvent être réalisées. Il est un environnement excellent pour la recherche interdisciplinaire.

Au cours de cette thèse d'abord quelques concepts de base de plasma ont été discutés. Ils ont été suivis par une discussion détaillée sur la formation des particules et leur comportement à différents fluxes. La dépendance sur le flux appliqué a été montré. Les raisons possibles pour le comportement observé ont été discutées. En plus, le changement du plasma a été étudié.

Les striations qui se produisent et des phénomènes de transport ne sont pas encore entièrement compris. D'autres études sur le changement dans les paramètres du plasma sont certainement nécessaires. Les processus de croissance dans des conditions de microgravité et sous l'utilisation d'autres gaz sont des sujets de recherche supplémentaires. Les connaissances acquises peuvent également conduire à un moyen plus efficace de nettoyer le tube.

Sur la section des plasmas complexes les charges des particules dans le plasma rémanent ont été décrites. L'influence d'un champ électrique a été démontrée de façon concluante. En plus, la dépendance à l'égard de la charge sur la taille des particules et de la position a été un sujet d'enquête. Malheureusement, certains des paramètres étudiés ne comportait pas de particules. En plus, il est souhaitable d'étudier la charge des particules dans les nuages aussi petits que possible. Les nuages plus petits et des tailles des particules manquantes peuvent compléter les expériences discutées.

Les expériences sur la rotation des nuages des particules ont montré la dépendance sur le champ électrique appliqué. Les données 3D ont des informations sur l'interaction verticale des particules et peuvent aider à la compréhension du mécanisme d'entraînement initial. Aussi la réponse aux autres excitations, par example dipôles et quadruples, reste à être étudiée. Les possibilités d'analyse 3D complète peuvent être illimitées si les problèmes avec la vitesse d'enregistrement et le post-traitement seront fixés.

Zusammenfassung

Die vorliegende Dissertation beschreibt Erkenntnisse aus einer Vielzahl verschiedener Experimente. Das Hauptziel dieser Arbeit galt der Beeinflussung des Teilchenwechselwirkungspotentials. Hierfür wurden zunächst grundlegenden Prinzipien der Plasmaphysik und des Teilchenwachstums beschrieben. Die durchgeführten Experimente zur Teilchenladung, einem der wichtigsten Parameter, wurden analysiert. Abschliessend wurden die Untersuchungen zum Wechselwirkungspotential dargestellt.

Zunächst wurden Konzepte zum Partikelwachstum und den damit verbundenen Veränderungen des Plasmas diskutiert. Des weiteren wurde das Verhalten der Partikel bei verschiedenen Neutralgasflüßen beschrieben. Mögliche Ursachen für das beobachtete Partikelverhalten und die Beeinflussung des Plasmas wurden diskutiert.

Da die Teilchenladung einer der wichtigesten Parameter in komplexen Plasmen ist, wurden Untersuchungen zur Ladungsreduktion durchgeführt. Die Teilchen wurden untersucht nachdem das umgebende Plasma relaxierte. Der Einfluss konstanter elektrischer Felder, der Teilchengröße, der Position und der Plasmaparameter auf die verbleibende Ladung wurden gezeigt.

In den verbleibenden Kapiteln wurden die Möglichkeiten zur Gestaltung des Wechselwirkungspotentials beschrieben. In früheren Experimenten wurde der Einfluss eines alternierenden Feldes entlang des elektrischen Feldes in der Plasmarandschicht gezeigt. Das veränderte Potential führte in diesem Fall zu langen Ketten entlang des angelegten elektrischen Feldes. Simulationen zu rotierenden elektrischen Feldern wurden durchgeführt. Um diese mit Experimenten zu vergleichen wurde eine zusätzliche leitende Glasbox eingebracht.

Zunäst wurde die Rotation des Clusters in Reaktion zu dem zusätzlichen elektrischen Feld beobachtet. Die Abhängingkeit der Rotationsgeschwindigkeit von der angelegten Frequenz wurde aufgezeigt.

In einer weiteren Serie wurden unter Verwendung holographischer Methoden 3D Daten der untersuchten Cluster gewonnen. Diese beinhalten Informationen über die interne Struktur des Clusters in vertikalen Teilchenketten und zylindrischen Schalen. Diese erhöhte innere Ordnung des Clusters ähnelt der strukturellen Veränderung des simulierten Systems.

Appendix A

Synchronization

A.1 Motivation

The Plasma Kristall 3 Plus (PK-3 Plus) setup saves next to the taken pictures also the parameters set as well as measured. These are saved to log files. Since the plasma parameters and environmental conditions are of vital importance to understand the particle behavior proper synchronization of the entries in the log files and the recorded pictures is necessary. The pictures and the log files can be synchronized by using the format numbers. These numbers are given both in the log files and in the pictures.

The rate the format numbers are written to the log files is however not constant. It is produced according to two programs which are used depending on whether the function generators are employed ('*Modtab.ini*') or not ('*Sorttab.ini*'). In both cases an internal clock is employed to call the entries in the according file and set values accordingly.

The two cases, the camera data format, the calculation, and the limitations will be discussed in this appendix.

A.2 Without Function Generators

If no function generators are used the entries in the log files are created and written one after the other according to Sorttab.ini. In total 128 data words can be written.The format number is set at every first data word. The time necessary for recording these is determined by the pick up period ('*Abholperiode*') p_{pick} and the period of one sort cycle p_{sort}. The values for these are given in '*System.ini*'. The time necessary to transfer and record all 128 data words is thus given by:

$$\begin{aligned} t_{rec} = \frac{p_{pick}}{p_{sort}} = \frac{3716}{1189200} s = 0.4s \\ \Rightarrow f_{rec} = 2.5Hz \end{aligned} \tag{A.1}$$

A.3 With Function Generators

In case function generators are employed to manipulate the particle behavior the entries written to the log files are chosen according to *'Modtab.ini'*. The readout timing is altered if function generators are used. It is now determined by the phase set 128 times per modulation (128 sampling points). It is divided into 128 phases as this is the number of data words that can be written. This is independent of whether or not the function generators are employed. Thus, also the time necessary to transfer and record these data words (t_{rec}) remains the same.

The sampling point distance is calculated if the generators are switched on, their frequency is changed, or if the amplitude is adjusted. The firs modulation phase once the timing of Sorttab.ini is finished. The modulation always starts with phase 32. The sampling point frequency f_{sam} is adjusted with respect to the modulation frequency f_{mod}:

$$f_{sam} = 128 \cdot f_{mod}. \tag{A.2}$$

If the modulation frequency is too high not every phase is set anymore and sampling points are left out. Assuming that n sampling points remain the sampling point frequency is reduced to:

$$f_{sam} = n \cdot f_{mod}. \tag{A.3}$$

This can be adjusted by reducing the set value 'stepwidthexponent', which gives the sampling step width in a power of two. The sampling point frequency is the time interval between setting the phase and production of all according measured values.

In difference to the way the entries are written if no function generators are employed now the entries are written in 32 quadruples. In each quadruples the phase of the function generator, the measured ion currents I_0 and I_1 and a measured value according to Modtab.ini are recorded. In the first quadruples this value always is the Modtab.ini number. The remaining 31 values can be chosen. For synchronization it is preferable if the format number is written at least once to this file.

The build-in computer is capable of transferring and saving to the log file with a frequency of $f_{rec} = 2.5$ Hz. In case it is not able to process the log files as fast as the modulation requires or the modulation cannot be filled by a normal number of quadruples a complicated sequence is written in order to write every phase of the modulation at least once. To a possible human reader of the log files this sequence caused by oversampling might look random.

A.4 Pictures

Every picture is taken during a 40 ms period. Afterwards the PAL (phase alternating line[1]) signal is read. In order to increase the frame rate to 50 Hz the even and odd lines of the

[1] for further explanations see for instance the wikipedia entry on the standard: http://en.wikipedia.org/wiki/PAL

Figure A.1: A picture as recorded by the cameras in the PK3 plus setup. On the lower edge the format number can be seen.

picture are read by two ports in parallel. The odd lines of the first picture are read by one channel, the even by the other. For the second picture this situation is reversed. In the lower edge the format number (FN), used as the main part in synchronizing the pictures and the housekeeping data, is given. Figure A.1 shows a picture as taken by the camera with the format number on the lower left corner as decoded in bright and dark regions.

The format number given on the picture is the one valid in the moment the rows in which it is present are read out and transfered and not in the moment the picture is actually taken. This has to be remembered when trying to synchronize the pictures with the housekeeping data later.

At some times the picture is read out in the moment the format number changes. In such cases half format numbers, as displayed in figure A.2(a), occur in the pictures. The broken format number is compared in this figure to the normal one, see figure A.2(b).

Note that in the PAL standard different amounts of lines are put between two pictures by the analog-to-digital converter (ADC) for synchronization. Before the odd frames 5 lines are included whereas before the even frames only 4 lines are included. To reach a frame rate of 50 Hz the pictures with 576 lines each as recorded by the camera are read by two PAL signal readout channels. If recording at 50 Hz an additional white line is

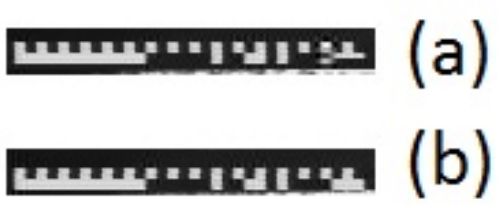

Figure A.2: Portion of pictures as shown in figure A.1 including only the format numbers. Each format number display in a picture consists of two rows. In the upper row a scale is displayed. From the white and black squares in the lower row the format number can be read. A white square represents a 0, a black one a 1. From left to right the square value decreases. Thus the format number displayed in (b) is an odd number. Panel (a) shows a broken format number. These are used to synchronize the pictures with the log files. In comparison to that a normal unbroken format number is shown in (b).

introduced on top or on bottom of the frames in order not to loose any information. This white line can be seen on the bottom in figure A.1. A sketch of the way the PAL standard is synchronized and the times needed to read a certain number of lines is displayed in figure A.3.

The three cameras are all controlled by one master chip. This ensures that these are synchronized. However, the chip also ensures that a picture has been taken to be read out if the PAL readout is ready. Thus it is possible that the cameras transmits slightly faster than the set frame rate which leads to uncertainties in the synchronization. Since the programming of the chip can neither be changed nor accessed anymore it is going to be assumed that the set frame rate is the one achieved. This assumption is of course for simplification. For further experiments it is advised to take as much care during the programming of the cameras and the log file saving routines as it has been taken in writing the log file routines in this setup.

A.5 Calculations

A.5.1 General

The aim of synchronization is to gain an information of the time elapsed until a certain number of frames has been taken:

First the broken format numbers are searched in the videos. These mark the times at which a new format number is generated and thus the old and the new format number are displayed in the video. Hence the format number is known to be an integer value. Since in the video only integer values can be displayed the broken numbers are the ones where the time of setting the new format number is best known. One frame recorded with a frame rate of 50 Hz is read out by two PAL channels. Of the first image one channel reads the odd, the other the even lines. For the second image the situation is mirrored. Since this would then, when combining the two images from both channels, lead to a gibbering in

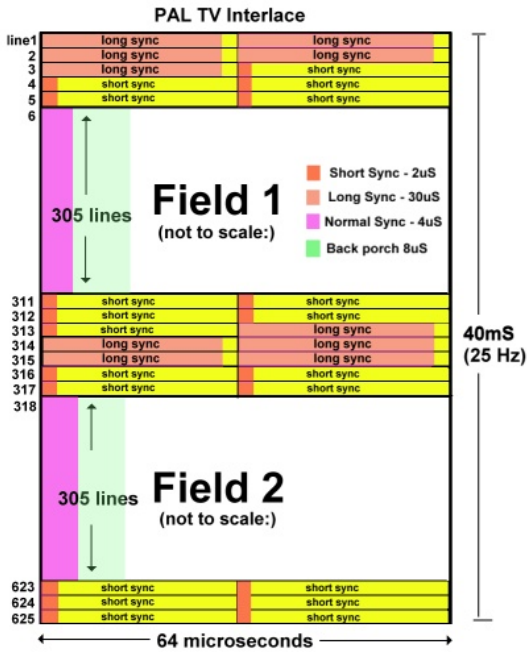

Figure A.3: Scheme to illustrate the PAL signal readout. This scheme is reproduced from [82].

the video additional white lines are saved.

If a broken format number occurs each readout channels read 285 lines before the format number has been changed. For the PAL synchronization 4 or 5 additional lines are taken depending on the frame number written. To write one line it takes 0.064 ms. The time it takes for the PAL readout to reach the line in which the new format number is set is then given by:

$$t_{PAL} = (4(5) + 285) \cdot 0.064ms, \tag{A.4}$$

depending on the frame number.

A.5.2 Without function Generators

In this case the format number frequency is constant. Thus the calculation of the number of frames recorded between setting two format numbers is:

$$n_{frames} = \frac{f_{camera}}{f_{rec}}, \tag{A.5}$$

with f_{camera} being the camera frame rate. If this is set to 50 Hz the resulting frame number is 20 frames. This ratio is very constant. Based on it the time elapses between producing two format numbers and thereby a correlation between the values in the log files and the cameras can be found.

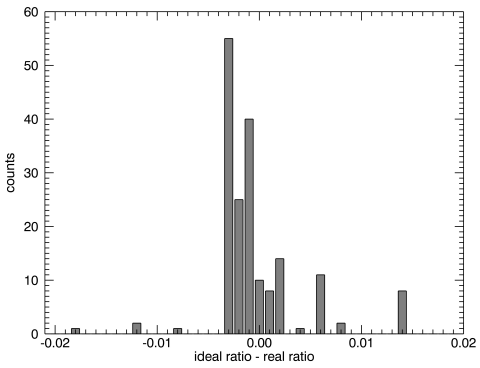

Figure A.4: Limitation to the synchronization as calculated from sequences recorded at 50 Hz. The ideal ratio of the phase set frequency to the camera frame rate minus the real ratio is displayed. The absolute mean difference between the two equals 0.00604.

A.5.3 With function Generators

As discussed the most constant frequency in case of employing the function generators found are the set values of the generators. Thus in the log files the integer format number and the corresponding phase and cycle number have to be found. Each cycle consists of 128 set points or phases. The first cycle starts with phase 32 since the current flowing to or from the chamber has to be zero for safety reasons on board the ISS. The following cycles start at phase 0. Since 128 phases are set to describe one cycle the time elapsed for each phase is determined by the phase set frequency:

$$t_{phase} = \frac{n_{cycles} \cdot 128 + n_{phase} - 33}{f_{phase}}. \tag{A.6}$$

Since the frequency of the function generators is set by 128 phases the phase set frequency f_{phase} can be calculated depending on the set generator modulation frequency $f_{alternation}$:

$$f_{phase} = 128 \cdot f_{alternation} \tag{A.7}$$

The number of full cycles n_{cycles} starts at zero. Since the first phase starts at 32, and the count there starts as well at 0 another 33 phases have to be subtracted to find the initial point of excitation. Knowing all these times the time elapsed between the beginning of the excitation and the change into a given format number is:

$$t_{el} = t_{phase} + t_{PAL}. \tag{A.8}$$

By multiplying this with the frame rate of 50 Hz one gains the number of frames taken since the excitation is on. Comparing this value to which the frame number in which the broken format number taken for synchronization has been observed results in the frame number in which the excitation has initially been introduced.

Please note that a change in amplitude should not change the relations whereas a change in frequency or switching the generators will. In these cases the synchronization has to be renewed.

Since the synchronization has been performed in a variety of cases throughout this thesis a good estimate of the synchronization limit can be given. The number of phases set per taken frame is calculated. If the camera would run at exactly 50 Hz this ratio at a sampling point frequency of 128 Hz would lead to a ratio of:

$$r_{ideal} = \frac{f_{phase}}{f_{camera}} = \frac{128Hz}{50Hz} = 2.56 \tag{A.9}$$

In figure A.4 the difference between the ideal ratio and the synchronization is displayed.

The absolute mean difference is calculated to be 0.00604. Assuming that the phase set frequency is constant a time limit to the synchronization can be calculated to about 0.27 frames which is equal to 5.4 ms. This is the reason for the inability of calculating the phases correctly in chapter 5. However, it is sufficient for most of the experiments conducted in this setup.

List of Figures

Bibliography

[MY1] L. Wörner, V. Nosenko, A. V. Ivlev, S. K. Zhdanov, H. M. Thomas, G. E. Morfill,M. Kroll, J. Schablinski, and D. Block, Phys. Plasmas **18**, 063706 (2011)

[MY2] L. Wörner, E. Kovacevic, J. Berndt, H. M. Thomas, M. H. Thoma, L. Boufendi, and G. E. Morfill, New J. Phys. **14**, 023024 (2012)

[MY3] L. Wörner, C. Räth, V. Nosenko, S. K. Zhdanov, H. M. Thomas, J. Schablinski, D. Block, and G. E. Morfill, accepted by Europ. Phys. Lett.

[1] E. Allahyarov, I. D'Amico, and H. Löwen, Phys. Rev. Lett. **81**, 1334 (1998)

[2] J. E. Allen, R. L. F. Boyd, and P. Reynolds, Proc. Phys. Soc. **B70**, 297 (1957)

[3] J. E. Allen, Physica Scripta. Vol. **45**, 497 (1992)

[4] O. Arp, D. Block, and A. Piel, Phys. Rev. Lett. **93**, 165004 (2004)

[5] O. Arp, D. Block, M. Klindworth, and A. Piel, Phys. Plasmas **12**, 122102 (2005)

[6] O. Arp, D. Caliebe, K. O. Menzel, A. Piel, J. A. Goree, IEEE Transactions on Plasma Science **38**, No. 4, 842 (2009)

[7] C. Arnas, M. Mikikian, and F. Doveil, Phys. Rev. E **60**, No. 6, 7420 (1999)

[8] C. Arnas, A. Mouberi, K. Hassouni, A. Michau, G. Lombardi, X. Bonnin, F. Bénédic and B. Pégouriè, J. Nucl. Mater. **390-391**, 140-143 (2009)

[9] C. Arnas, M. Mikikian, G. Bachet, and F. Doveil, Phys. Plasmas **7**, 4418 (2000)

[10] Y. Ando, J. Kuwabara, K. Suzuki, and A. Sawabe, Diamond and Rel. Mat. **13**, 1975 (2004)

[11] N. Angert, CERN **94-01**, 619 (1994)

[12] J. C. Angus and C. C. Hayman, Science **241**, 913 (1988)

[13] B. M. Annaratone, T. Antonova, C. Arnas, P. Bandyopadhyay, M. Chaudhuri, C.-R. Du, Y. Elskens, A. V. Ivlev, G. E. Morfill, V. Nosenko, K. R. Sütterlin, M. Schwabe and H. M. Thomas, Plasma Sources Sci. Technol. **19**, 065026 (2010)

[14] W. D. Arnett and D D. Clayton, Nature **227**, 780(1970)

[15] R. Basner, F. Sigeneger, D. Loffhagen, G. Schubert, H. Fehske, and H. Kersten, New J. Phys. **11**, 013041 (2009)

[16] H. Baumgartner, D. Block, and M. Bonitz, Contrib. Plasma Phys. *49*, 281 (2009)

[17] J. Beckers, W. W. Stoffels, and G. M. W. Kroesen, J. Phys. D: Appl. Phys. **42**, 155206 (2009)

[18] J. Beckers, T. Ockenga, M. Wolter, W. W. Stoffels, J. van Dijk, H. Kersten, and G. M. W. Kroesen, Phys. Rev. Lett. **106**, 115002 (2011)

[19] J. Berndt, E. Kovavcevic, I. Stefanovic, O. Stepanovic, S. H. Hong, L. Boufendi, and J. Winter, Contrib. Plasma Phys. **49**, No. 3 (2009)

[20] J. Berndt, E. Kovacevic, and L. Boufendi, J. Appl. Lett. **106**, 063309 (2009)

[21] D. Block, S. Käding, A. Melzer, A. Piel, H. Baumgartner, and M. Bonitz, Phys. Plasmas **15**, 040701 (2008)

[22] D. Block, J. Carstensen, P. Ludwig, W. J. Miloch, F. Greiner, A. Piel, M. Bonitz, and A. Melzer, accepted by Contr. Plasma Phys.

[23] B. E. Blue, C. E. Clayton, C. L. OConnell, F.-J. Decker, M. J. Hogan, C. Huang, R. Iverson, C. Joshi, T. C. Katsouleas, W. Lu, K. A. Marsh, W. B. Mori, P. Muggli, R. Siemann, and D.Walz, Phys. Rev. Lett. **90**, 214801 (2003)

[24] D. Bohm, E. H. S. Burhop, and H. S. W. Massey, McGraw-Hill Book Company, Inc., New York (1949)

[25] M. Bonitz, C. Henning, and D. Block, Rep. Prog. Phys. **73**, 066501 (2010)

[26] X. Bonnin, G. Lombardi, K. Hassouni, A. Michau, F. Bénédic, and C. Arnas, J. Nuc. Mat. **363-365**, 1191 (2007)

[27] J. E. Borovsky, Phys. Fluids **29**, 718 (1986)

[28] A. Bouchoule, *Dusty Plasma*s, John Wiley and Sons LTD, Chichester, first edition (1999)

[29] L. Boufendi, A. Plain, J. Ph. Blondeau, A. Bouchoule, C. Laure, and M. Toogood, Appl. Phys. Lett. **60**, 169 (1992)

[30] L. Boufendi, A. Bouchoule, and T. Hbid, J. Vac. Sci. Technol. A **14**, 572 (1996)

[31] L. Boufendi, J. Gaudin, S. Huet, G. Viera, and M. Dudemaine, Appl. Phys. Lett. **79**, 4301 (2001)

[32] L. Boufendi and A. Bouchoule, Plasma Sources Sci. Technol. **11**, A211 (2002)

[33] P. C. Brandt, A.V. Ivlev, and G.E. Morfill, J. Chem. Phys. **130**, 204513 (2009)

[34] P. C. Brandt, Dissertation, Ludwig Maximilian Universität, München (2010)

[35] P. C. Brandt, A.V. Ivlev, and G.E. Morfill, J. Chem. Phys. **132**, 234709 (2010)

[36] I. N. Bronstein, K. A. Semendjajew, G. Musiol, and H. Mühlig, Wissenschaftlicher Verlag Harri Deutsch GmbH, 7. Auflage (2008)

[37] M. A. Cappelli, T. G. Owano, and C. H. Kruger, J. Mater. Res. **5(11)**, 2326 (1990)

[38] J. Carstensen, F. Greiner, L.-J. Hou, H. Maurer, and A. Piel, Phys. Plasmas **16**, 013702 (2009)

[39] J. Carstensen, F. Greiner, and A. Piel, Phys. Plasmas **17**, 083703 (2010)

[40] J. Carstensen, H. Jung, F. Greiner, and A. Piel, Phys. Plasmas **18**, 033701 (2011)

[41] J. Carstensen, F. Greiner, D. Block, J. Schablinski, W. J. Miloch, and A. Piel, Phys. Plasmas **19**, 033702 (2012)

[42] P. Casavecchia, N. Balucani, M. Alagia, L. Cartechini, and G. G. Volpi, Acc. Chem. Res. **32**, 503 (1999)

[43] F. F. Chen, Plasma Sources Sci. Technol. **18**, 035012 (2009)

[44] S. J. Choi and M. J. Kushner, J. Appl. Phys **74**, 853 (1993)

[45] S. J. Choi, P. L. G. Ventzek, R. J. Hoekstra, and M. J. Kushner, Plasma Sources Sci. Technol. **3**), 418 (1994)

[46] J. H. Chu and I. Lin, Phys. Rev. Lett., **72**, 4009 (1994)

[47] L. Couëdel, M. Mikikian, and L. Boufendi, Physical Review E **74**, 026403 (2006)

[48] L. Couëdel, A. Mezeghrane, A. A. Samarian, M. Mikikian, Y. Tessier, M. Cavarroc, and L. Boufendi, Contrib. Plasma Phys. **49**, No.4-5, 235 (2009)

[49] L. Couëdel, M. Mikikian, A.A. Samarian, and L. Boufendi, Phys. Plasmas **17**, 083705 (2010)

[50] L. Couëdel, V. Nosenko, A. V. Ivlev, S. K. Zhdanov, H. M. Thomas, and G. E. Morfill, Phys. Rev. Lett. **104**, 195001 (2010)

[51] C. Cui and J. Goree, IEEE Trans. Plasma Sci. **22**, 151 (1994)

[52] R. P. Dahiya, G. V. Paeva, W. W. Stoffels, E. Stoffels, G. M. W. Kroesen, K. Avinash, and A. Bhattacharjee, Phys. Rev. Lett. **89**, 125001 (2002)

[53] J. E. Daugherty, R. K. Porteus, and D. B. Graves, J. Appl. Phys. **73**, 1617 (1993)

[54] K. de Bleecker, A. Bogaerts, and W. Goedheer, Phys. Rev. E **73**, 026405 (2006)

[55] I. Denysenko, J. Berndt, E. Kovacevic, I. Stefanovic, V. N. Selenin, and J. Winter, Phys. Plasmas **13**, 073507 (2006)

[56] M. A. Dopita, B. A. Groves, R. S. Sutherland, and L. J. Kewley, The Astrophys. Journal **583**, 727 (2003)

[57] J. Dorschner and T. Henning, The Astron. Astrophys. Rev. **6**, 271 (1995)

[58] S. C. Eaton and M. K. Sunkara, Diamond and Related Materials **9**, 1320 (2000)

[59] C. A. Eckert, B. L. Knutson, and P. G. Debenedetti, Nature **383**, 313(1996)

[60] P. S. Epstein, Phys. Rev. **23**, 710 (1924)

[61] Y. Feng, J. Goree, and B. Liu, Rev. Sci. Instr. **78**, 053704 (2007)

[62] A. A. Fridman, L. Boufendi, T. Hbid, B. V. Potapkin, and A. Bouchoule, J. Appl. Phys, **79** (3), 1303 (1996)

[63] T. Fujii, J. Appl. Phys. **82**, 2056 (1997)

[64] V. E. Fortov, A. P. Nefedov, V. M Tochinskii, V. I. Molotkov, A. G. Khrapak, O. F. Petrov, and K. F. Volykhin, JETP Lett. **64**, 92 (1996)

[65] V. E. Fortov, A. P. Nefedov, V. I. Molotkov, M.Y. Poustylnik, and V. M. Torchinsky, Phys. Rev. Lett. **87**, 205002 (2001)

[66] V. E. Fortov, A. G. Khrapak, S. A. Khrapak, V. I. Molotkov, and O. F. Petrov, Physics - Uspekhi **47**, 447 (2004)

[67] V. E. Fortov, O. F. Petrov, A. D. Usachev, and A. V. Zobnin, Phys. Rev. E **70**, 046415 (2004)

[68] V. E. Fortov, A. V. Ivlev, S. A. Khrapak, A. G. Khrapak, and G. E. Morfill, Physics Reports **421**, 1-103 (2005)

[69] V. Fortov, G. Morfill, O. Petrov, M. Thoma, A. Usachev, H. Hoefner, A. Zobnin, M. Kretschmer, S. Ratynskaia, M. Fink, K. Tarantik, Yu. Gerasimov, and V. Esenkov, Plasma Phys. Contrl. Fusion **47**, B537 (2005)

[70] B. Friedel and S. Greulich-Weber, small **7**, 859(2006)

[71] D. Gahan, S. Daniels, C. Hayden, D. O'Sullivan, and M. B. Hopkins, Plasma Sources Sci. Technol. **21**, 015002 (2012)

[72] A. Garscadden, B. Ganguly, P. Haarland, and J. Williams, Plasma Sources Sci. Technol. **3**, 239 (1994)

[73] S. Girshik and P. Agarwal, private communications, ICOPS and WPDP (2012)

[74] C. K. Goertz and G. E. Morfill, Icarus **53**, 219 (1983)

[75] A. de Graaf, M. F. A. M. van Hest, M. C. M. van de Sanden, K. G. Y. Letourneur, and D. C. Schram, Appl. Phys. Lett. **74**, 2927 (1999)

[76] J. Goree, Plasma Sources Sci. Technol. **3**, 400 (1994)

[77] J. Goree, G. E. Morfill, V. N. Tsytovich, and S. V. Vladimirov, Phys. Rev. E **59**, 7055 (1999)

[78] O. Havnes, C. K. Goertz, G. E. Morfill, E. Grün, and W. Ip, J. Geophys. Res. **92**, 2281 (1987)

[79] Y. Hayashi and K. Tachibana, Jpn. J. Appl. Phys. **33**, L804 (1994)

[80] R. Heidemann, S. Zhdanov, K. R. Sütterlin, H. M. Thomas and G. E. Morfill, Europ. Phys. Lett. **96**, 15001 (2011)

[81] R. Hewins, R. Jones, and E. Scott, Cambridge University, Cambridge (1996)

[82] http://martin.hinner.info/vga/pal.html

[83] http://www.microparticles.de/

[84] S. Hofmann and G. Münzenberg, Rev. Mod. Phys., **72**, 733 (2000)

[85] S. Hong, J. Berndt, and J. Winter, Plasma Sources Sci. Technol. **12**, 46 (2003)

[86] P. Huber, Dissertation, Ludwig Maximilian Universität, München (2011)

[87] M. Hundt, P. Sadler, I. Levchenko, M.Wolter, H. Kersten, and K. Ostrikov, J. Appl. Phys. **109**, 123305 (2011)

[88] H. Ikezi, Physics of Fluids **29**, 1764 (1986)

[89] H. Imanaka, B. N. Khare, J. E. Elsila, E. L. O. Bakes, C. P. McKay, D. P. Cruikshank, S. Sugita, T. Matsui, and R. N. Zare, Icarus **168**, 344 (2004)

[90] T. Inoue, H. Tachibana, K. Kumagai, K. Miyata, K. Nishimura, K. Kobashi, and A. Nakaue, J. Appl. Phys. **67**, 7329 (1990)

[91] C.-W. Io, C.-L. Chan, and L. I, Phys. Plasmas **17**, 053703 (2010)

[92] Y. Ivanov and A. Melzer, Phys. Rev. E **79**, 036402 (2009)

[93] A. V. Ivlev, U. Konopka, and G. Morfill, Phys. Rev. E **62**, 2739 (2000)

[94] A. V. Ivlev, M. Kretschmer, M. Zuzic, G. E. Morfill, H. Rothermel, H. M. Thomas, V. E. Fortov, V. I. Molotkov, A. P. Nefedov, A. M. Lipaev, O. F. Petrov, Yu. M. Baturin, A. I. Ivanov, and J. Goree, Phys. Rev. Lett. **90**, 055003 (2003)

[95] A. V. Ivlev, G. E. Morfill, H. M. Thomas, C. Räth, G. Joyce, P. Huber, R. Kompaneets, V. E. Fortov, A. M. Lipaev, V. I. Molotkov, T. Reiter, M. Turin, and P. Vinogradov, Phys. Rev. Lett. **100**, 095003 (2008)

[96] J. A. Johnson and R. Ramaiah, Phys. Rev. A **36**, No. 2, 774 (1987)

[97] A. V. Ivlev, P. C. Brandt, G. E. Morfill, C. Räth, H. M. Thomas, G. Joyce, V. E. Fortov, A. M. Lipaev, V. I. Molotkov, and O. F. Petrov, IEEE Transactions on Plasma Science **38**, 733 (2010)

[98] A. V. Ivlev, M. H. Thoma, C. Räth, G. Joyce, and G. E. Morfill, Phys. Rev. Lett. **106**, 155001 (2011)

[99] H. Kersten, H. Steffen, D. Vender, and H. E. Wagner, *Vacuum* **48(3)**, 305 (1995)

[100] T. Kewitz and H. Kersten, Galvanotechnik **4**, 866 (2010)

[101] S. A. Khrapak, D. Samsonov, G. Morfill, H. Thomas, V. Yaroshenko, H. Rothermel, T. Hagl, V. Fortov, A. Nefedov, V. Molotkov, O. Petrov, A. Lipaev, A. Ivanov, and Y. Baturin, Phys. Plasmas **10**, 1-4 (2003)

[102] S. A. Khrapak, S. V. Ratynskaia, A. V. Zobnin, A. D. Usachev, V. V. Yaroshenko, M. H. Thoma, M. Kretschmer, H. Höfner, G. E. Morfill, O. F. Petrov, and V. E. Fortov, Phys. Rev. E **72**, 016406 (2005)

[103] S. A. Khrapak, H. M. Thomas, and G. E. Morfill, Europ. Phys. Lett. **91**, 25001 (2010)

[104] S. A. Khrapak, P. Tolias, S. Ratynskaia, M. Chaudhuri, A. Zobnin, A. Usachev, C. Rau, M. H. Thoma, O. F. Petrov, V. E. Fortov, and G. E. Morfill, Europ. Phys. Lett. **97**, 35001 (2012)

[105] C. Killer, A. Schella, T. Miksch, and A. Melzer, Phys. Rev. B **84**, 054104 (2011)

[106] B. Klumov, P. Huber, S. Vladimirov, H. Thomas, A. Ivlev, G. Morfill, V. Fortov, A. Lipaev, and V. Molotkov, Plasma Phys. Control. Fusion **51**, 124028 (2009)

[107] R. Kompaneets, S. V. Vladimirov, A. V. Ivlev, V. Tsytovich, and G. Morfill, Phys. Plasmas **13**, 072104 (2006)

[108] R. Kompaneets, Dissertation, Ludwig Maximilian Universität, München (2007)

[109] R. Kompaneets, G.E. Morfill und A.V. Ivlev, Physics of Plasmas **16**, 043705 (2009)

[110] J. Kong, T. W. Hyde, L. Matthews, K. Qiao, Z. Zhang, and A. Douglass, Physical Review E **84**, 016411 (2011)

[111] U. Konopka, Dissertation, Ruhr Universität, Bochum (2000)

[112] U. Konopka, G. E. Morfill, and L. Ratke, Phys. Rev. Lett. **84**, 891 (2000)

[113] U. Kortshagen and U. Bhandarkar, Phys. Rev. E **60**, 887 (1999)

[114] E. Kovacevic, I. Stefanovic, J. Berndt, and J. Winter, J. Appl. Lett. **93**, 2924 (2003)

[115] E. Kovacevic, I. Stefanovic, J. Berndt, Y. Pendleton, and J. Winter, Astrophys. J. **623**, 242 (2005)

[116] E. Kovacevic, Dissertation, Ruhr Universität, Bochum (2006)

[117] M. Kroll, S. Harms, D. Block, and A. Piel, Phys. Plasmas **15**, 063703 (2008)

[118] M. Kroll, J. Schablinski, D. Block, and A. Piel, Phys. of Plasmas **17**, 013702 (2010)

[119] M. Kroll, L. Mühlfeld, and D. Block, IEEE Trans. Plasma Sci. **38**, 897 (2010)

[120] M. Kroll, Dissertation, Christian Albrecht Universität, Kiel (2010)

[121] M. J. Kushner, J. Appl. Phys. **63**, 2532 (1988)

[122] M. Lampe, G. Joyce, G. Ganguli, and V. Gavrishchaka, Phys. Plasmas **7**, 3851 (2000)

[123] M. Lampe, G. Joyce, and G. Ganguli, IEEE Transactions on Plasma Science **33**, 57 (2005)

[124] V. Land and W. J. Goedheer, New J. Phys. **10**, 123028 (2008)

[125] V. Land, B. Smith, L. Matthews, and T. Hyde, IEEE Trans. Plasma Sci. **38**, 768 (2010)

[126] E. J. Lerner, Ind. Phys. **6**, 16 (2000)

[127] M. A. Lieberman and V. A. Godyak, IEEE Transactions on Plasma Science **26**, 955 (1998)

[128] M. A. Lieberman and A. J. Lichtenberg, *Principles of Plasma Discharges and Materials Processing*, John Wiley and Sons, Inc, Hoboken, New Jersey, second edition (2005)

[129] A. M. Lipaev, S. A. Khrapak, V. I. Molotkov, G. E. Morfill, V. E. Fortov, A. V. Ivlev, H. M. Thomas, A. G. Khrapak, V. N. Naumkin, A. I. Ivanov, S. E. Tretschev, and G. I. Padalka, Phys. Rev. Lett. **98**, 265006 (2007)

[130] L. B. Loeb, Phys. Rev. **76**, No. 2, 255 (1949)

[131] P. Ludwig, H. Kählert, and M. Bonitz, Plasma Phys. Control. Fusion **54**, 045011 (2012)

[132] 3M GMBH Deutschland, Industriestraße, 55743 Idar-Oberstein

[133] J. E. Martin, J. Odinek, T. C. Halsey, and R. Kamien, Phys. Rev. E **57**, 756 (1998)

[134] K. Matyash, R. Schneider, R. Ikkurthi, L. Lewerentz, and A. Melzer, Plasma Phys. Control. Fusion **52**, 124016 (2010)

[135] H. R. Maurer, V. Schneider, M. Wolter, R. Basner, T. Trottenberg, and H. Kersten, Contrib. Plasma Phys. **51**, No. 2-3, 218 (2011)

[136] P. F. McMillan and H. E. Stanley, Nature Physics **6**, 479 (2010)

[137] F. Melandsø, T. Aslaksen, and O. Havnes, Planet. Space Sci. **41**, 321 (1993)

[138] A. Melzer, A. Hofmann, and A. Piel, Phys. Rev. E **53**, 2757 (1996)

[139] A. Melzer, V. A. Schweigert, and A. Piel, Phys. Rev. Lett. **83**, 3194 (1999)

[140] A. Melzer, Plasma Souces Sci Technol. **10**, 303 (2001)

[141] A. Melzer, Phys. Rev. E **73**, 056404 (2006)

[142] A. Melzer, B. Buttenschön, T. Miksch, M. Passvogel, D. Block, O. Arp, and A. Piel, Plasma Phys. Control. Fusion **52**, 124028 (2010)

[143] R. L. Merlino, Am. J. Phys. **75**, 12(2007)

[144] A. Michau, G. Lombardi, C. Arnas, L. Colina Delacqua, M. Redolfi, X. Bonnin, and K. Hassouni, Plasma Sources Sci. Technol. **19**, 034023 (2010)

[145] A. Michau, G. Lombardi, C. Arnas, X. Bonnin, K. Hassouni, J. Nucl. Mater. **415**, pp. S1077-S1080 (2011)

[146] A. Michau, G. Lombardi, L. C. Delacqua, M. Redolfi, C. Arnas, P. Jestin, X. Bonnin, K. Hassouni, Plamsa Chemnistry and Plasma Processing 32, 451(2012)

[147] G. Mie, Ann. Phys. **25**, 377 (1908)

[148] M. Mikikian, L. Boufendi, A. Bouchoule, H. M. Thomas, G. E. Morfill, A. P. Nefedov, V. E. Fortov, and the PKE Nefedov team, New J. Phys. **5**, 19 (2003)

[149] M. Mikikian, L. Couëdel, M. Cavarroc, Y. Tessier, and L. Boufendi, New. J. Phys. **9**, 268 (2007)

[150] M. Mikikian, L. Couëdel, M. Cavarroc, Y. Tessier, and L. Boufendi, Eur. Phys. J. Appl. Phys. **49**, 13106 (2010)

[151] W. J. Miloch, M. Kroll, and D. Block, Phys. Plasmas **17**, 103703 (2010)

[152] L. Minnhagen, Journal of the Optical Society of America **63**, No 10, 1185 (1973)

[153] S. Mitic, R. Sütterlin, A. V. Ivlev, H. Höffner, M. H. Thoma, S. Zhdanov, and G. E. Morfill, Phys. Rev. Lett. **101**, 235001 (2008)

[154] S. Mitic, M. Y. Pustylnik, G. E. Morfill, and E. Kovacevic, Optics letters **36**, No. 18, 3699 (2011)

[155] M. Moravej and R. F. Hicks, Chem. Vap. Deposition **11**, 469 (2005)

[156] G. E. Morfill, E. Grün, and T. V. Johnson, Planet. Space Sci. **28**, 1087 (1980)

[157] G. E. Morfill and H. M. Thomas, Icarus **2**, 539 (2005)

[158] G. E. Morfill, U. Konopka, M. Kretschmer, M. Rubin-Zuzic, H. M. Thomas, S. K. Zhdanov, and V. Tsytovich, New J. Phys. **8**, 7 (2006)

[159] G. E. Morfill, A. V. Ivlev, Reviews of Mod. Physics **81**, 1353 (2009)

[160] Y. Mori, K. Yoshii, K. Yasutake, H. Kakiuchi, H. Ohmi, K. Wada, Thin Solid Films **444**, 138 (2003)

[161] H. M. Mott-Smith and I. Langmuir, Physical Review **28**, 727 (1926)

[162] T. Mussenbrock, R. P. Brinkmann, M. A. Lieberman, A. J. Lichtenberg, and E. Kawamura, Phys. Rev. Lett. **101**, 085004 (2008)

[163] T. Nagai, Z. Feng, A. Kono, and F. Shoji, Phys. Plasmas **15**, 050702 (2008)

[164] Y. Nakamura, J. Phys. D: Appl. Phys. **43**, 365201 (2010)

[165] W. L. Nighan and W. J. Wiegand, Phys. Rev. A **10**, No. 3, 922 (1974)

[166] V. Nosenko, A. V. Ivlev, S. K. Zhdanov, M. Fink, and G. E. Morfill, Phys. Plasmas **16**, 083708 (2009)

[167] V. Nosenko, S. K. Zhdanov, A. V. Ivlev, C. A. Knapek, and G. E. Morfill, Phys. Rev. Lett. **103**, 015001 (2009)

[168] M. A. Olevanov, Yu. A. Mankelevich, and T. V. Rakhimova, Tech. Phys. **48**, 1270 (2003)

[169] J. K. Olthoff and K. E. Greenberg, J. Res. Natl. Inst. Stand. Technol. **100**, No. 4, 327 (1995)

[170] N. Osterman, I. Poberaj, J. Dobnikar, D. Frenkel, P. Ziherl und D. Babić, Phys. Rev. Lett. **103**, 228301 (2009)

[171] C. Plank, Biological Chemistry **384**, 737 (2003)

[172] B. Povh, K. Rith, C. Scholz, F. Zetsche, Springer, 8. Auflage, XII, (2009)

[173] L. C. Qin, D. Zhou, A. R. Krauss, and D. M. Gruen, Appl. Phys. Lett. 72, 3437 (1998)

[174] Yu. P. Raizer, *Gas Discharge Physics*, Springer, Berlin (1991)

[175] V. A. Rakov and M. A. Uman, Cambrige University Press, Thrid printing (2005)

[176] S. Ratynskaia, S. Khrapak, A. Zobnin, M. H. Thoma, M. Kretschmer, A. Usachev, V. Yaroshenko, R. A. Quinn, G. E. Morfill, O. Petrov, and V. Fortov, Phys. Rev. Lett. **93**, No. 8, 085001 (2004)

[177] L. Ravi and S. L. Girshik, Phys Rev. E **79**, 026408 (2009)

[178] C. J. Olson Reichhardt, C. Reichhardt, A. R. Bishop, Phys. Rev. Lett. **92**, 016801 (2004)

[179] E. Riedel, Anorganische Chemie, de Gruyter, Berlin-New York, 5. Aufl. (2002)

[180] H. S. Robertson, Phys. Rev. **105**, No. 2, 386 (1957)

[181] S. Robertson and Z. Sternovsky, Phys. Rev. E **67**, 046405 (2003)

[182] H. Rothermel, T. Hagl, G. E. Morfill, M. H. Thoma, and H. M. Thomas, Phys. Rev. Lett. **87**, No. 17, 175001 (2002)

[183] W. D. Suranga Ruhunusiri and J. Goree, Phys. Rev. E **85**, 046401 (2012)

[184] Y. Saito, T. Yoshikawa, M. Inagaki, M. Tomita, and T. Hayashi, Chem. Phys. Lett. **204**, 277 (1993)

[185] A. A. Samarian, O. S. Vaulina, A. P. Nefedov, V. E. Fortov,1 B. W. James, and O. F. Petrov, Phys. Rev. E **64**, 056407 (2001)

[186] A. A. Samarian and B. W. James, Plasma. Phys. Controlled Fusion **47**, B629 (2005)

[187] D. Samsonov and J. Goree, Phys. Rev. E **59**, No. 1, 1047 (1999)

[188] J. Schablinski, D. Block, A. Piel, A. Melzer, H. Thomsen, H. Kählert, and M. Bonitz, Phys. Plasmas **19**, 013705 (2012)

[189] A. Schella, T. Miksch, A. Melzer, J. Schablinski, D. Block, A. Piel, H. Thomsen, P. Ludwig, and M. Bonitz, Phys. Rev. E **84**, 056402 (2011)

[190] M. Schwabe, Dissertation, Ludwig Maximilian Universität, München (2009)

[191] H. Setyawan, M. Shimada, Y. Hayashi, K. Okuyama, and S. Winardi, J. Appl. Phys. **97**, 043306 (2005)

[192] P. Sheng and W. Wen, Annu. Rev. Fluid Mech. **44**, 143 (2012)

[193] T. Shimizu, J. L. Zimmermann and G. E. Morfill, New J. Phys. **13**, 023026 (2011)

[194] F. Shoji, Z. Feng, A. Kono, and T. Nagai, Appl. Phys. Lett. **89**, 171504 (2006)

[195] P. K. Shukla and A. A. Mamun, *Introduction to Dusty Plasma Physics*, Institute of Physics Publishing, London (2002)

[196] P. K. Shukla and B. Eliasson, Rev. Mod. Phys. **81**, 25 (2009)

[197] A.V. Silhanek, M. V. Milosevic, R. B. G. Kramer, G. R. Berdiyorov, J. Van de Vondel, R. F. Luccas, T. Puig, F. M. Peeters, and V. V. Moshchalkov, Phys. Rev. Lett. **104**, 017001 (2010)

[198] R. Stanway, J. L. Sproston, und A. K. El-Wahed, Smart Materials and Structures **5**, 464 (1996)

[199] V. Steinberg, R. Sütterlin, A. V. Ivlev, and G. E. Morfill Phys. Rev. Lett. **86**, 4540 (2001)

[200] H. Stöcker, Bibliografische Information Der Deutschen Bibliothek, 5. Auflage (2004)

[201] S. Stoykov, C. Eggs, and U. Kortshagen, J. Phys. D: Appl. Phys. **34**, 2160 (2001)

[202] K. D. Supulver and D. N.C. Lin, Icarus **146**, 525 (2000)

[203] M. Thoma, H. Höffner, M. Kretschmer, S. Ratynskaia, G. E. Morfill, A. Usachev, A. Zobin, O. Petrov, and V. Fortov, Microgravity Sci. Technol. **XVII-3/4**, 47 (2006)

[204] H. M. Thomas, G. E. Morfill, V. Demmel, J. Goree, B. Feuerbacher, and D. Möhlmann, Phys. Rev. Lett., **73**(5), 652 (1994)

[205] H. M. Thomas and G. E. Morfill, Nature **379**, 806(1996)

[206] H. M. Thomas, G. E. Morfill, V. E. Fortov, A. V. Ivlev, V. I. Molotkov, A. M. Lipaev, T. Hagl, H. Rothermel, S. A. Khrapak, R. K. Suetterlin, M. Rubin-Zuzic, O. F. Petrov, V. I. Tokarev, and S. K. Krikalev, New J. Phys. **10**, 033036 (2008)

[207] V. N. Tsytovic, Phys. Usp. 40, 53 (1997)

[208] O. S. Vaulina, S. A. Khrapak, A. A. Samarian, and O. F. Petrov, Phys. Scripta T **84**, 229 (2000)

[209] O. Vaulina und S. Khrapak, J. Exp. Theor. Phys. **90**, 287 (2000)

[210] S. Veprek, S. Reiprich, and L. Shizi, Appl. Phys. Lett. **66**, 2640 (1995)

[211] Z. W. Wang, H. P. Fang, Z. F. Lin, L. W. Zhou Phys. Rev. E **61**,6837 (2000)

[212] J. Waskoenig and T. Gans, Appl. Phys. Lett. **96**, 181501 (2010)

[213] Y. Watanabe, M. Shiratani, and K. Koga, Plasma Sources Sci. Technol. **11**, A229 (2002)

[214] G. Wattieaux and L. Boufendi, Phys. Plasmas **19**, 033701(2012)

[215] S. J. Weidenschilling, Icarus **127**, 290 (1997)

[216] R. B. Wilson IV and N. K. Podder, Phys. Rev. E **76**, 046405 (2007)

[217] W. M. Winslow, J. Appl. Phys. **20**, 1137 (1949)

[218] J. Winter, Phys. Plasmas **7**, 3862 (2000)

[219] W. A. Yarbrough and R. Messier, Science **247**, 688 (1990)

[220] V. V. Yaroshenko, B. M. Annaratone, S. A. Khrapak, H. M. Thomas, G. E. Morfill, V. E. Fortov, A. M. Lipaev, V. I. Molotkov, O. F. Petrov, A. I. Ivanov, M. V. Turin, Phys. Rev. E **69**, 066401 (2004)

[221] K. Yasutake, H. Ohmi, Y. Kirihata, H. Kakiuchi, Thin Solid Films **517**, 242 (2008)

[222] J. H. Yoo und N. M. Wereley, J. Intelligent Mat. Syst. and Structures **13**, 679 (2002)

[223] T. Yoshida, Y. Kousaka, and K. Okuyama, Ind. Eng. Chem. Fundam. **15**, 37 (1976)

[224] C. Yunming and L. Ming, J. Phys. D Appl. Phys. **26**, 1007 (1993)

[225] Yi Zeng, S. W. Lee, L. Gao, and C. X. Ding, J. Eurp. Ceramic Society **22**, 347 (2002)

[226] S. Zhdanov, M. H. Thoma, C. A. Knapek, and G. E. Morfill, New Journal Phys. **14**, 023030 (2012)

[227] A. V. Zobnin, A. D. Usachev, O. F. Petrov, and V. E. Fortov, Phys. Plasmas **15**, 043705 (2008)

[228] M. Rubin-Zuzic, H. M. Thomas, S. K. Zhdanov, and G. E. Morfill, New J. Phys. **9**, 39 (2007)

Acknowledgements

First of all I want to thank Prof. Dr. Dr. h. c. G. E. Morfill and Prof. Dr. L. Boufendi for offering me the possibility to study at both their institutes. I am very grateful for the opportunities, support, and guidance offered by them during my thesis.

Next, I want to thank Dr. H. M. Thomas for his patience and support. I want to take this opportunity to tell how much I appreciate his guidance.

My special thanks go to Dr. E. Kovacevic without whom the time in France would not have been half as much fun as it was. She and her husband Dr. J. Berndt knew the answers to all my questions.

Many thanks go to Dr. V. Nosenko who introduced me to the concepts of plasma physics. He is the best supervisor any student can possibly ask for.

I want to thank Dr. A. V. Ivlev, Dr. S. Zhdanov, Dr. M. H. Thoma, Dr. C. Räth, Dr. R. Sütterlin, Dr. L. Couëdel, Dr. P. Huber, and Dr. P. Brandt for their patience and persistence in helping me solving my problems.

I want to thank J. Schablinski, Dr. M. Kroll, and Dr. D. Block for the good cooperation and the great time we spend together in Kiel.

I want to thank C. Du and Dr. L. Talizadeh, for being the best office mates. I had an amazing time with the two of you! Thank you for lightening up my mood whenever needed!

Furthermore, I want to thank Dr. U. Konopa, Dr. C. Knapek, Dr. M. Schwabe, Dr. S. Mitic, R. Heideman, J. Jeon, M. Fink, Dr. T. Antonova, Dr. L. Balika, H. Tawidian, and the remaining colleagues from MPE Munich, IHED Moscow, Gremi Orléans, and CAU Kiel. Working in such a lively group of experts has inspired me.

Special thanks to Dr. J. Zimmerman for coffee breaks. Thank you for listening and being there when I needed support! In line with her I want to thank A. Langer for more than only administrative help.

I want to thank H. Modest, A. Weißmann, and Dr. G. 'Dr. Gre' Rossmanith, for many controversial discussions. The time spend with you in the office, on the Wiesn and anywhere else was great!

Last but definitely not least I want to thank the engineers at both institutes, namely C. Rau, C. Deysenroth, K. Taratnik, T. Hagl, S. Dozias, and T. Lecas. I want to thank especially S. Albrecht for technical support, scientific explanations, and thrilling ideas.